Universidad de Valladolid

ESCUELA DE INGENIERÍAS INDUSTRIALES

UNIVERSITY OF VALLADOLID

SCHOOL OF INDUSTRIAL ENGINEERINGS

Master's in Chemical Engineering

MASTER'S THESIS

Hydrogenation of D-Xylose molecules in the presence of solid foam catalysts in a stirred tank reactor

Author:

Goicoechea Torres, Alberto

Supervisors:

García Serna, Juan

University of Valladolid

Tapio Salmi

Laboratory of Industrial Chemistry and Reaction Engineering
Åbo Akademi University

Valladolid, July 2022

Hydrogenation of D-Xylose molecules in the presence of solid foam catalysts in a stirred tank reactor

Master's Thesis

Alberto Goicoechea Torres

Johan Gadolin
Process Chemistry Centre

Laboratory of Industrial Chemistry and Reaction Engineering
Faculty of Science and Engineering/Chemical Engineering
Åbo Akademi University
Turku/Åbo, Finland, 2022

TFM REALIZADO EN PROGRAMA DE INTERCAMBIO

TÍTULO:	Hydrogenation of D-Xylose molecules in the presence of solid foam catalysts in a stirred tank reactor
ALUMNO:	Alberto Goicoechea Torres
FECHA:	12 de julio de 2022
CENTRO:	Faculty of Science and Engineering
UNIVERSIDAD:	Åbo Akademi University
TUTOR:	Tapio Salmi

Abstract

BACKGROUND: A significant portion of the world's energy carriers and material products are derived from fossil fuel refineries. The practicality of exploitation of fossil fuels is expected to diminish in the near future due to ongoing price increases, uncertain availability, and environmental concerns. As a result, alternative solutions capable of mitigating climate change and reducing the use of fossil fuels should be promoted. The use of biomass as a raw material for fuel and chemical production instead of oil is an intriguing possibility that is driving the development of biorefinery complexes. In this perspective, using lignocellulosic biomass as a raw material for the chemical industry is a viable approach that has received a lot of attention in recent years, such as the manufacture of sugar alcohols. Thus, these polyols generated from the hydrogenation of sugar molecules are flexible compounds with a wide range of applications, including low-calorie sweeteners, medicinal excipients, anti-caries agents, and so on. The aim of this thesis was to improve a novel open-cell foam catalyst based on ruthenium supported on carbon. Thus, heterogeneous catalyst was used in order to perform kinetic experiments for the selective hydrogenation of D-Xylose into its sugar alcohol D-Xylitol. To do so, a wide range of different experiments were carried out at different temperatures (60-90^{o}C), pressures (20-40 bar) and D-Xylose initial concentrations (0.065, 0.13, 0.26 M), to investigate the role of each of them on the reaction rate. The solid open-cell foam catalyst used in this thesis comprised the following preparation steps: cutting the open-cell aluminum foam piece, followed by an anodic oxidation pretreatment, next a carbon coating with an acid pretreatment afterwards, to finish with a ruthenium impregnation step and an Ex-Situ reduction.

RESULTS: D-Xylose conversions up to 100 % were accomplished, depending on the reaction conditions. Some by-product formation was also detected, affecting the quality of the selectivity, though it only supposed 2% wt. The catalyst was characterized by scanning electron microscopy (SEM), transmission electron microscopy (TEM), X-ray photoelectron spectroscopy (XPS) and inductively coupled plasma optical emission spectrometry (ICP-OES). Regarding the kinetic modeling, Langmuir Hinshelwood assumptions were proposed for the reaction and, to determine the numerical values of the kinetic parameters, a nonlinear regression was used.

CONCLUSIONS: The kinetic models developed in this thesis was able to predict the sugar hydrogenation process at different temperatures and hydrogen pressures, taking into account the reaction byproducts. Thus, all the kinetic parameters were determined.

Abstract

BAKGRUND: En betydande del av världens energibärare och material härstammar från fossila bränsleraffinaderier. Enligt förväntningarna kommer utnyttjandet av fossila bränslen att minska inom en kort framtid på grund av ständig prisökning, osäker tillgänglighet och miljöproblem. Därför ska alternativa lösningar som kan mildra klimatförändringen och minska användningen av fossila bränslen befrämjas. Användningen av biomassa som råvara för bränsle och kemisk produktion istället för olja är en spännande möjlighet som driver utvecklingen av moderna bioraffinaderier. I detta perspektiv är användningen av lignocellulosabaserad biomassa som råmaterial för kemisk industri ett livskraftigt tillvägagångssätt som har fått mycket uppmärksamhet under de senaste åren, t.ex. tillverkning av sockeralkoholer. Dessa polyoler som framställs genom katalytisk hydrering av sockermolekyler är flexibla föreningar med ett brett spektrum av tillämpningar, t.ex. sötningsmedel med låg kalorihalt, medicinska hjälpämnen och antikariesmedel. Syftet med denna avhandling var att förbättra en ny skumkatalysator med öppna celler, där rutenium på aktivt kol är den katalytiskt verksamma komponenten. Denna heterogena katalysator användes i kinetiska experiment för selektiv hydrering av D-xylos till sockeralkoholen D-xylitol. En omfattande serie avkinetiska experiment genomfördes i en reaktorautoklav vid olika temperaturer (60-90^{o}C), vätetryck (20-40 bar) och begynnelsekoncentrationer av D-Xylos (0,065, 0,13, 0,26 M) för att undersöka dessa parametrars inverkan på reaktionshastigheten. Den fasta skumkatalysatorn med öppna celler som användes i detta arbete omfattade följande beredningssteg: skärning av aluminiumskumbitar med öppna celler, anodisk oxidation av skummet, kolbeläggning med syraförbehandling, ruteniumimpregnering och ex-situ-reducering.

RESULTAT: Fullständing (100%) omsättning av D-xylos uppnåddes i flesta experiment beroende på reaktionsbetingelserna. Bildning av biprodukter upptäcktes också, vilket påverkade selektiviteten, även om biprodukterna utgjorde endast 2 viktprocent. Katalysatorn karakteriserades genom svepelektronmikroskopi (SEM), transmissions-elektronmikroskopi (TEM), röntgenfotoelektronspektroskopi (XPS) och induktivt kopplad plasmaoptisk emissionsspektrometri (ICP-OES). I kinetisk modellering tillämpades Langmuirs och Hinshelwoods antaganden för reaktionsmekanismen och för bestämning av numeriska värden på de kinetiska parametrarna användes olinjär regression.

SLUTSATSER: De kinetiska modellerna som utvecklades i denna avhandling kunde förutsäga sockrets hydreringsprocess vid olika temperaturer och vätetryck, med hänsyn till de upptäckta reaktionsbiprodukterna. Sålunda bestämdes alla kinetiska parametrar med god noggrannhet.

Abstract

ANTECEDENTES: Una parte importante de los portadores de energía y de los productos materiales del mundo se derivan de las refinerías de combustibles fósiles. Se espera que la viabilidad de la explotación de los combustibles fósiles disminuya en un futuro próximo debido a los continuos aumentos de precio, la disponibilidad incierta y las preocupaciones medioambientales. Por ello, deben promoverse soluciones alternativas capaces de mitigar el cambio climático y reducir el uso de combustibles fósiles. El uso de la biomasa como materia prima para la producción de combustibles y productos químicos en lugar del petróleo es una posibilidad intrigante que está impulsando el desarrollo de complejos de biorrefinería. En esta perspectiva, el uso de la biomasa lignocelulósica como materia prima para la industria química es un enfoque viable que ha recibido mucha atención en los últimos años, como la fabricación de polialcoholes. Así, estos polioles generados a partir de la hidrogenación de moléculas de azúcar, son compuestos flexibles con una amplia gama de aplicaciones, incluyendo edulcorantes bajos en calorías, excipientes medicinales, agentes anticaries, etc. El objetivo de esta tesis fue mejorar un novedoso catalizador de espuma de célula abierta basado en rutenio soportado sobre carbono. Así, se utilizó un catalizador heterogéneo para realizar experimentos cinéticos para la hidrogenación selectiva de la D-Xilosa en su alcohol de azúcar D-Xilitol. Para ello, se llevó a cabo una amplia gama de experimentos diferentes a distintas temperaturas (60-90^{o}C), presiones (20-40 bar) y concentraciones iniciales de D-Xilosa (0,065, 0,13, 0,26 M), para investigar el papel de cada una de ellas en la velocidad de reacción. El catalizador sólido de espuma de célula abierta utilizado en esta tesis comprendía los siguientes pasos de preparación: corte de la pieza de espuma de aluminio de célula abierta, seguido de un pretratamiento de oxidación anódica, a continuación un recubrimiento de carbono con un pretratamiento ácido posterior, para terminar con un paso de impregnación de rutenio y una reducción Ex-Situ.

RESULTADOS: Se lograron conversiones de D-Xilosa de hasta el 100 %, dependiendo de las condiciones de reacción. También se detectó cierta formación de subproductos, que afectó a la calidad de la selectividad, aunque sólo supuso un 2% en peso. El catalizador se caracterizó mediante microscopía electrónica de barrido (SEM), microscopía electrónica de transmisión (TEM), espectroscopia de fotoelectrones de rayos X (XPS) y espectrometría de emisión óptica con plasma acoplado inductivamente (ICP-OES). En cuanto a la modelización cinética, se propusieron las hipótesis de Langmuir Hinshelwood para la reacción y, para determinar los valores numéricos de los parámetros cinéticos, se utilizó una regresión no lineal.

CONCLUSIONES: Los modelos cinéticos desarrollados en esta tesis fueron capaces de predecir el proceso de hidrogenación del azúcar a diferentes temperaturas y presiones de hidrógeno,

teniendo en cuenta los subproductos de la reacción. Determinandose así todos los parámetros cinéticos.

Acknowledgements

First and foremost, I would like to express my deep and sincere gratitude to my research supervisors, professor Juan García Serna from Universidad de Valladolid, and professor Tapio Salmi from Åbo Akademi University, for allowing me to live this experience abroad. Your patience, motivation, enthusiasm and immense knowledge have helped me a lot throughout this incredible adventure. I would also like to thank each and every person at the TKR laboratory. I have never seen a lab like this before, consisting of amazing scientists as well as kind individuals who are always willing to help. It has the vibe of a family. I will never forget all the saunas, BBQs, our performances in Toimmisto, Dynamo...

I would want to offer my heartfelt appreciation to German. This thesis would not have been feasible without your assistance. You are an outstanding scientist who always had a solution to the issues we encountered. Thank you so much for everything, for welcoming me in my initial days, for sharing your expertise, for your corrections and for your endless patience. You are a wonderful person, and I am grateful for everything you have done for me. This thesis is partly thanks to you. Thank you very much.

Thank you so much from the bottom of my heart to all the friends I made throughout my time in Finland. Karo, Henry, Anka, Maria, Clara, Elyn, Alejandro, Zuzana, Clemenz, Mio, Lucia, Sharon... My panita Ben, who was always there and always made me laugh, a real friend, and claudià, the most incredible person I have ever met and one of the most important in my life. Thank you for being my family in Finland and supporting me in both good and terrible times. I consider myself really fortunate to have met you.

This experience would not be completed without my lab partner Alvaro. You are responsible for many of my fondest memories. I will never forget our "Muro Español", our breathtaking performances in Toimmisto, our performances in Assarin, our "Vamos al gym que hoy toca berzas", cross-country skiing, the sauna of the lake, your frights, our trips, staying until late in the lab... You have been like my big brother in Finland, and I cannot wait to meet you again back in Spain.

Finally, one of the best persons I am taking with me from this adventure is Iraide. Thank you so much for these astonishing 6 months, filled with incredible adventures and better moments. From hugging each other under a festival of northern lights, to hike the fjords, going through an unforgettable trip to Venice, or a lovely sunset in the Baltic Sea. This experience has been incredible, and it is largely thanks to you. Finland is named after you crack. Ya sabes que eres la perdición de mi máster y el objeto de todas mis luj...

I am also extremely grateful to my family for its love, prayers, caring and sacrifices for educating and preparing me for my future. This thesis is yours.

Abbreviations

A'_1	Lumped pre-exponential factor reaction 1.
A'_2	Lumped pre-exponential factor reaction 2.
A'_3	Lumped pre-exponential factor reaction 3.
A'_s	Lumped pre-exponential factor.
a	Slope in HPLC calibration curves.
A_{HPLC}	Area in HPLC graphs.
Ara	Concentration of D-Arabitinol.
$C_{Calc,i}$	Estimated concentration of the component i.
C_{Ery}	Concentration of Erythritol.
$C_{Exp,i}$	Experimental concentration of the componenti.
C_i	Concentration of the component i.
C_{Mean}	Mean concentration.
CAGR	Compound annual growth rate.
Ea'_1	Lumped activation energy factor reaction 1.
Ea'_2	Lumped activation energy factor reaction 2.
Ea'_3	Lumped activation energy factor reaction 3.
Ea'_s	Lumped activation energy factor.
EDX	Energy dispersive X-ray analysis.
EPS	Earnings per share.
Ery	Concentration of Erythritol.
FA	Furfuryl alcohol.
H_2	Pressure of hydrogen.
ICP-OES	Inductively coupled plasma atomic emission spectroscopy.
IWI	Incipient wetness impregnation.
K_1	Kinetic constant reaction 1.
K_2	Kinetic constant reaction 2.
K_3	Kinetic constant reaction 3.
K_{Ara}	Adsorption constant D-Arabitinol.
K_{Ery}	Adsorption constant Erythritol.
K_{H_2}	Adsorption constant Hydrogen.
K'_i	Arrhenius K.
K_S	Adsorption constant D-Xylose.
K_{SOH}	Adsorption constant D-Xylitol.
mcat	Mass of catalyst.
PFA	Poly(furfuryl alcohol).

Q	Objective function.
R_2	Coefficient of determination.
r_1	Reaction rate reaction 1.
r_2	Reaction rate reaction 2.
r_3	Reaction rate reaction 3.
S	Concentration of D-Xylose.
SEM	Scanning electron microscope.
SOH	Concentration of D-Xylitol.
SRS	Sum of residual squares.
T	Temperature.
TEM	Transmission electron microscopy.
TPR	Temperature-programed reduction.
V_L	Reaction volume.
XPS	X-ray photoelectron spectroscopy.

ρ_B	Bulk density.
θ	Catalyst free site.
θ_{Ara}	Adsorbed D-Arabitinol molecule.
θ_{Ery}	Adsorbed Erythritol molecule.
θ_{H_2}	Adsorbed Hydrogen molecule.
θ_S	Adsorbed D-Xylose molecule.
θ_{SOH}	Adsorbed D-Xylitol molecule.

To my family and friends.

Contents

List of Figures

List of Tables

Chapter 1

Introduction

1.1 Fossil Fuels Situation

The sustainable development goals (SDGs) established in 2015 by the United Nations General Assembly aim to achieve a better and more sustainable future for all the people and the world in the framework of the 2030 Agenda. Nevertheless, the growing population, with a projected value of 10 billion by 2057 [18] and the environment deterioration is imposing serious drags to the completion of goals such as "zero hunger" and "climate action". Pollution, climate change, global warming, waste disposal, and natural resource depletion, in particular, have escalated at an alarming rate, and these problems are mostly the result of uncontrolled harmful human activities on our Mother Earth [19]. Fossil fuels, mainly composed of coal, oil and gas, have played and keep playing a dominant role in the world when it comes to energy sources. As a matter of fact, their use is increasing as the years go by.

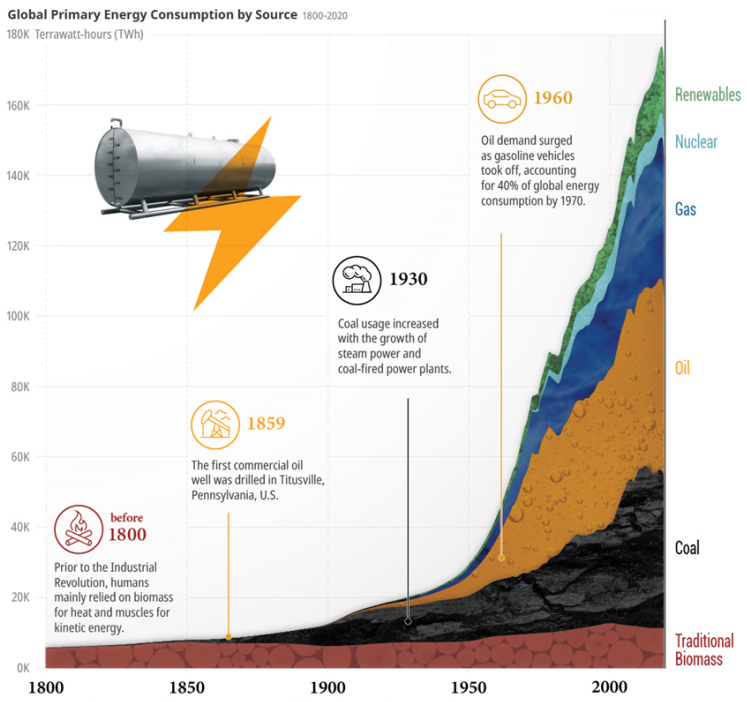

Figure 1.1: *BP Statistical review of world energy [1, 2].*

Throughout the history, fossil fuels have been used without control, emitting carbon dioxide to the atmosphere with no limit, lifting the atmospheric CO_2 concentration up to 400 ppm, the highest level since 803,719 BCE and increasing [20].

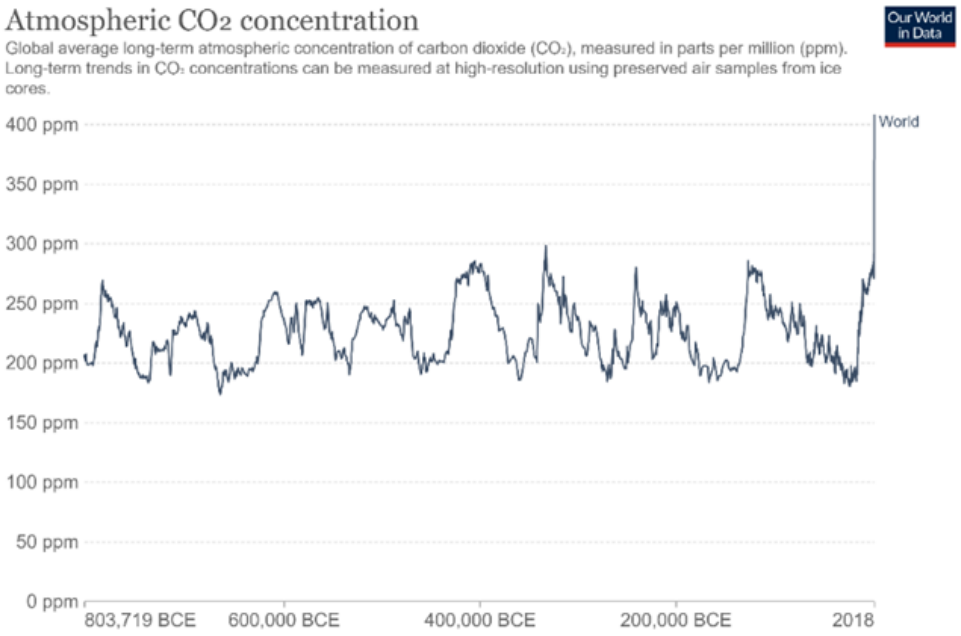

Figure 1.2: *Historical CO_2 global atmospheric concentration [3].*

In fact, global temperatures have risen sharply to approximately 0.7°C higher than the 1961-1990 and, when looking back to 1850, the temperatures were 0.4°C colder. All of which has resulted in an overall temperature change worth 1.1°C in less than 200 years [20].

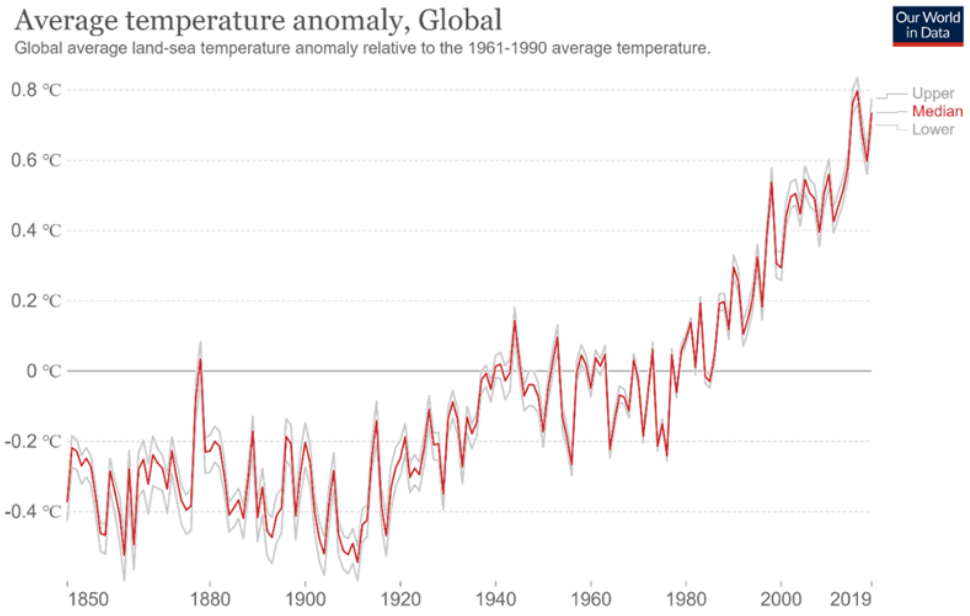

Figure 1.3: *Global average temperature anomaly [4].*

Furthermore, according to 2017 U.S. Climate Science Special Report [21], if annual emissions continue to rise at their current rate, as they have since 2000, models predict that by the end of the century, global temperatures would be at least 5 degrees Fahrenheit higher than the 1901-1960 average, around 80 years' time worst-case scenario.

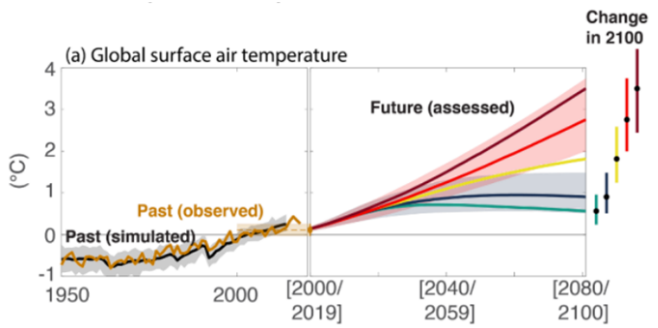

Figure 1.4: *Global surface air temperature prediction [4].*

Not only that but, in addition, by using the longest time estimate, it would take less than 270 years to completely deplete all petroleum on Earth, making it necessary to explore other alternatives to oil, since the time required to replenish reserves naturally is about 280 million years [22].

As a result, these global challenges require an urgent solution in which the circular bioeconomy may play a vital role, and a low carbon economy will undoubtedly assist to overcome these difficulties, particularly on climate change by limiting global warming to 1.5 degrees Celsius in the future [23–25] .

1.2 Biorefinery Concept

A biorefinery is a facility that combines biomass conversion techniques and equipment to create fuels, electricity, chemicals, and value-added products from biomass. According to the US Department of Energy, a biorefinery is a processing plant where biomass feedstocks are transformed and processed into a variety of useful products [5]. A scheme of what a biorefiney looks like is shown as follows:

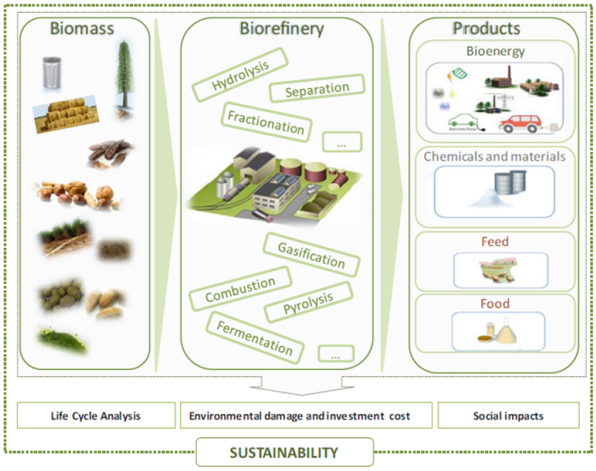

Figure 1.5: *Scheme of biorefinery concept [5].*

In a broad sense, biomass is defined as the whole organic matter produced by biological processes [5]. The choice of biomass feedstock must be considered, taking into account factors like availability, potential use, characteristics ... since the final product will depend on that [26]. Hence, there are a wide range of different sources of biomass on earth, such as:

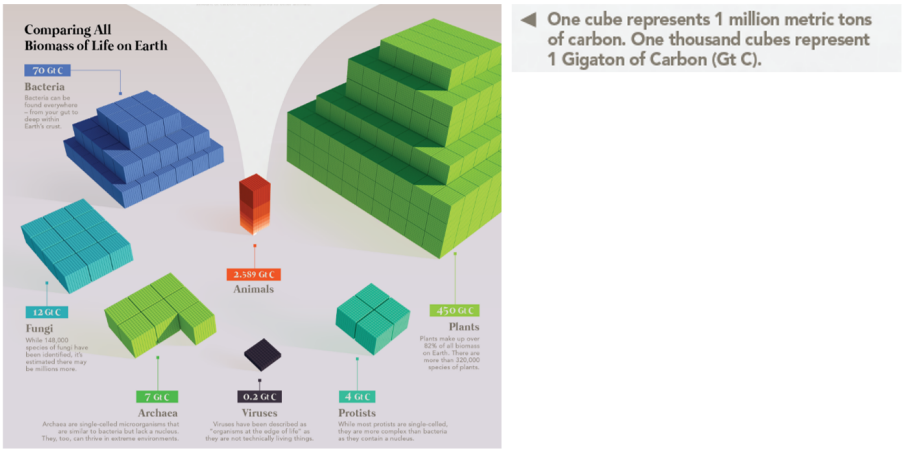

Figure 1.6: *The biomass distribution on Earth [6, 7].*

The use of diverse biomass feedstock has resulted in the specialized development of processes for each raw material, which, combined with the interest in the production of several specific compounds, has leaded to a significant separation between processing models, resulting in the creation of different types of biorefinery generations; the first and the second one [27].

1.2.1 Second Biorefinery generation

The term "second-generation biorefinery" refers to the use of lignocellulosic biomass as raw materials; this feedstock is primarily composed of cellulose, hemicellulose, and lignin, and this biomass represents a significant opportunity due to the wide range of products that can be formed from this biomass, such as biochemicals, biomaterials, and biofuels [28–30].

Because cellulose is made up of glucose monomers, it is feasible to split and ferment the cellulose glucan to produce liquid biofuels such as bioethanol by enzymatic hydrolysis and fermentation. Lignin is a biopolymer that may be utilized to synthesize aromatic chemicals, syngas products, heavy metal sequestrants, and antibacterial agents, among other things. Finally, hemicellulose is regarded as a valuable source for the manufacture of compounds with high added value, such as XOs, which have potential use in the culinary and medicinal industries [31–34].

There are several co-products that may be derived from lignocellulosic materials via various processing branches. They are formic acid, ethylene glycol, acetic acid, lactic acid, sorbitol, glycerol, glycolic acid, and, of course, bioethanol in the case of cellulose. For Lignin, quinones, phenol benzene, syringaldehyde, pyruvate, and other lipids. XOs, xylose, furfural, hydroxymethylfurfural (HMF), levulinic acid, and pentane may all be obtained from hemicelluloses like xylan [35, 36]. This large range of products is determined by the kind of processing, the primary purpose of the biorefinery, and societal necessity [37].

This thesis starts from this point, since the main goal is to take one sugar product, D-Xylose in this case, and take it one step ahead by turning it into its main sugar alcohol D-Xylitol.

The conversion pathway from lignocellulosic biomass to sugar alcohols is illustrated in Figure 1.7:

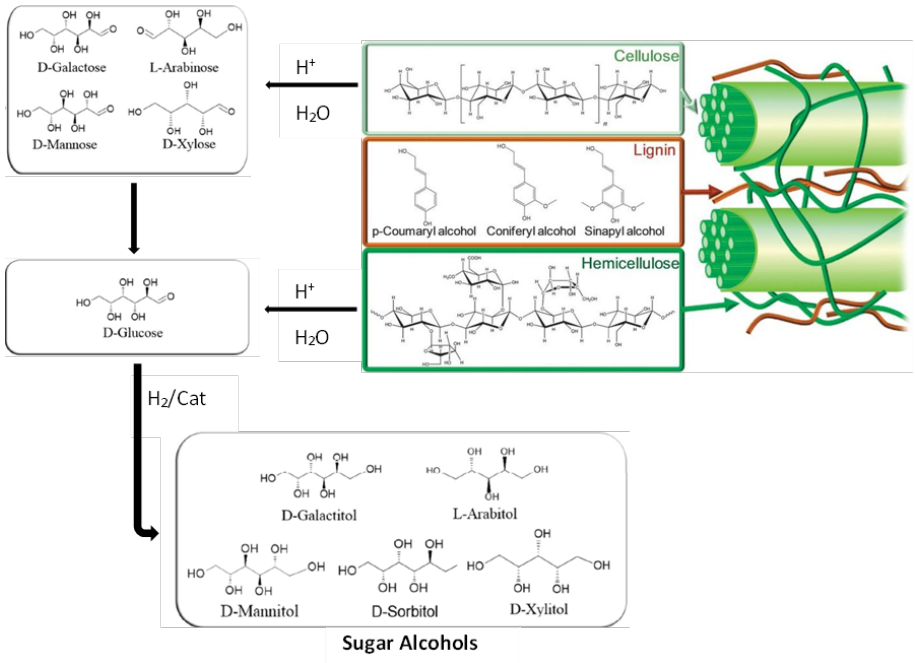

Figure 1.7: *Sugar alcohols from lignocellulosic biomass [8].*

1.3 Sugar Alcohols

Sugar alcohols are polyhydric alcohols (or polyols) formed when the carbonylgroup of the monosaccharideis is reduced to a hydroxyl group. [38]. They are white, water-soluble solids that can occur naturally or be produced industrially by hydrogenation of sugars [39]. The typical formula for sugar alcohols is $HOCH_2(CHOH)_nCH_2OH$. Their relative orientation (stereochemistry) of these –OH groups further distinguish them, and they do not exist as rings, as opposed to sugars. They may, however, be dehydrated to produce cyclic ethers too.

The prioritization of mental and emotional wellbeing by health-conscious consumers along with the rising in prevalence of various health-related issues, such as diabetes, obesity, and heart diseases are increasing the demand for sugar alcohols and boosting the market growth [40]. Thus, the global sugar alcohol market was valued at $ 3,360 million in 2019, and is projected to reach $ 4,800.4 million by 2027, registering a CAGR of 5.9% from 2021 to 2027 [9].

Figure 1.8: *Forecast of the sugar alcohol market by type [9].*

Sorbitol is the most relevant one, such was the case that in 2019 accounted for the highest sugar alcohol market share. With about 35-60% of the sweetness of sucrose, it is used as a sweetener and flavouring agent. It is also hygroscopic and therefore is used as a humectant [38].

Mannitol, on the other hand, is widely distributed in nature and occurs in the exudates of many plants. It has about half the sweetness of sucrose. Clinically, mannitol is administered intravenously as an osmotic diuretic in patients with acute renal failure. It is not metabolized appreciably and is not reabsorbed by the tubules; hence, it is excreted in urine [38].

Xylitol, the second most industrially relevant sugar alcohol and the model molecule of this work, is widely distributed in the plant kingdom. It has about twice the sweetness of sucrose. A potential benefit of xylitol would be the prevention of dental caries. However, it has many other beneficial properties for health [38].

1.3.1 Xylitol

Xylitol is classified as a sugar alcohol or polyalcohol (alditol). It is an achiral isomer of pentane-1,2,3,4,5-pentol with the formula $CH_2OH(CHOH)_3CH_2OH$. It is present in low amounts in the fibers of many fruits and vegetables and can be extracted from berries, oats, and mushrooms, as well as fibrous material such as maize husks and sugar cane bagasse. Industrial manufacture, on the other hand, begins with xylan (a hemicellulose) derived from hardwoods or corncobs, which is hydrolyzed into xylose and catalytically hydrogenated into xylitol [41].

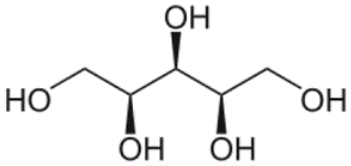

Figure 1.9: *D-Xylitol molecule.*

Table 1.1: *D-Xylitol properties [17].*

Properties	Characteristics/values
Empirical formula	$C_5H_{12}O_5$
Chemical name	1,2,3,4,5 Pentahydroxy pentane
Synonyms	Hydrogenated xylose; Xylite
Molecular weight	152.15 g/mol
Saccharide class/sub-class	Monosaccharide/hydrogenated monosaccharides
Generic form	Pentitol
Appearance	Crystalline powder
Color	White
Taste	Sweet
Odor	Odorless
Melting point	92–96 °C
Boiling point	216 °C (1 atm)
pH (in aqueous solution 10 %)	5–7
Density	1.03 g/ml (aqueous solution 10 %) 1.23 g/ml (aqueous solution 60 %)
Solubility in water at 20 °C	64.2 g/100 g solution
Solubility in methanol	6.0 g/100 g solution methanol 96 %
Solubility in ethanol	1.2 g/100 g solution ethanol 96 %
Viscosity at 20 °C	1.23 cP (aqueous solution 10 %) 20.63 cP (aqueous solution 60 %)
Hygroscopicity (in high humidity)	More than sucrose and less than sorbitol
Solution heat (endothermic)	34.8 cal/g
Relative sweetness	Similar to sucrose, greater than sorbitol or mannitol
Caloric value	2.4 cal/g
Stability	Stable at 120 °C (does not caramelizes)
Refractive index at 25 °C	1.35 (aqueous solution 10 %)
Specific rotation	Optically inactive
Heat of combustion	16.96 kJ/g

1.3.1.1 Xylitol benefits

Because of its similar sweetening capacity to sucrose, xylitol has mostly been utilized as a sugar replacement in meals. However, as compared to regular sugar, it offers significant advantages. One of them is its excellent chemical and microbiological stability, which enables it to be used as a preservative in food goods, therefore increasing their shelf life [42].

Xylitol also has several benefits, when comparing to other sweeteners. Because it has a sweetening strength similar to sucrose, it can be used alone to replace this sugar, whereas other polyols such as sorbitol, arabitol, and mannitol have a lesser sweetening power and must be combined with other sweeteners to get the required sweet taste [43].

It is also a moisturizer, stabilizer, cryoprotectant, and freezing point reducer. When used in ice creams, for example, xylitol may act as a bulking agent, sweetener, and crystallization inhibitor [44]. Moreover, it is also an effective humectant when used in cakes and muffins, since it binds the moisture within the product, improving the texture and shelf-life of baked products [45].

Diabetes

One of the key advantages of xylitol over sucrose is that diabetics can ingest it. Controlling the rate of glucose in the blood is critical in people with this metabolic condition, which is characterized by a deficit in carbohydrate metabolism. Unlike traditional sugars, xylitol does not require insulin to be digested by the body. As a result, people with type I or type II diabetes tolerate it well [46–48]. Therefore, xylitol is regarded as a sweetener suitable for diabetics [49].

Hemolytic Anaemia

G6PDH (glucose 6-phosphate dehydrogenase) is a critical enzyme for cell survival, since it is responsible for maintaining enough NADPH (a reduced coenzyme important in oxidative biological processes). In humans, a lack of the enzymes G6PDH causes a disease known as hemolytic anaemia. Because cells are unable to replenish NADPH, this shortage promotes erythrocyte decrease [50].This pathology is the most common human enzymopathy and affects about 400 million people worldwide [51].

People with G6PDH impairment can utilize xylitol as a medicinal treatment because this enzyme is not necessary for its metabolism. By oxidizing L-xylulose, xylitol provides NADPH to the cell and aids in the maintenance of red blood cell membrane integrity [49, 52].

Oral Health

In brief, xylitol helps the oral health in four different ways:

1. It minimizes the occurrence of caries and stabilizes those that have developed. Over the course of two years, a research found that replacing sucrose with xylitol reduced the incidence of dental cavities by 85 percent [53].

2. It promotes saliva production and stabilizes calcium and phosphate ions in saliva [39, 54].

3. It inhibits the development of Lactobacillus and Streptococcus mutans in the saliva. Different studies have found that individuals who consumed xylitol had a substantial reduction in the weight of the total plaque as well as the number of S. mutans present in the plaque and saliva [53].

4. The pH decrease from the tooth surface is prevented by oral cleaning with xylitol solution. The amounts of certain enzymes are also elevated, improving the saliva's buffering capacity and bacteriostatic action. The oral environment is hence less conducive to the growth of microorganisms [55].

Acute otitis media

Acute otitis media, the second most frequent illness in children, is caused by nasopharynx bacteria that enter the middle ear through the Eustachian tube [56], Because it suppresses the growth of the bacteria Streptococcus pneumoniae, the major cause of sinusitis and middle ear infections, Xylitol has shown to be effective in avoiding or fighting this condition [57].

A daily dose of 8.4 g of xylitol given in the form of two pieces of chewing gum (chewed for 5 min each) to children is effective to combat this disease, reducing by 40 % the incidence of this infection [58].

Osteoporosis

Osteoporosis is a disease characterized by a reduction in calcium deposition in bones, resulting in volume and biomechanical property loss. This condition predominantly affects the femur, which becomes brittle and readily fractures. Xylitol fights osteoporosis by increasing calcium absorption in the gut and boosting blood flow to the bone. The calcium content of bones is therefore increased, lowering the requirement for resorption [59].

Respiratory Infections

In brief, xylitol boosts the lungs' natural defense mechanism by delaying or avoiding the development of bacterial diseases such as pneumonia [60]. It also inhibits the growth of the bacteria S. pneumoniae and Haemophilus influenzae, which cause sinusitis and respiratory infections, and

reduces their attachment to epithelial cells, lowering the incidence of infection processes [61].

Colon diseases

Because xylitol is a low-digestible carbohydrate, it is only partially absorbed in the upper intestine. Approximately half of the eaten amount is absorbed in the lower intestine, where it is fermented by helpful commensal bacteria in the colon, such as Bifidobacterium and Lactobacillus species. Human colonic and faecal microflora have been observed to be influenced by xylitol use too [62].

1.3.1.2 Market overview

The global xylitol market has been valued to be USD$ 447.88 M in 2020 [63], and it is expected to keep growing up at a compound annual growth rate (CAGR) of 6.9%, reaching a value of USD$ 891.5 M by the end of 2027 [10]. Thus, the xylitol market size by year and by application would be divided as shown in Figure 1.10:

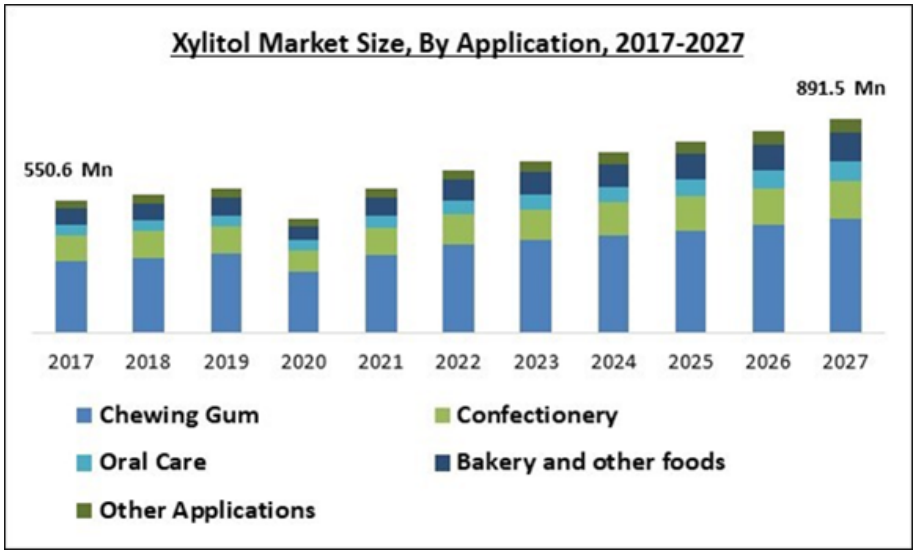

Figure 1.10: *Xylitol market size by application 2017-2027 [10].*

Being the oral care the major significant use of this sugar alcohol as of 2018. Regarding the region, the major key players in the next forecasted years will be North America along with Europe, as is shown below:

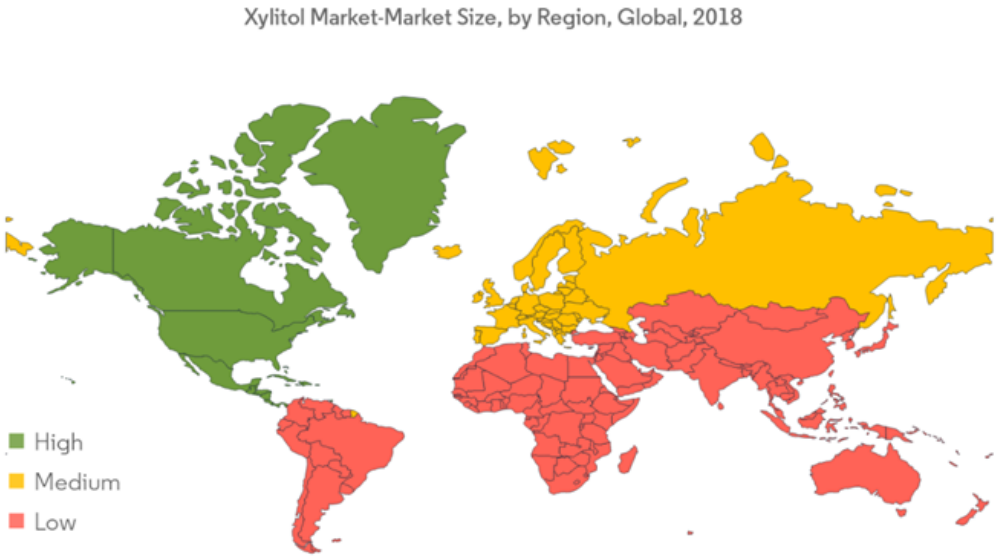

Figure 1.11: *Xylitol market size by region 2018 [11].*

As for the competitive landscape, xylitol market is still a fragmented market in development, in which there is a highly competitiveness without dominant players, what makes it an outstanding opportunity to get into it owing to the fact that xylitol is becoming more and more popular (CAGR of 6.9%).

As a matter of fact, xylitol has overcome all the rest of sugar alcohols by far when it comes to searching on google. Since 2008 it has become the one that gathers the highest number of consults on the network, being Finland the country that search for it the most.

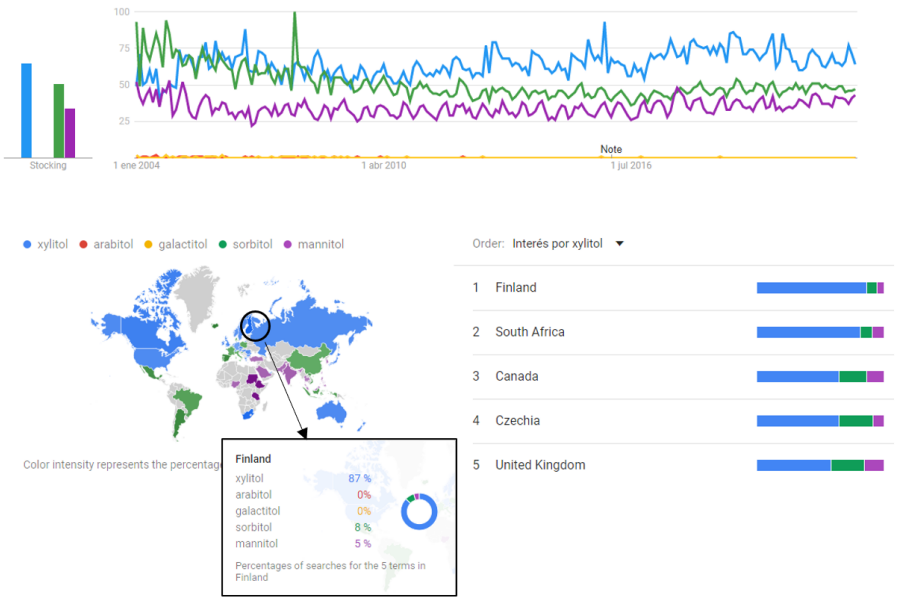

Figure 1.12: *Google trends - Xylitol,Arabitol,Galactitol,Sorbitol and Mannitol [12].*

This surge in popularity can also be reflected in the stock market through the most important

companies in the sector since they have been "bullish" these past years. Thus, reaching returns over 270%.

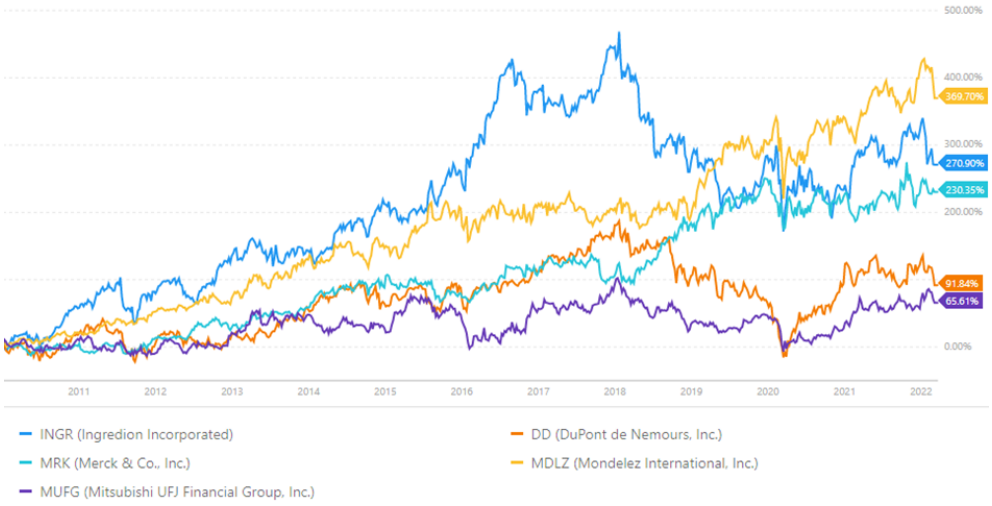

Figure 1.13: *Stock charts of the main sugar alcohol companies [13].*

Which has triggered an increase in the TEV (total enterprise value) of each of the companies in the last 15 years, as it can be seen in Figure 1.14:

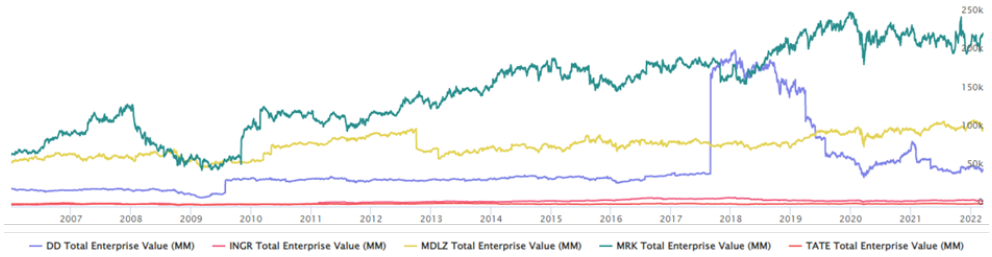

Figure 1.14: *Total enterprise value evolution of the main sugar alcohol companies [14].*

Furthermore, to truly measure the performance of these companies along the years, an EPS (earnings per share) study is also presented, where all the companies perform outstandingly, providing around $5 profit per share as average throughout the years.

Figure 1.15: *Earnings per share evolution of the main sugar alcohol companies [14].*

1.3.1.3 Xylitol in the supermarkets

The main xylitol based products available in supermarkets in Finland have to mainly do with chewing gums as well as toothpaste:

Figure 1.16: *Xylitol products in the supermarket.*

1.4 Catalytic Production of Sugar Alcohols

Carbohydrate hydrogenation is a significant process in the fine chemical (food) industry [64,65] that, historically, has been carried out over skeletal Ni catalyst [64–70].

One of the benefits of using Ni catalyst is its low price cost in compare to other more costly catalyst systems [66]. However, it has also some drawbacks that must be considered, since leaching has also been observed during reaction [64,65], which leads to the formation of harmful by-products as well as the catalyst deactivation.

In fact, as an immunotoxic and carcinogenic substance, Ni itself can induce several health problems, starting from contact dermatitis, cardiovascular illness and asthma for low exposures, until lung fibrosis and respiratory tract cancer in worse cases [71].

As a result, other heterogeneous catalysts, including supported metals such as cobalt, platinum, palladium, rhodium, and ruthenium, have been investigated, resulting the supported ruthenium the most promising ones [66–68]. As a matter of fact, recently DFT calculations has confirmed that Ru has the higher activity among conventional metals used for xylose hydrogenation: Ru > Rh Ni> Pd> Pt [72].

Ruthenium itself provides the best activity while not being that harmful as Ni. However, ruthenium itself can easily become toxic if ingested in large quantities [73]. Ruthenium (or ruthenium-based compounds) can act also as blocking agents, preventing hazardous metals from freely flowing in your body [74]. This isn't the only function it can play in boosting wellbeing; some study has looked into ruthenium complexes' potential utility in cancer treatment [75]. Moreover, Ruthenium complexes have a DNA-binding mechanism that appears to have caused good anti-tumor effects in various cases, even making some tumors resistant [76]. Despite its toxicity when consumed in excess, ruthenium can be advantageous to health.

On the other hand, Ru/C catalyst have demonstrated exceptional performance and stability when it comes to D-Xylose hydrogenation [77–79].

1.5 Reaction mechanism

Regarding the kinetic model of sugar hydrogenation, D-Xylose in this case, prior sources have proposed a reaction process in which the reactants (sugar and hydrogen) are adsorbed on the active sites of the catalyst. Following that, the adsorbed sugar molecules react with hydrogen on the catalyst's surface to generate the corresponding products, which are then desorbed. In general, it is assumed that the reaction between adsorbed sugar species and adsorbed hydrogen is the rate-determining step, whilst reactant adsorption and product desorption are quick enough [72,79–84].

When it comes to sugar hydrogenation, there is a debate whether the simultaneous adsorption of sugar molecules and hydrogen is competitive or non-competitive, owing to the huge different

molecule sizes of both species. As a matter of fact, both models have been implemented in recent literature, being the competitive one the most used when working with D-Xylose over ruthenium catalyst [78, 81].

Furthermore, T.Salmi et al. [84] also presented an alternative semi-competitive process. The notion is that bigger molecules (sugar molecules) are adsorbed at the principal sites of the catalyst surface, leaving some accessible interstitial sites for small species like hydrogen (in atomic or molecular form).

1.6 Solid Foam Catalyst

Structured catalysts are made comprised of a support that has been preshaped into a certain 3D form and a layer of catalytic material. [85] The form and material of the support are determined by the process applications, whilst the coating qualities dictate the reactivity of the structured catalyst in a specific reaction. Ceramic (Al2O3, cordierite, and SiC), metallic (single elements, i.e., Al, Ni, Cu, Co, or alloy, i.e., stainless steel, Inconel, FeCrAl, NiCrAl, FeNiCrAl), and carbonaceous materials (activated carbon, reticulated vitreous carbon) structures are used in a variety of 3D forms, such as honeycomb monolith, open-cell foam, gauze, wire-mesh, corrugated sheet and fiber [15].

Open-cell foams are 3D cellular materials composed of interconnecting solid struts that surround cavities (the cells) and communicate with one another via windows (the pores). They offer a disruptive and convoluted flow channel, resulting in extraordinary mixing as well as heat supply or release to/from the reactor walls, particularly in the case of metallic foams [15]. More than thirty companies throughout the world have commercialized this kind of material in the last two decades [86], and numerous types of materials with acceptable quality and cost levels are also available [87].

The selection of this kind of catalyst is owing to two main reasons [85]: the tolerance of operation conditions such as high temperatures or oxidative and corrosive chemicals, which needs the use of a stable alloy, or when the heat transfer is a crucial factor. In this case, aluminium, a highly thermal conductive material, might be used for temperatures ranging below 500^{o}C and reducing atmospheres. And the second one is due to the high effectiveness factors to achieved operating under continuous mode thanks to the thin catalyst layers [88, 89].

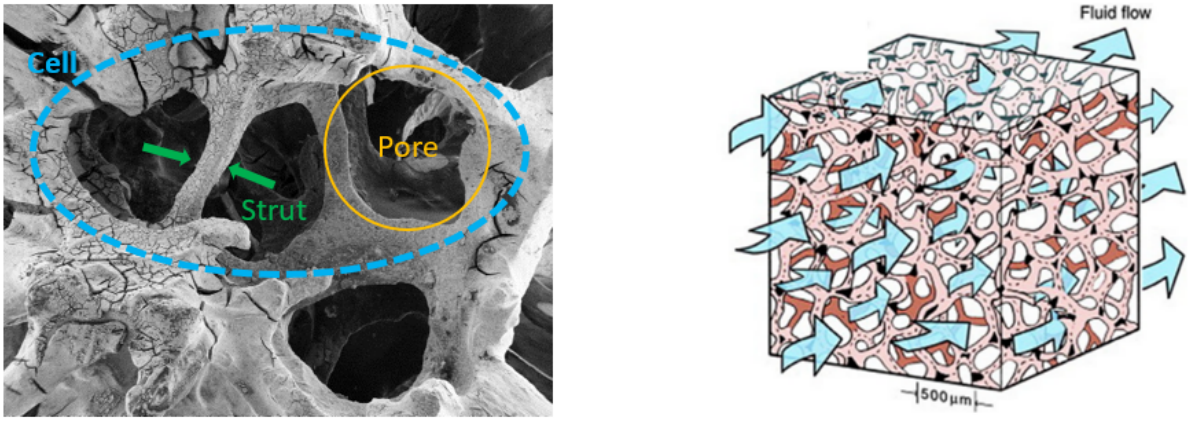

Figure 1.17: *SEM image of an open-cell foam and tortuous flow path of the fluid passing through [15].*

However, the absence of micropores in carbon and metal foams, on the other hand, results in a reduced surface area for catalyst deposition [90], which must be wash coated afterwards [91], thus creating a micro-mesoporous structure on which a highly catalytically active species, such as metal nanoparticles, can be deposited [92].

Previous research covers several methods for increasing the surface area of the foams by generating porous titania and alumina washcoats and zeolite layers when it comes to open-cell foams [93–95]. Moreover, a carbon porous layer on open-cell foams has also been explored as a support [96–99].

Vergus et al. [100], proposed poly(furfuryl alcohol) as a carbon precursor. This compound (furfuryl alcohol polymer) is well-known for its usage as a starting material in the fabrication of carbon molecular sieves, since it provides high carbon yields 50% [100], as well as coming from a renewable biomass [99]. Under acidic conditions, furfuryl alcohol (FA) can polymerize even at ambient conditions [101, 102].

The methodology used in this thesis to polymerize FA starts from the one proposed by F.Lali et al. [99] and replicated afterwards by A.Najarnezhadmashhadicet al. [103]. They both used furfuryl alcohol as the carbon yielding binder, oxalic acid as catalyst and, for this special work, PEG along with water have been used as a pore former, since bigger pore sizes were aimed.

1.7 Incipient wetness impregnation (IWI)

In order to generate ruthenium nanoparticles over the carbon layer achieved in previous section, two possible methods can be applied: homogenous deposition precipitation (HDP) and incipient-wetness impregnation. For this thesis, the last one has been performed. Incipient-wetness impregnation, (IWI), consisting of wetting the foam drop by drop, with the volume of solution containing the active metal precursor corresponding to its pore volume. Once it gets filled up, it is then dried in an oven [103]. By using this method, it is prevented the deposition on the external surface of the catalyst by the nanoparticles, as well as limiting waste [104].

1.8 Research strategy

The main goal of this master thesis was to implement as well as improve the preparation method of the novel open-cell solid foam Ru/C catalysts through the incorporation of polyethylene glycol as pore-former and study their catalytic activity for the hydrogenation case of D-Xylose in different condition of temperature, hydrogen pressure and initial concentration. Thus, the following tasks were carried out:

- Preparation of open-cell foam Ru/C catalyst through the polymerization of furfural alcohol (FA) in the presence of polyethylene glycol in the carbon-coating step.
- Perform of kinetic hydrogenation experiments with D-xylose to explore the product selectivity, reactant conversion, product yield, and influence of the pressure, temperature and initial concentration on the reaction rate and product distribution.
- Fitting the experimental data to a plausible kinetic model considering the pressure term.
- Application of catalyst characterization techniques that contribute to the clarification of the results.

Chapter 2

Catalyst Preparation

The catalyst preparation is based on six general steps: Firstly, cutting the open-cell aluminium foam pieces, followed by an anodic oxidation pretreatment, next a carbon coating with an acid pretreatment afterwards, to finish with a ruthenium impregnation step and an ex-Situ reduction:

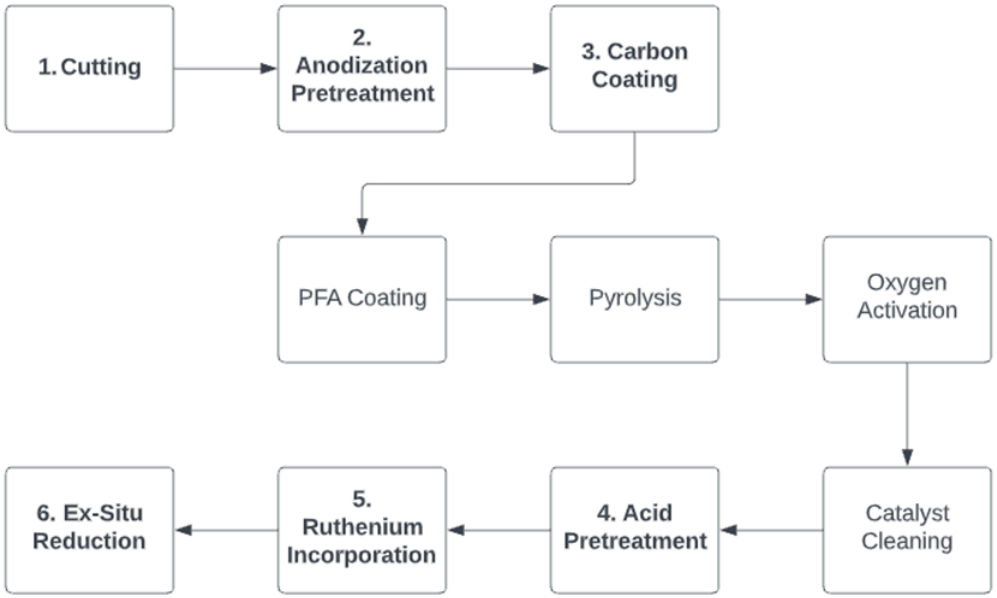

Figure 2.1: *Overview of the solid foam catalyst preparation process.*

A total of seven catalysts were prepared under different conditions, so most of the catalyst parameters could be investigated. Table 2.1 shows the general information of them.

Table 2.1: *Batch codes and general information of the prepared catalysts.*

Batch Code	Foam Code	Initial Mass (Al foam) [g]	Anodic Oxidation Pretreatment	PEG content in Coating [wt.%]	Cleaning	Ruthenium Incorporation Method
0*	B0-F1		Yes	-	No	IWI
1	B1-F1	0,6292	Yes	10%	No	IWI
	B1-F2	0,6341	Yes		No	IWI
	B1-F3	0,6308	Yes		No	IWI
2	B2-F1	0,6217	Yes	5%	No	IWI
	B2-F2	0,614	Yes		No	IWI
	B2-F3	0,591	Yes		No	IWI
3	B3-F1	0,641	Yes	15%	No	IWI
	B3-F2	0,5932	Yes		No	IWI
	B3-F3		Yes		No	IWI
4	B4-F1	0,6159	Yes	20%	No	IWI
	B4-F2	0,6296	Yes		No	IWI
	B4-F3		Yes		No	IWI
5	B5-F1	0,6708	Yes	5%	No	IWI
	B5-F2	0,6637	Yes		No	IWI
	B5-F3	0,6465	Yes		No	IWI
6	B6-F1	0,6387	Yes	5%	No	IWI
	B6-F2	0,6395	Yes		No	IWI
	B6-F3	0,6336	Yes		No	IWI
7	B7-F1	0,6462	Yes	5%	Yes	IWI
	B7-F2	0,6276	Yes		Yes	IWI
	B7-F3	0,6311	Yes		Yes	IWI

2.1 Cutting

The foams pieces were obtained from an aluminium foam sheet by cutting cylinders of 33 mm length and 11 mm diameter. The pore density of the samples was 40 PPI (Goodfellow Cambridge Ltd), and a diamond hole saw was used in the cutting process. Then, the foam pieces were sonicated for 15 min in acetone and then oven-dried for 2 hours at a temperature of 70°C, followed by an overnight at room temperature.

Figure 2.2: *Cutting of aluminium foam pieces.*

2.2 Anodic Oxidation

In order to improve the adhesion of the carbon on the foam, aall the samples went through an anodic oxidation pretreatment. Previous observations has shown that included this step generates a more homogenous and regular carbon layer [16]. Thus, an aluminium foam piece coming from the previous step was attached to a thin platinum flat strip using PTFE tape, to keep the contact stable during the process. Then, it was connected to the anode (working anode) of a power supply (Autolab PGSTAT100N), as an aluminum plate with an immersed area of 18 cm^2 was connected to its cathode (counter electrode), keeping 2.5 cm distance among them.

The anodization process was carried out in 100 mL of sulphuric acid at 1.6M (Sigma-Aldrich; 96%), along with 60 g/L of aluminium sulfate hexadecahydrate (Fluka; 98%), so the dissolution of aluminium could be controlled along the process [95, 105].

Regarding the electrical current, it was set to be 2A throughout 1h, and the voltage was monitored with the General-Purpose Electrochemical System (GPES) version 4.1 software. Moreover, the temperature was also set to be 40^{o}C using a thermostat (Grant GR150 GP200), by circulating oil through the jacked vessel of the anodic oxidation container. The electrolyte solution was constantly stirred during the process to homogenize the temperature and concentration.

The same process was repeated with all the foam pieces coming from the previous step. Once all of them were done, they were dried for 30 minutes at 70°C and, afterwards, they were calcinated for 4h at 600°C.

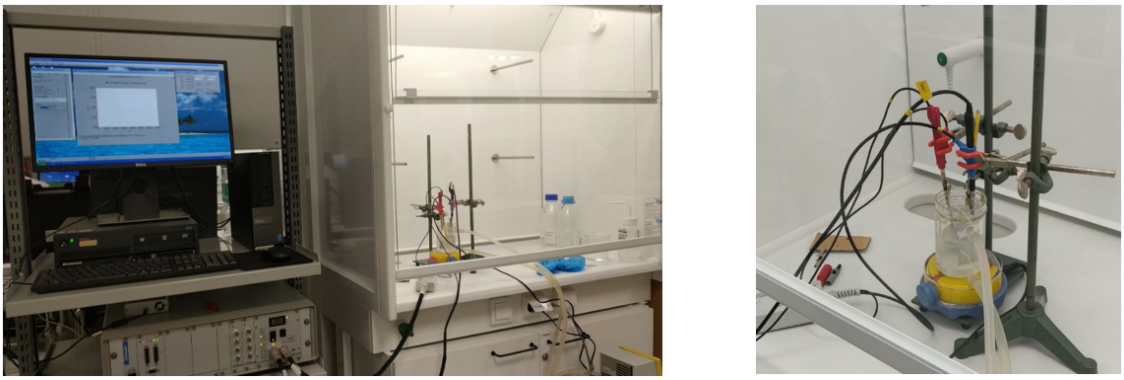

Figure 2.3: *Anodic oxidation setup.*

2.3 Carbon Coating

The carbon-coated foam batches were made up of two or three pieces that were connected to a crossed blade stirrer shaft with thin stainless-steel wires and placed in a 300 mL metallic jar with an electric band heater (Ogden Mighty-Tuff MT-03015-0424). Following that, the jar was filled with 136.2 g of furfuryl alcohol (Sigma Aldrich; 98 wt. percent), 0.42 g of oxalic acid dihydrate (Sigma Aldrich; 99.5 wt. percent), and 16.7 g of distilled water.

Using a temperature process controller (The CAL 9500P), the heating rate of the electrical band was changed at 2 Kmin-1 from ambient temperature (approximately 20°C) to 120°C. During the polymerization process, a Heidolph RZR 2021 mechanical stirrer was also used to rotate the foams. The stirring speed was set to 200 rpm.

Under the conditions described above, the mixture remained between 20 and 110 degrees Celsius for 55-60 minutes. When the temperature reached 110°C, the water began to evaporate. However, due to the reaction enthalpy the temperature increased dramatically along with the viscosity of the mixture; therefore, the automatic heating was turned off, and the temperature was manually adjusted to reach 120°C within 45-60 minutes, allowing the water to slowly evaporate and the crossliking of the poly(furfural alcohol) to take place.

An adequate amount of polyethylene glycol with a molar mass of 8kDa (Sigma Aldrich) was added around 50th minute of the curing stage (between 110 and 120°C) to obtain a mixture with a PEG content as specified in Table 2.1. To allow the proper incorporation of PEG, the rotation speed was increased to 400 rpm until total dissolution was achieved, then 0.42 g of oxalic acid was poured into the mixture to compensate for the dilution effect that PEG has on the reaction system [106].

Finally, the excess of the mixture over the foams was removed by rotating the foams at 1000 rpm for 5 min. The experimental setup is shown as follows:

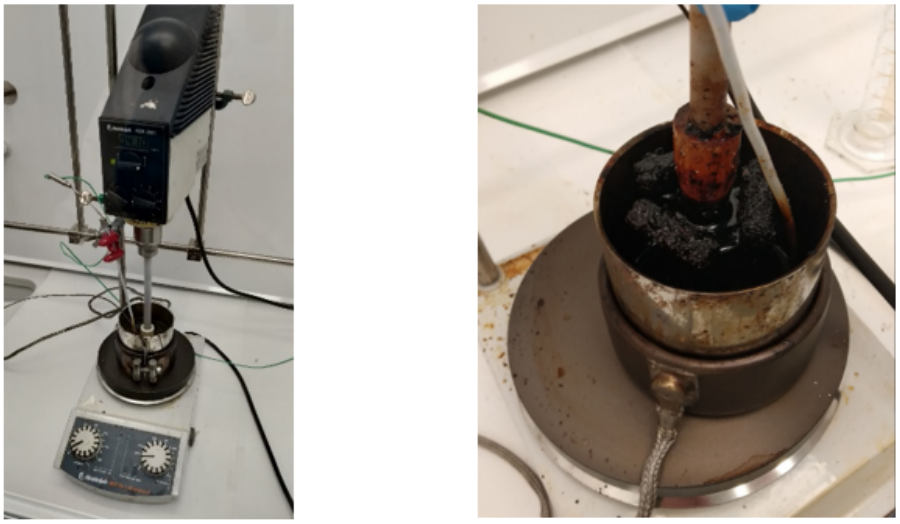

Figure 2.4: *Carbon coating setup.*

The PFA-coated foams were then pyrolyzed in a furnace (Carbolite CTF 12/100/900) heated up to 550°C at 5 $Kmin^{-1}$ and kept for 5 hours in a nitrogen stream of 1 Lh^{-1}. The resulting carbon on the surface of the foams was activated in a 2 Lh^{-1} oxygen stream and heated from room temperature up to 380°C at 5 $Kmin^{-1}$ up to 380°C and held at this temperature for 2 hours.

Once this process was done, the catalysts were cleaned using the so-called hydrothermal treatment with hot water with the aim of eliminating the potential impurities from the surface, such as polyethylene glycol remaining, or unreacted poly(furfuryl alcohol). Therefore, the foams were tied to the stirrer of a laboratory-scale batch reactor as the one described on section 2.7, and rotated at 600 rpm in deionized water at 210°C and a total pressure of 23 bar, using argon, the total duration of the cleaining process was of 4h [107].

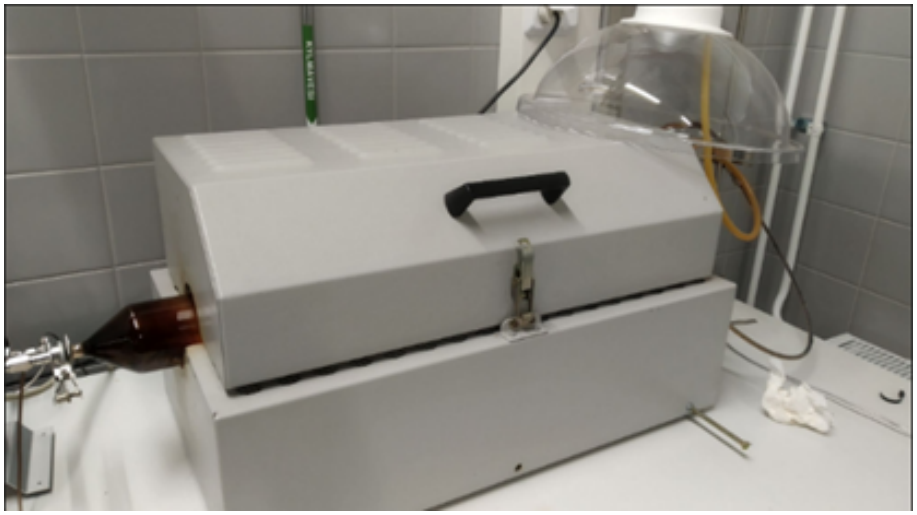

Figure 2.5: *Pyrolysing furnace.*

2.4 Acid Pretreatment

In order to enhance the incorporation of ruthenium on the carbon surface, an acid pretreatment step is necessary to create surface oxygen-containing spicies. Thus, the foams were poured into 300 ml of a dissolution of nitric acid (Sigma-Alrich;70 wt.%) at 5% for 2 hours. Thereafter, the foams were washed in deionized water and dried at 80°C for 3 hours and overnight at room temperature.

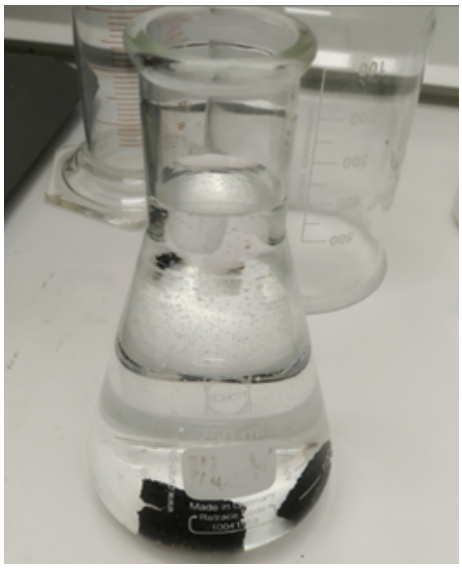

Figure 2.6: *Acid pretratment photo.*

2.5 Ruthenium Incorporation

When it comes to ruthenium incorporation, two different methods can be used, incipient wetness impregnation (IWI) and homogenous deposition precipitation (HDP). In this thesis, the first one IWI was the chosen one. Thus, a solution of Ru (III) nitrosyl nitrate (diluted in nitric acid; Sigma-Aldrich) was tested at 1.4 wt%.

Using an appropriate number of impregnation stages, the precursor solution was dripped to spread it as uniformly as possible on the surface of the carbon-coated foams, avoiding overflowing, until reaching the desired nominal ruthenium loading. After each impregnation step, the foams were dried at 110°C for 24 h in an oven.

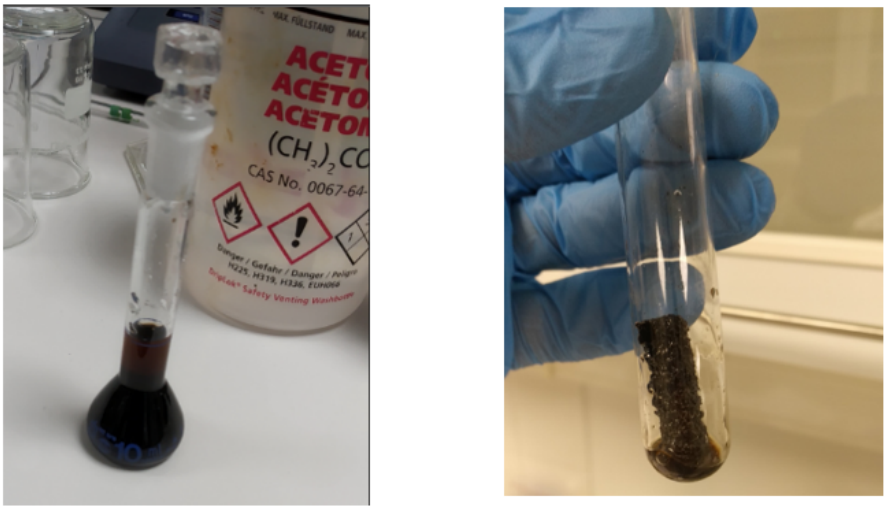

Figure 2.7: *IWI method photo.*

2.6 Ex-Situ Catalyst Reduction

The ex-situ reduction of the catalyst was carried out in a furnace (Carbolite CTF 12/100/900), by using 100 mL min^{-1} of hydrogen stream, with a ramp of 3°C min^{-1} until 300°C, and held for 5 hours. Prior reduction, the furnace was purged with argon for 10 minutes. This working temperature is based on TPR measurements held in this thesis, explained in chapter 3.1.5.

Figure 2.8: *Reduction oven setup.*

2.7 Kinetic Experiments and Setup

The experiments were conducted in a 0.3 L laboratory-scale semi-batch reactor (Parr 4561) fully equipped with baffles, a sampling line with a sintered filter (7 µm), a heating jacket, a temperature and stirring rate controller (Parr 4843), a cooling coil, a pressure display module (Parr 4843), and a bubbling chamber. During the trials, two foam catalyst pieces were attached at the terminus of the mechanical agitating shaft to serve as the stirrer.

In other to study the effect of temperature over the reaction rate, a set of experiments a different temperature (60, 80, 90, 100 and 120°C) were conducted at a constant hydrogen pressure of 40 bar. On the other hand, experiments at a fixed temperature of 90°C and variable hydrogen pressure (20, 30, 40, 50 and 60 bar) were performed.

Prior to every experiment, the reactor was flashed 5 times with Argon and then with hydrogen another 5 times in order to remove the air inside the reactor. Then, the foam catalyst was

in-situ reduced for 2 hours at 5 bar of hydrogen pressure and 120°C. After reducing the catalyst, 130 mL of sugar solution were pumped into the bubbling chamber and purged with hydrogen for 15 minutes. Thereafter, the hydrogen pressure and the temperature were adjusted, and the hydrogen-saturated solution was straightly injected into the reactor, thereby beginning the reaction under the desired conditions.

For all trials, a stirring rate of 600 rpm was used. The concentration of reactants and products was measured taking samples coming from the reactor at different reaction times.

A High-Performance Liquid Chromatograph (HITACHI Chromaster HPLC) equipped with a refractive index (RI) detector was used to analyze the concentrations of the chemicals coming from the reactor (HITACHI 5450 RI Detector). The mobile phase was 1.2 mM $CaSO_4$ solution (0.3 $mLmin^{-1}$ flow rate), the oven temperature was 50°C, and an injection volume of 10µL was employed on a Biorad HPX-87C carbohydrate column. The PID diagram is shown as follows:

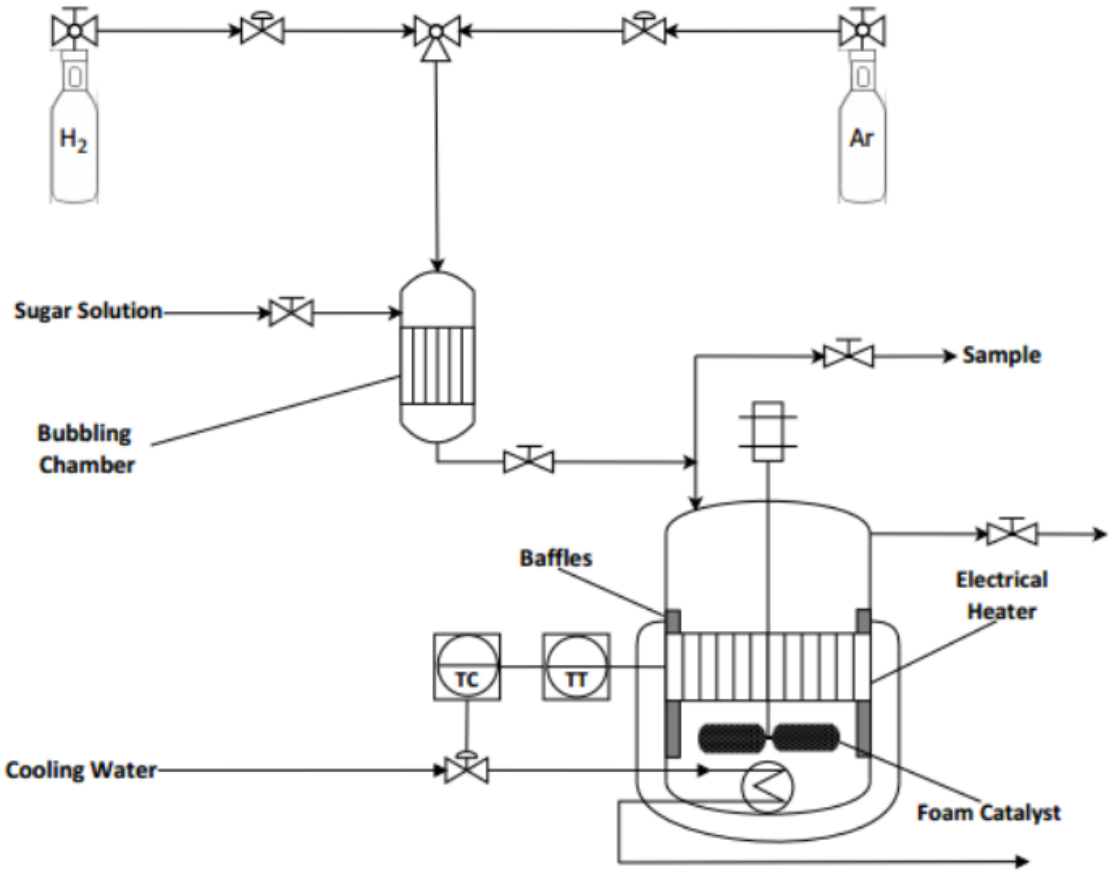

Figure 2.9: *Overview of the setup for sugar hydrogenation experiments [16] .*

Chapter 3

Results and Discussion

3.1 Catalyst Preparation Results

3.1.1 Anodic Oxidation

In order to increase carbon cohesiveness in the coating process, the aluminium foam samples were subjected to anodic oxidation pretreatment to induce surface roughness. Due to the noble characteristics of the platinum strip utilized, the foam piece was completely immersed and maintained good contact throughout the process. For all treated pieces, the measured voltage exhibited typical behaviour [108, 109]: the potential climbed at first until it reached a maximum, then fell to a steady value of roughly 3 V. Since the aluminium foams were getting oxidated, its initial silver colour got darker, which indicates a well-distributed oxide layer (Figure).

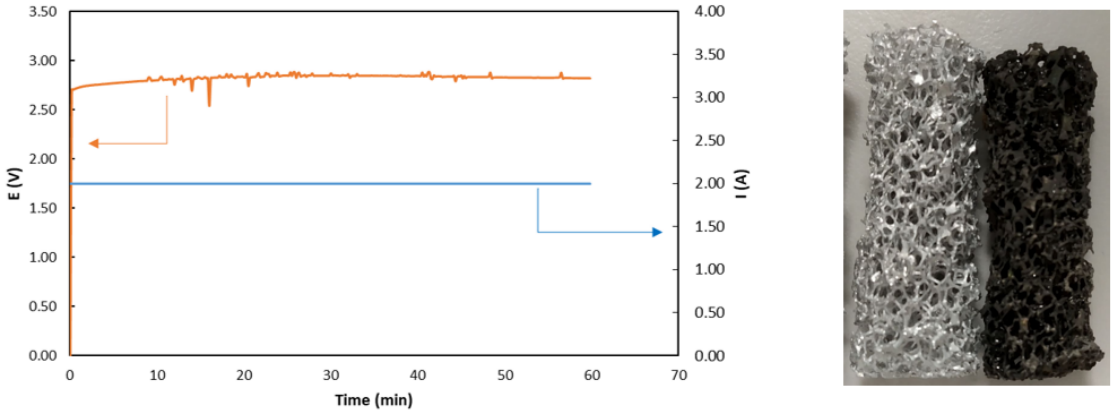

Figure 3.1: *Potential variation during anodic oxidation step and catalyst changes.*

According to Araujo-Barahona et al. [16], after analysing the micrographs of the foams before and after this process, it was demonstrated that calcination is a necessary step in order to obtain a more uniform pore pattern as well as eliminate surface sub-holes [110]. Thus, this impact was attributed to the diffusion of ambient oxygen and aluminium from the substrate through the existing aluminium oxide layer, which both combine to generate more alumina [111].

3.1.2 Carbon Coating

The carbon coating of the aluminium foams involves four steps; a controlled polymerization of furfuryl alcohol along with polyethylene glycol addition as pore-former, followed by a pyrolysis step, then carbon activation in an oxygen stream, surface cleaning by using hot water. Thus, a series of seven batches, three foams each, were performed as Table 3.1 shows:

Table 3.1: *Carbon-coating conditions of the prepared batches.*

Batch Number	Foam Code	Initial Mass [g]	Rotation speed [rpm]	PEG [wt.%]	Time [min]		PFA Loaded [wt.%]	Carbon After Pyrolisis [wt.%]	Carbon After Oxidation [wt.%]	Final Mass of Carbon [g]
					20 - 100 °C	110-120 °C				
0*	B0-F1			0						
1	B1-F1	0,6292	400	10%	55	70	43	18	7	0,043
	B1-F2	0,6341					44	19	11	0,0764
	B1-F3	0,6308					43	19	6	0,0349
2	B2-F1	0,6217	200	5%	55	63	64	44	41	0,3925
	B2-F2	0,614					64	43	38	0,3371
	B2-F3	0,591					66	50	49	0,5347
3	B3-F1	0,641	200	15%	55	79	49	24	25	0,1817
	B3-F2	0,5932					53	30	30	0,2597
	B3-F3						46	20	18	0,1398
4	B4-F1	0,6159	200	20%	53	62	78	53	x	x
	B4-F2	0,6296					77	52	x	x
	B4-F3						75	45	x	x
5	B5-F1	0,6708	200	5%	53	62	58	32	22	0,1662
	B5-F2	0,6637					52	26	31	0,2782
	B5-F3	0,6465					54	30	18	0,1223
6	B6-F1	0,6387	200	5%	56	82	76	56	54	0,7138
	B6-F2	0,6395					77	59	55	0,7429
	B6-F3	0,6336					78	58	59	0,8601
7	B7-F1	0,6462	200	5%	51	43	81	67	64	1,0558
	B7-F2	0,6276					81	69	68	1,2257
	B7-F3	0,6311					81	74	73	1,6102

Following the procedures described in the Chapter 2, the process could be split into two parts. A first part, in which the mixtures were heated up until 110°C under automatic temperature control, and a second one in which the mixture was taken up to 120°C by manual control. When reaching 110°C, a sudden water evaporation appeared, producing a peak in temperature. That was the moment when the manual control took over. The evolution of temperature along time is shown in Figure:

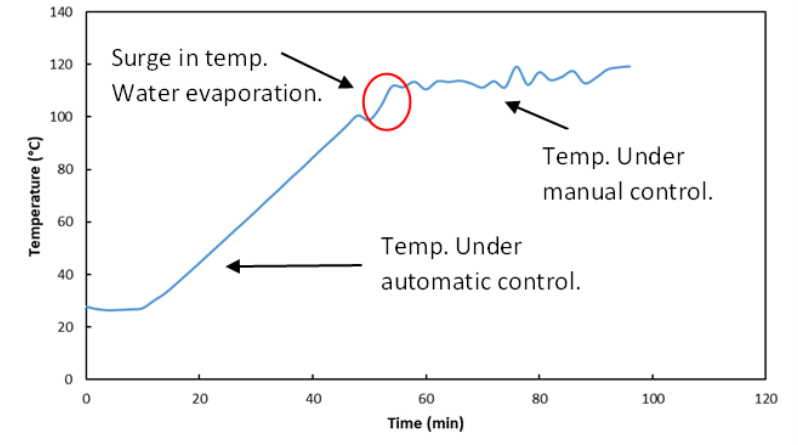

Figure 3.2: *Temperature pattern during PFA coating step.*

Even though that the exact reaction mechanism performed in this polymerization of furfuryl alcohol step is still uncertain [112, 113], it is widely accepted that, when working under acidic conditions, the main product that results it is a linear aliphatic structure of repeating units of polyfurfuryl alcohol linked by methylene bridges, which is produced by the condensation of the OH groups [114].

The mixture then grows darker and more viscous, since the linear PFA branches and cross-links are happening. Moreover, owing to the exothermic nature of these phase events, the water vaporizes, which produces holes in the polymer, which allows it to turn into a good active carbon precursor [115].

Furthermore, polyethylene glycol was also added when the polymer was coming to form, so it mixed up with the PEG. The aim of this component is to enhance the pore size distribution in the following step, since it is a large molecule which, when pyrolysing, will create bigger cavities on the catalyst carbon. The resulting mixture as well as the aspect of the catalyst are shown in figure:

Figure 3.3: *PFA coating results.*

3.1.3 Pyrolizing

The aim of this step is to generate the carbon layer on the surface of the foam support. Thus, a thermogravimetric analysis (TGA) study of the resulting mixture, as well as the added PEG was conducted, in order to investigate the decomposition patterns of the involved polymers.

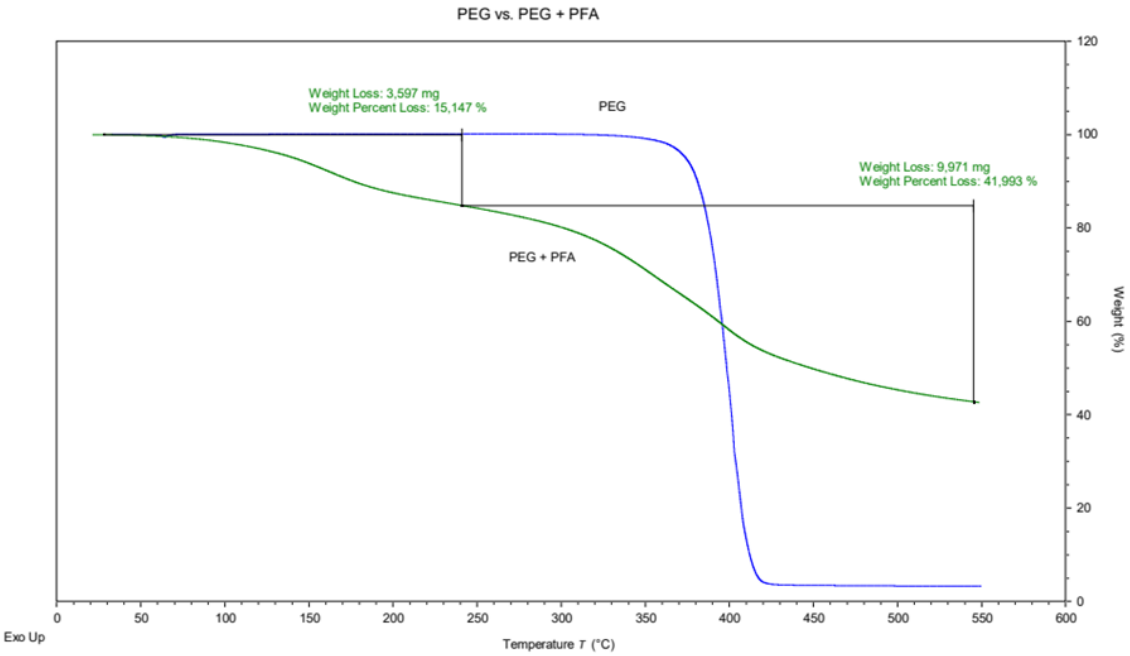

Figure 3.4: *TGA study of PEG and PFA+PEG.*

Which matches perfectly with T.Vergunst et al. [100]. Thus, the required temperature to assure no PEG remains on the foam is around 400-450°C, thus being 550°C the selected one, since it allows to get rid of the PEG whilst leaving a carbon layer on the foam.

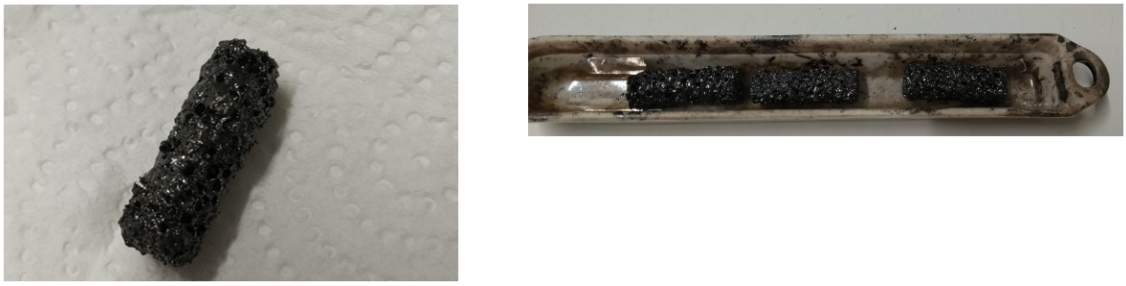

Figure 3.5: *Catalyst after pyrolysis.*

3.1.4 Ruthenium Incorporation

The method used to impregnate the surface of the carbon-coated foams with ruthenium was the well-known incipient wetness impregnation, (IWI). Thus, a solution of Ru (III) nitrosyl nitrate 1.4 wt.% Ru was utilized. The amount of precursor solution used per impregnation was determined as the greatest liquid volume that the support could adsorb without overflowing. The features reached in each of them are shown in Table 3.2.

Table 3.2: *Ruthenium incorporation results of all batches under IWI method.*

Batch Code	Foam Code	Anodic Oxidation Mass [g]	Mass After Ru deposition [g]	Carbon %	Carbon [g]	Solution Mass in foam [g]	ICP Ruthenium Concentration (mg/Kg)	Impregnation Days [d]	Ruthenium Incorporation Method
2	B2-F1	0.6217	1.149	45.89 %	0.53	4.5915	13631	10	IWI
	B2-F2	0.614	0.9516	35.48 %	0.34	4.5819			IWI
	B2-F3	0.591	1.1225	47.35 %	0.53	4.581			IWI
3	B3-F1	0.5466	0.7547	27.57 %	0.21	2.9948		6	IWI
	B3-F2	0.543	0.8736	31.98 %	0.28	2.73887			IWI
	B3-F3	0.6263	0.7905	20.77 %	0.16	2.7308			IWI
5	B5-F1	0.6708	0.769	21.61 %	0.17	1.41543		5	IWI
	B5-F2	0.6637	0.881	30.53 %	0.27	2.6653			IWI
	B5-F3	0.6465	0.7251	18.49 %	0.13	1.8538			IWI
6	B6-F1	0.5992	1.313	54.36 %	0.71	3.0638		7	IWI
	B6-F2	0.6058	1.3487	55.08 %	0.74	3.0994			IWI
	B6-F3	0.5961	1.4562	59.06 %	0.86	3.1801			IWI
7	B7-F1	0.6462	0.5997	64.39 %	1.08	4.4217	6083	10	IWI
	B7-F2	0.6276	0.5784	68.81 %	1.28	4.3969			IWI
	B7-F3	0.6311							IWI

*Not all the catalysts reached this step, so it could not be tried it in all the batches.

Table 3.3: *Comparison of the reactivity and physical properties of batches 2 and 7.*

Batch Code	Total Carbon Mass (Two foams) [g]	ICP Ru Conc. [mg/Kg]	Ru loading [g]	D-Xylose conv. after 4h. 40 Bar 100°C
2	1.06	13631	0.01443	95.75 %
7	2.36	6083	0.014359	95.98 %

Resulting in two batches of foams with same amount of ruthenium, which allowed them to perform almost identically.

After this step, the catalyst appearance was like:

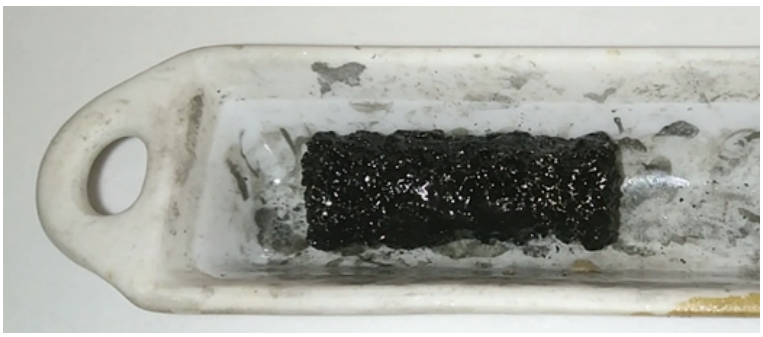

Figure 3.6: *Catalyst after ruthenium incorporation.*

3.1.5 Catalyst Reduction

In order to identify the suitable temperature to assure the correct ex-situ reduction conditions a temperature-programmed reduction (TPR) test was performed. Thus, two hydrogen consumption peaks were obtained around 230°C and 550°C, figure 3.7. The first one is attributable to the reduction of ruthenium oxides, RuO_x [116, 117], whereas the second one is caused by the methanation reaction of the support, confirmed by mass spectrometry.

Therefore, after TPR results, the reduction temperature used was set to 300°C. Besides, the reduction time was set to 5h, by using a temperature ramp worth 3°C*min^{-1}.

After this step, the catalyst was already done and able to start reactions. Moreover, before every experiment took place, the catalyst undertook another reduction, this time a in-situ one, so it could provide the best performance when carrying out the reaction. Thus, it was reduced at 120°C and 5 bar for 2h under the presence of hydrogen, as explained in section.

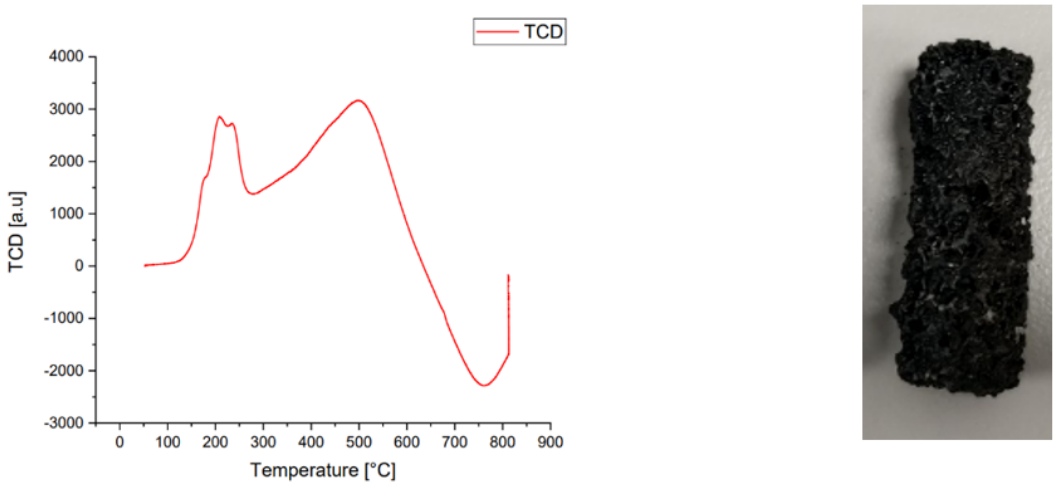

Figure 3.7: *Hydrogen TPR profile and catalyst after reduction step.*

3.2 Catalyst Characterization

3.2.1 Scanning Electron Microscopy (SEM)

SEM (Zeiss Leo Gemini 1530) was utilized to investigate the carbon morphology of the prepared catalyst and the effect of PEG addition on it (see Figure 3.8). As shown in Figure 3.8, there is an observable increase in the presence of depressions and porosity with increasing amount of PEG.

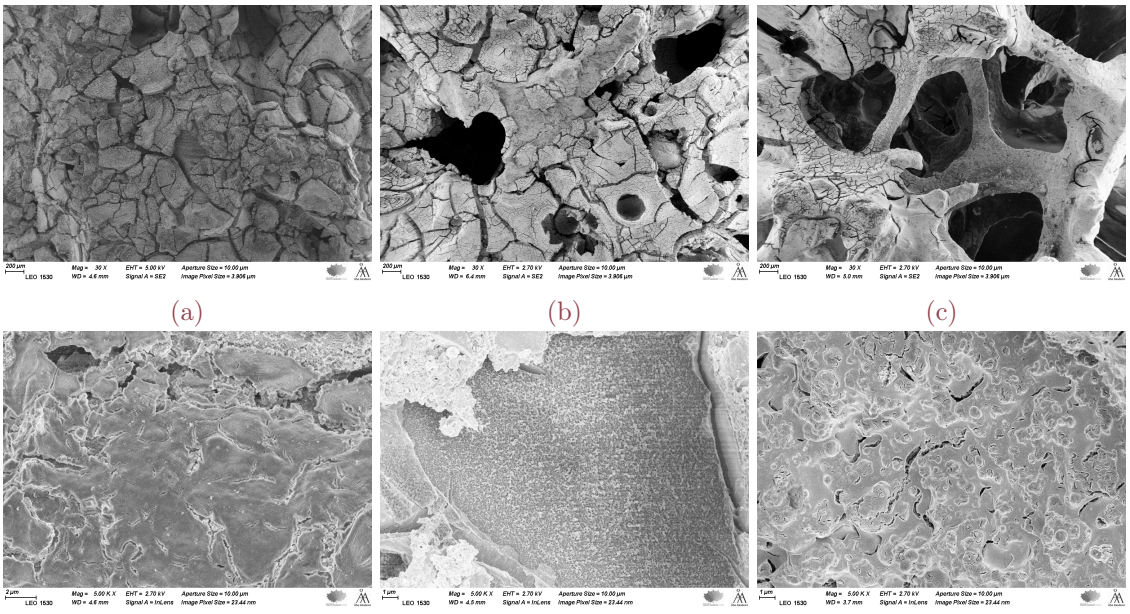

(a) (b) (c)

(d) (e) (f)

Figure 3.8: *SEM micrographs. a) No PEG 30x, b) 5% PEG 30x, c) 15% PEG 30x, d) No PEG 5kx, e) 5% PEG 5kx, f) 15% PEG 5kx.*

These differences were further studied by nitrogen physisorption, resulting in a pore size distribution ranging from 1 to 2 nm for the 0% PEG sample, and much more developed porosity in the 0% PEG sample. of the 5% PEG sample (see Figure3.9).

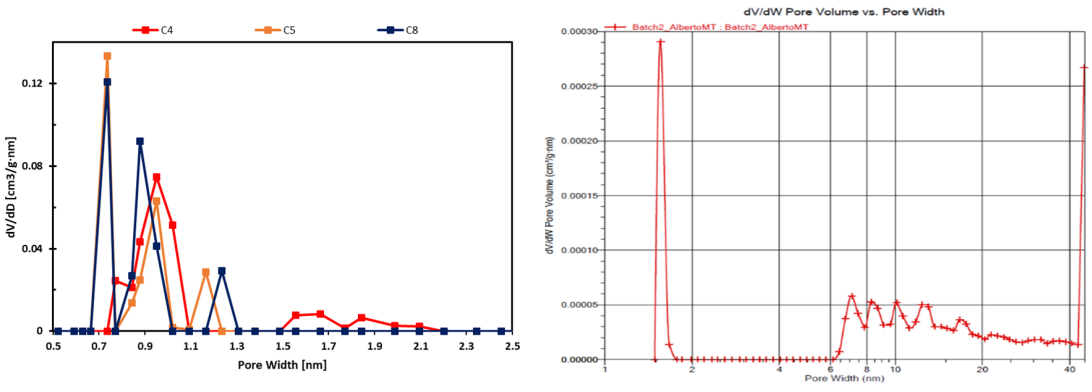

(a) (b)

Figure 3.9: *Pore size distribution of carbon coated foams using (a) 0% PEG and (b) 5%.*

According to the observations reported by Araujo-Barahona et al. [16], the foams prepared without PEG, that is, through the pyrolysis of poly(furfuryl) alcohol, are mainly microporous. In this sense, the addition of a high molar mass PEG during the coating step, triggers the formation of larger pores during the pyrolysis [100], eneabling larger molecules to penetrate the carbon layer where the actives sites are dispersed.

Previous studies have been carried out using a mixture of PFA/PEG to prepare carbonaceous materials with improved porosity [100].

3.2.2 Transmission Electron Microscopy (TEM)

The ruthenium nanoparticle size distribution on the foam catalyst was investigated by using Transmission Electron Microscopy (JEM 1400 Plus Transmission Electron Microscope) of fresh and spent catalyst. A total of 350 particles were measured per sample using Image J software

The TEM measurement right after finishing the catalyst preparation is shown below:

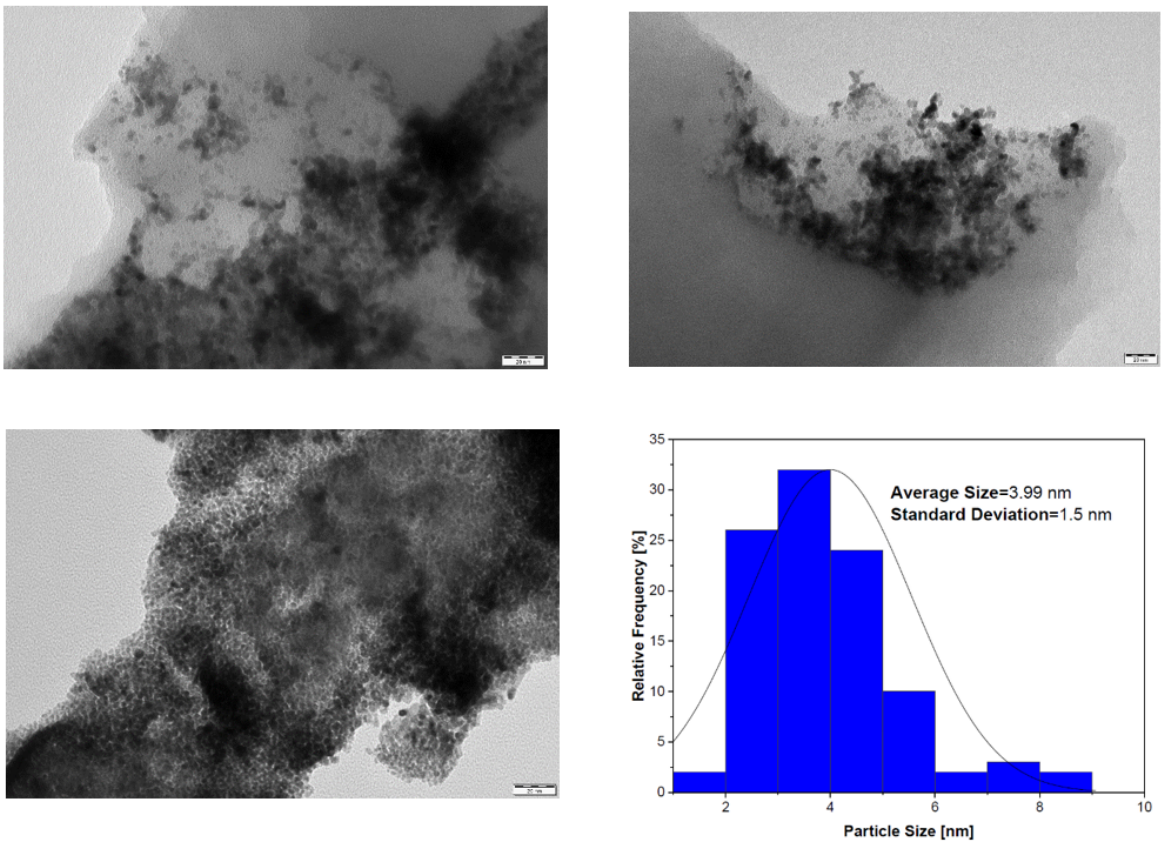

Figure 3.10: *TEM images of a finished catalyst and its particle size distribution.*

The TEM study of the spent catalyst is explained in Section 3.3.

3.2.3 Hydrogen Temperature Programmed Reduction (TPR)

The catalysts produced via incipient wetness impregnation were studied using Temperature Programmed Reduction (Microtrac MRB Catalyst Analyzer Belcat II) measurements. TPR studies were carried out in a stream of hydrogen and argon from 30°C to 700°C, with a temperature ramp of 10°Cmin^{-1} (5% hydrogen in argon). TPR measurement shown previously, in Section 2.6.

3.2.4 Inductively Coupled Plasma Atomic Emission Spectroscopy (ICP-OES)

ICP-OES was utilized to determine the ruthenium content of the catalysts employed in the kinetic experiments (Perkin Elmer, Optima 5300 DV). Prior to analysis, the carbon coating (0.1 g) of the catalyst samples was decomposed in a microwave oven with a combination of acids (3 mL of sulfuric acid (Sigma-Aldrich; 96% wt.) + 3 mL of nitric acid (Sigma-Aldrich; 65% wt)). ICP results shown previously, in Figure 3.3. Additionally, the leaching of ruthenium from the catalyst was monitored by analyzing a liquid sample before and after each experiment and determining the Ru concentration.

3.2.5 XPS

The chemical state of the catalytic species on the support was investigated using an X-ray photoelectron spectroscopy (XPS) approach (Axis Ultra DLD spectrometer with a monochromatized Al Ka X-ray source with charge neutralization).

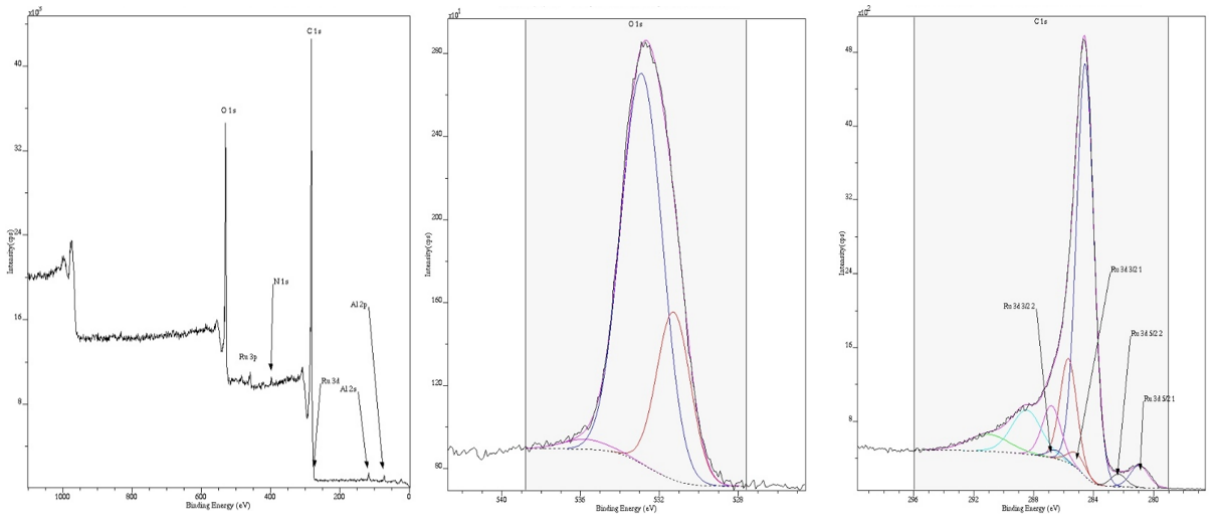

Figure 3.11: *XPS of a finished catalyst.*

3.3 Repetitiveness & Deactivation

About repetitiveness, three different experiments, at the same conditions, were carried out after 9, 54 and 99h of use of the catalyst. Its performance was more than acceptable, providing almost the same values of conversion for each experience figure. The average standard deviation resulted to be around 0.0259 of D-xylose conversion.

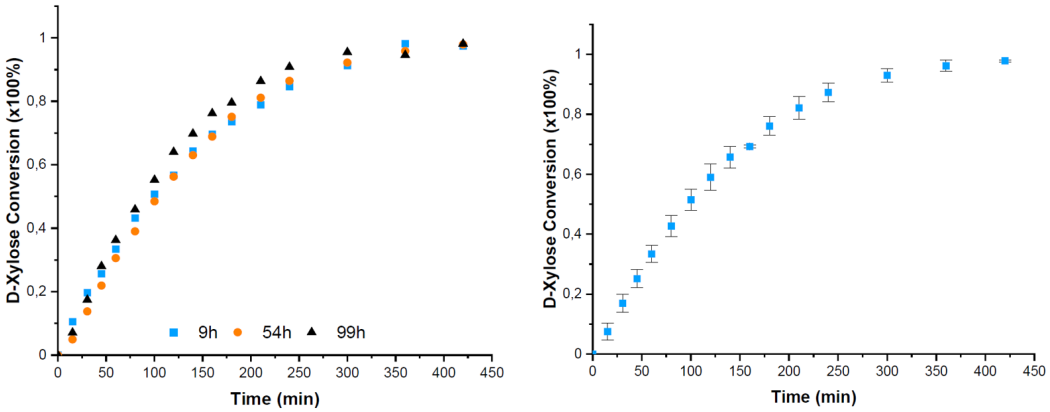

Figure 3.12: *Catalyst repetitiveness experiments under 90°C and 30 bar.*

On the other hand, after 180 h of use, catalyst 7 showed a decrease in its activity (see Figure 3.13). Even if 100% conversion of D-xylose is still reached after 200 min of reaction, there is a drop in the reaction rate at 100 min of around 13%.

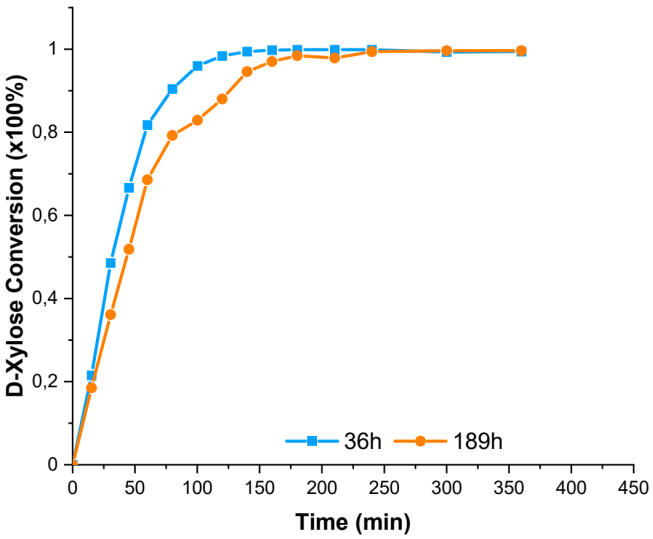

Figure 3.13: *Catalyst deactivation experiment under 120°C and 40 bar.*

Figure 3.14 shows the TEM micrograms of the spent catalyst, the average particle size obtained was 8 nm with a standard deviation of 2.6 nm. These results indicate that after 189 h of use, the average particle size doubled its value, since no ruthenium leaching was detected during the experiments (detection limit: <0.03 mg/L) and it is known that sugar hydrogenation is a highly structure-sensitive reaction [118], the nanoparticle agglomeration could be identified as the main cause of deactivation [65].

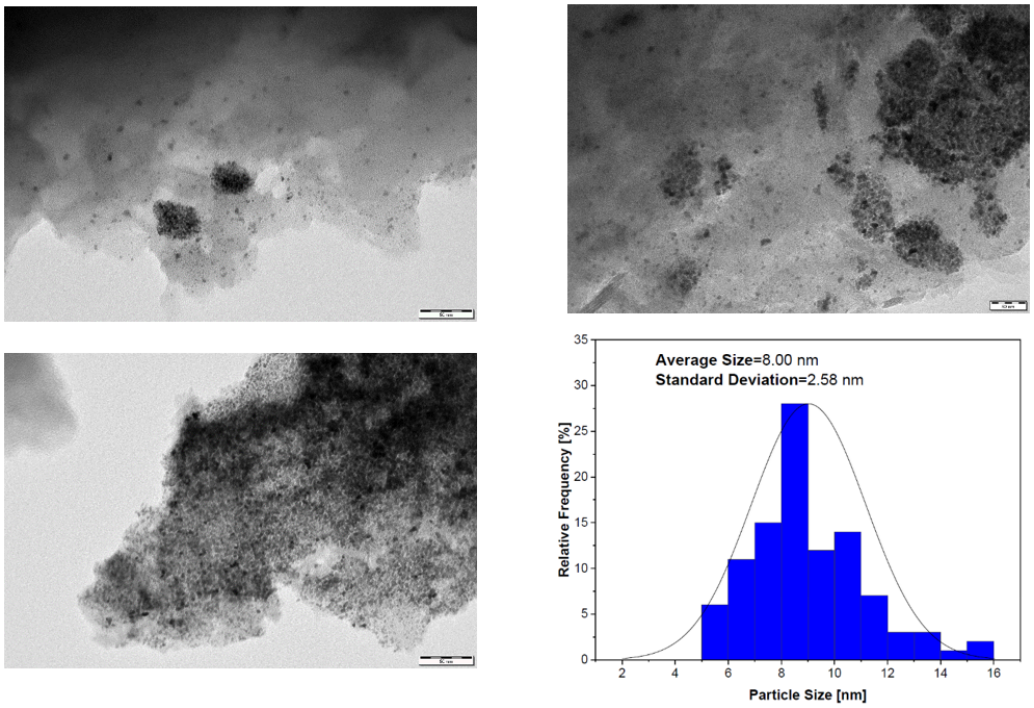

Figure 3.14: *TEM images of a spent catalyst and its particle size distribution.*

3.4 Kinetic Results

3.4.1 Analytics Proposed Reaction Pathway

In order to identify the chemicals present in the reaction mixture and to propose a possible reaction pathway for the hydrogenation of D-xylose, a GC-MS analysis of a sample at 100% conversion was performed, the results are shown in Figure 3.15:

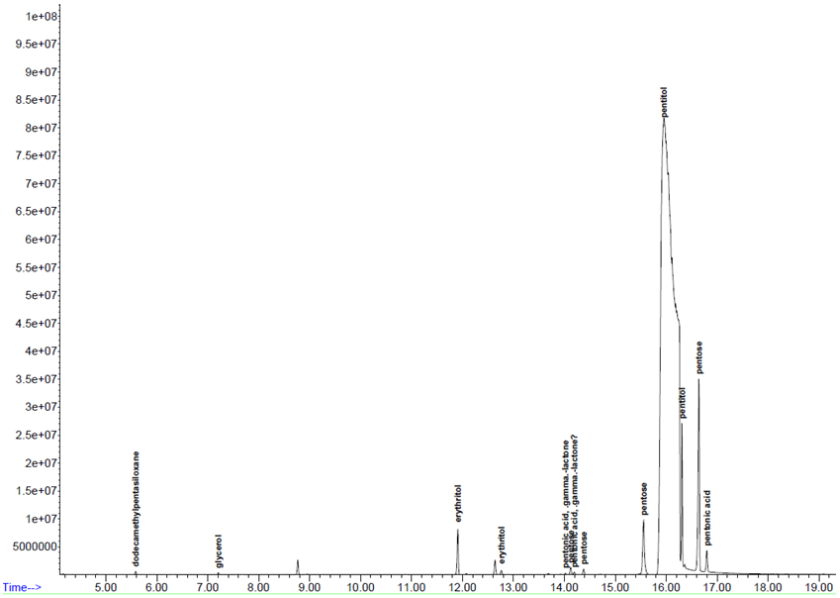

Figure 3.15: *GC-MS test out of a reactor sample.*

Even though GC-MS results show a wide range of chemicals, the HPLC was only capable of

detecting those whose concentration was above the limit of detection, thereby resulting in only 5; D-Xylose, D-Xylitol, D-Arabitol, Erythritol and a product that could not be identified. Figure 3.16 shows a typical HPLC chromatogram of the reaction mixture:

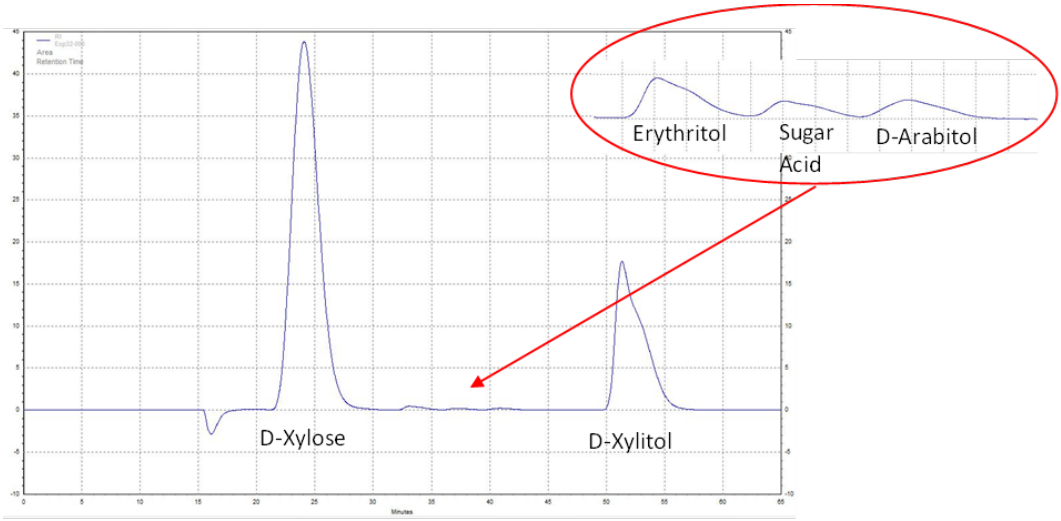

Figure 3.16: *HPLC chromatograph.*

Component	a	Retention Time (min)
D-Xylose	0,323828361	24
Erythritol	0,366974811	32,9
D-Arabitol	0,322578739	40,773
D-Xylitol	0,311061923	51,167

Figure 3.17: *HPLC retention times.*

Being the parameter "a" defined as $C_{Sample} = a \cdot A_{HPLC} \cdot 10^{-8}$.

Since it had been working with foam catalyst over Ru/C conditions, D-Xylose is widely known for producing D-Xylitol under the presence of hydrogen to, afterwards, isomerizes to its epimer D-Arabitol [77, 80]. Regarding the Erythritol, some literature states that, through retro-Claisen reactions, D-Xylose turns to Erythritol under Ru/C catalyst too [119]. Hence, the proposed reaction pathway is shown in Figure 3.18:

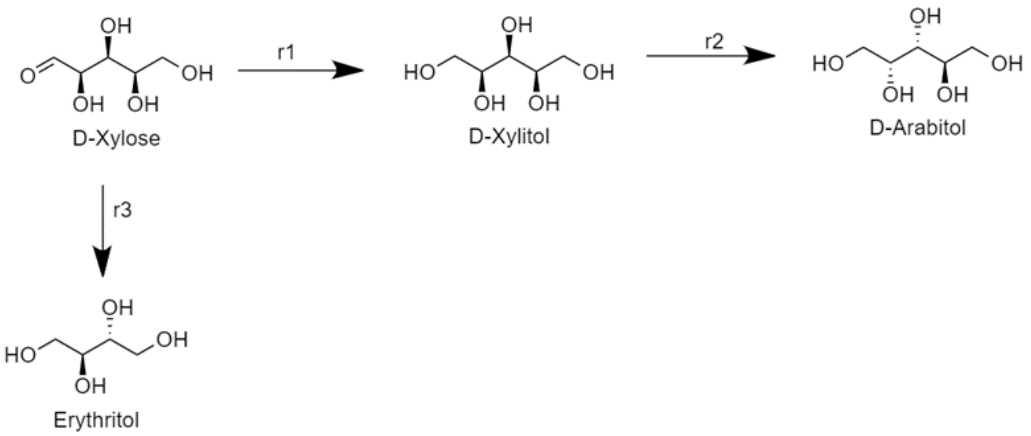

Figure 3.18: *Proposed reaction pathway for D-Xylose hydrogenation.*

3.4.2 Temperature and pressure Influence

Whilst temperature showed a significant influence on the reaction rate for Xylitol, pressure did not seem to be a key parameter. Moreover, the effect of temperature was successfully described by Arrhenius's law through modeling, see Section 3.5. With regard to the selectivity, the catalyst showed to be very selective, reaching values around 98%, and around 95% yields. Thus, the temperature influence is shown as follows:

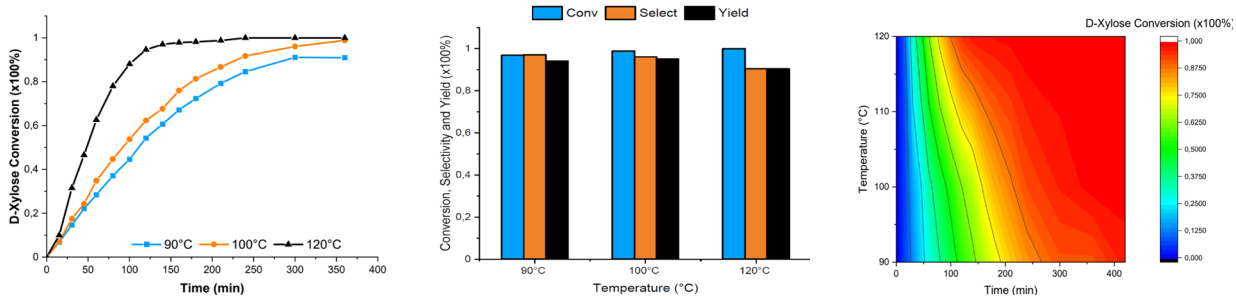

Figure 3.19: *Temperature influence under 20 bar.*

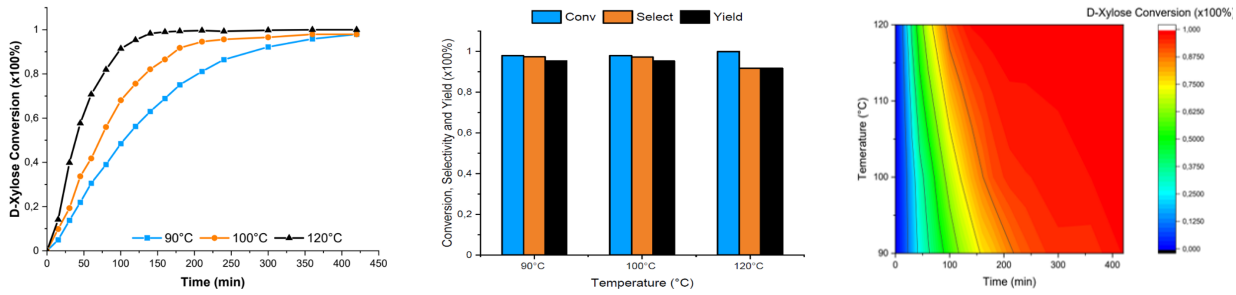

Figure 3.20: *Temperature influence under 30 bar.*

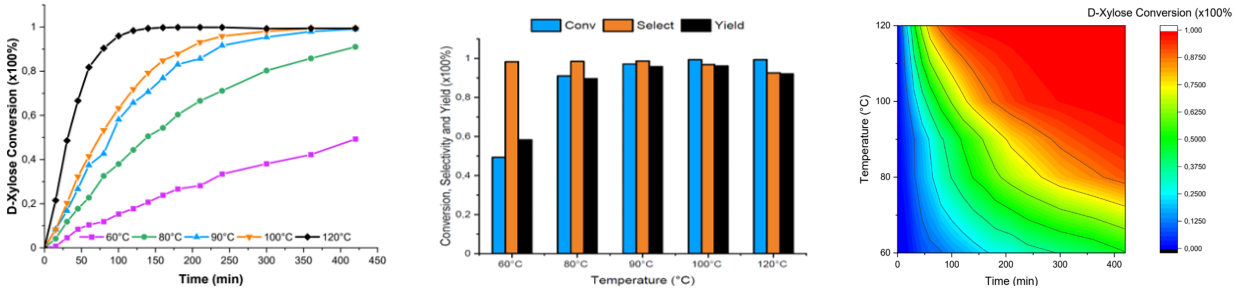

Figure 3.21: *Temperature influence under 40 bar.*

With regard to the hydrogen pressure, as mentioned before, it does not play a key role, thereby not having a big influence in the performance of the reaction.

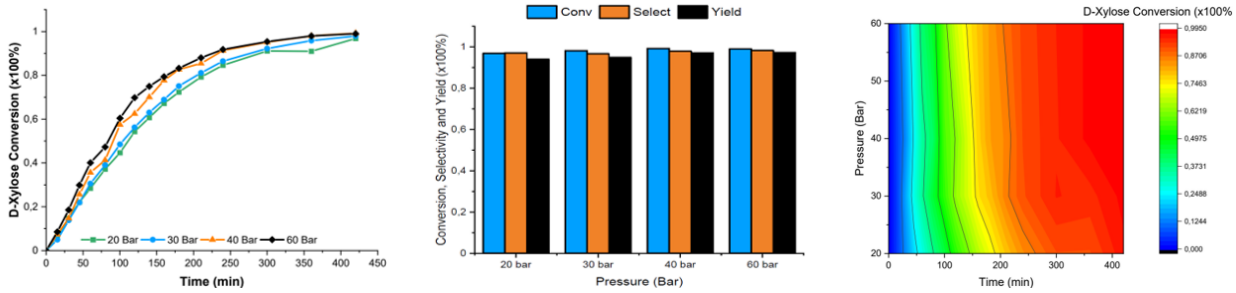

Figure 3.22: *Pressure influence under 90°C.*

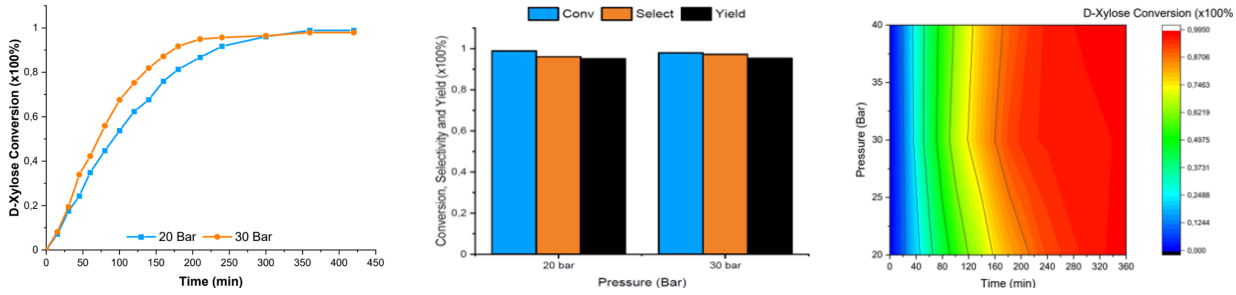

Figure 3.23: *Pressure influence under 100°C.*

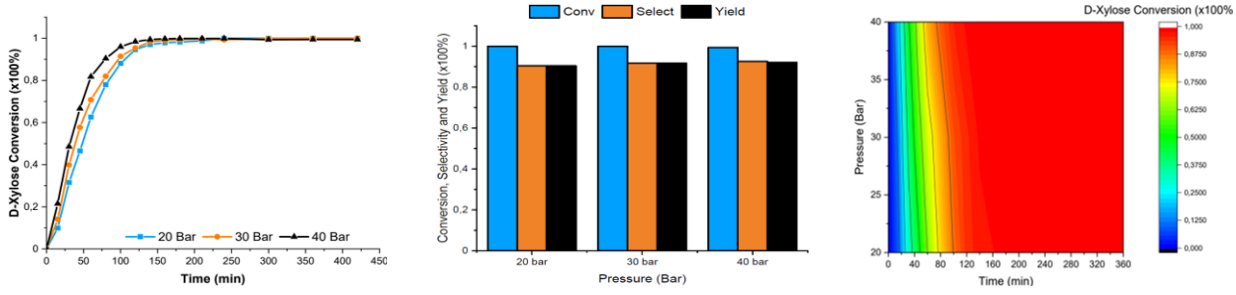

Figure 3.24: *Pressure influence under 120°C.*

These presented results match the observations reported by Samikannu et al. [77], who studied the same process, D-Xylose hydrogenation over Ru/C, but using powder catalyst. Despite that,

the author found the same behaviour, the higher the temperature, for a given pressure, the faster the reaction rate. Same behaviour was also reported regarding the pressure, even though this one was less pronounced.

Furthermore, the results also match the ones obtained by Sifontes Herrera et al. [78],who by using powder catalyst, found the same strong temperature dependence on the reaction rate, while pressure had minimal effect.

3.4.3 Initial concentration influence

It was also studied the way the initial D-Xylose concentration affects the reaction rate. Thus, three experiences were carried out, one with the double and another with the half of the initial concentration has been using in all the previous experiments. The results are shown in figure:

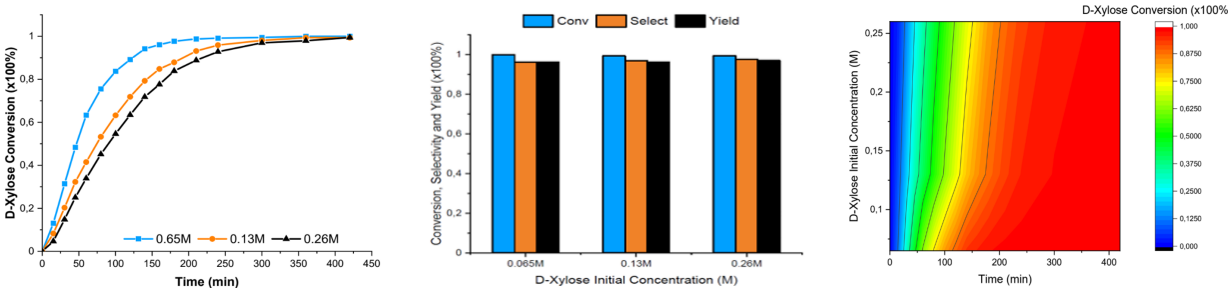

Figure 3.25: *Initial concentration influence under 100°C and 40 bar.*

The behavior displayed in Figure 3.25, in which the reaction rate decreases as the initial concentration decreases, can be explained in terms of the available active sites on the surface of the catalyst and its capacity to adsorb the reactants molecules.
Furthermore, it can also be appreciable the fact that, since the initial concentration influence the reaction rate, the kinetics degree must be order 1 or greater.

3.4.4 Selectivity Analysis and Reaction Optimization

One of the most important aspects that must be optimized when working with chemical reactions is selectivity. Since this thesis focuses on the hydrogenation of D-Xylose, the main desired product was D-Xylitol, thereby the purer, the better. In order to find the best working conditions to maximize the production of D-xylitol, the selectivities of all the key components were determined at different temperatures, pressures as well as initial concentrations. Figure 3.26:

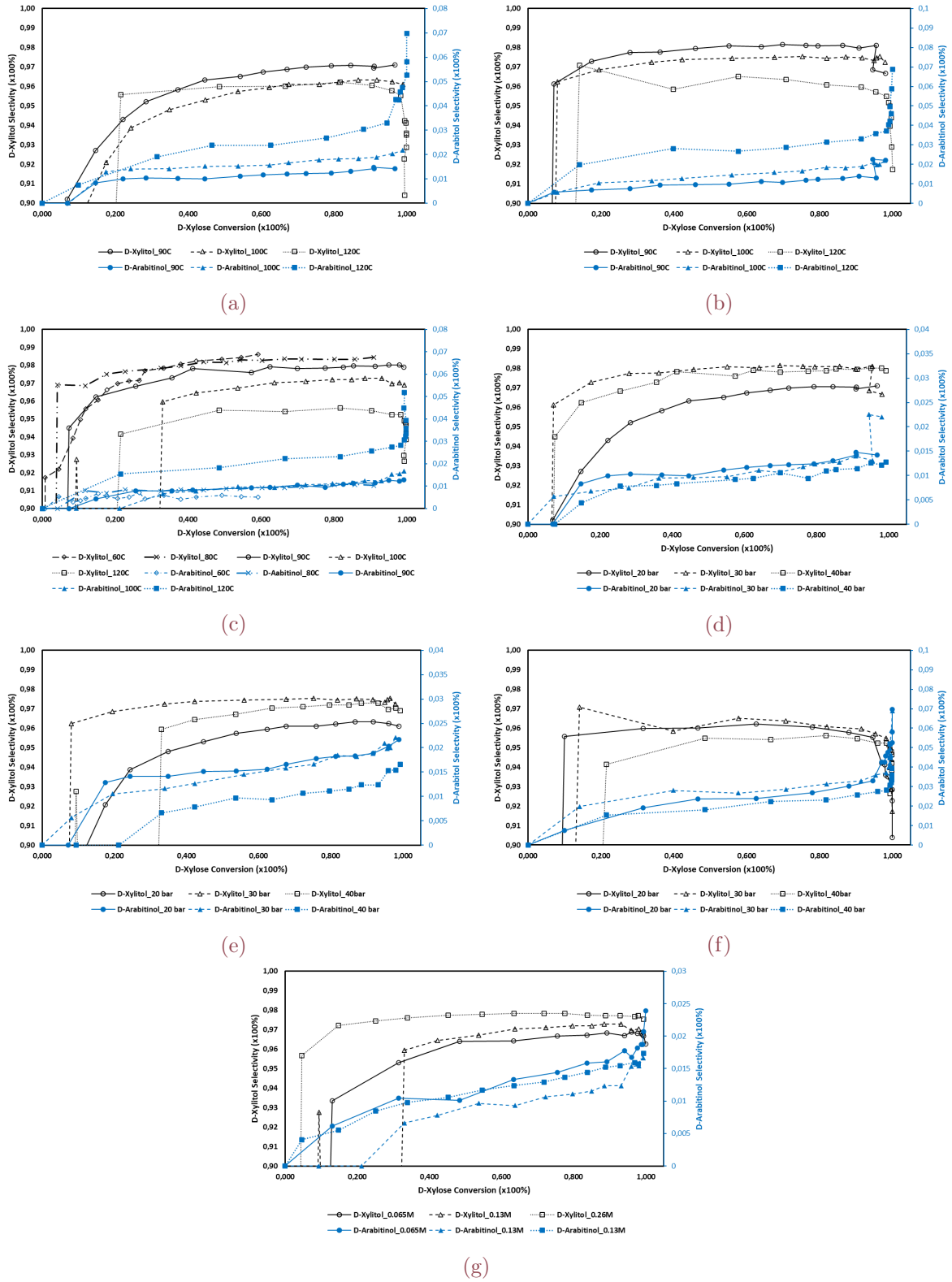

Figure 3.26: *D-Xylitol and D-Arabitinol selectivty against D-Xylose conversion charts at: a) 20 bar, b) 30 bar, c) 40 bar, d) 90°C, e) 100°C, f) 120°C and g) 100°C and 40 bar.*

D-Xylitol

Temp/Press	60°C	80°C	90°C	100°C	120°C
20 Bar	-	-	96.5 %	95.7 %	96.2 %
30 Bar	-	-	98.1 %	97.5 %	96.5 %
40 Bar	98.4 %	98.1 %	97.8 %	96.7 %	95.4 %
50 Bar	-	-	97.1 %	-	-
60 Bar	-	-	98.0 %	-	-

D-Xylitol

Temp/Press	60°C	80°C	90°C	100°C	120°C
20 Bar	-	-	97.1 %	96.2 %	96.1 %
30 Bar	-	-	97.3 %	97.4 %	96.1 %
40 Bar	-	98.3 %	98.7 %	97.2 %	95.6 %
50 Bar		-	97.5 %	-	-
60 Bar	-	-	98.2 %	-	-

Erythritol

Temp/Press	60°C	80°C	90°C	100°C	120°C
20 Bar	-	-	2.4 %	2.7 %	1.4 %
30 Bar	-	-	1.0 %	1.1 %	0.8 %
40 Bar	1.0 %	1.0 %	1.5 %	2.3 %	2.3 %
50 Bar	-	-	1.9 %	-	-
60 Bar	-	-	1.2 %	-	-

Erythritol

Temp/Press	60°C	80°C	90°C	100°C	120°C
20 Bar	-	-	1.6 %	2.0 %	1.3 %
30 Bar	-	-	1.5 %	0.7 %	0.8 %
40 Bar	-	0.61 %	0.3 %	1.6 %	2.1 %
50 Bar	-	-	0.6 %	-	-
60 Bar	-	-	0.8 %	-	-

D-Arabitinol

Temp/Press	60°C	80°C	90°C	100°C	120°C
20 Bar	-	-	1.1 %	1.5 %	2.4 %
30 Bar	-	-	1.0 %	1.5 %	2.7 %
40 Bar	0.5 %	0.9 %	0.9 %	1.0 %	2.2 %
50 Bar	-	-	1.0 %	-	-
60 Bar	-	-	0.8 %	-	-

D-Arabitinol

Temp/Press	60°C	80°C	90°C	100°C	120°C
20 Bar	-	-	1.3 %	1.8 %	2.7 %
30 Bar	-	-	1.2 %	1.8 %	3.1 %
40 Bar	-	1.07 %	1.1 %	1.2 %	2.3 %
50 Bar	-	-	2.1 %	-	-
60 Bar	-	-	0.9 %	-	-

Figure 3.27: *Selectivity analysis under 50 and 80% of D-Xylose conversion, varying the temperature and pressure.*

D-Xylitol

Conc.(M) / Conv.	0.5	0.8	1
0.065 M	96.4 %	96.7 %	96.3 %
0.13 M	96.7 %	97.2 %	96.9 %
0.26 M	97.7 %	97.7 %	97.5 %

Erythritol

Conc.(M) / Conv.	0.5	0.8	1
0.065 M	2.6 %	1.7 %	1.4 %
0.13 M	2.0 %	1.5 %	1.3 %
0.26 M	1.2 %	2.1 %	0.7 %

D-Arabitinol

Conc.(M) / Conv.	0.5	0.8	1
0.065 M	1.0 %	1.6 %	2.4 %
0.13 M	1.0 %	1.1 %	1.7 %
0.26 M	1.1 %	1.8 %	1.7 %

Figure 3.28: *Selectivity analysis under 80% of D-Xylose conversion, varying the initial concentration of D-Xylose.*

Selectivities around 96-98% were achieved for D-Xylitol, the key compound, whereas regarding the byproducts, around 1-2% was also obtained for both D-Arabitol and Erythritol.

In general, lower temperatures and higher hydrogen pressures were found to tend to decrease the production of undesired compounds and thus maximizing selectivity towards D-xylitol

Therefore, from the point of view of the industrial production of xylitol, temperature in the range of 80-90°C and pressures of 40-60 bar hydrogen would allow operating with an adequate reaction time while maintaining selectivity levels that facilitate downstream separation processes.

3.4.5 PEG Influence and Improvements

In order to investigate the influence of polyethylene glycol and the average pore size, two kinetic experiments at the same conditions were carried out with catalyst 0 [16] (No PEG, 1.73% Ru/C, 0.0409 g Ru) and catalyst 7 (5% PEG, 0.014 g Ru). Thus obtaining:

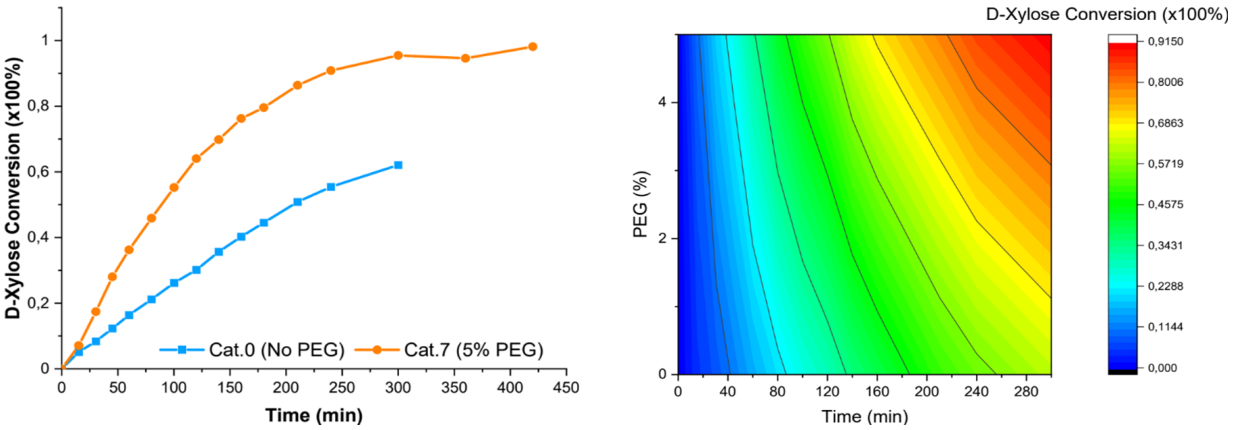

Figure 3.29: *Influence of PEG under 90°C and 30 bar.*

This notorious increment in the sizes of the porous leaded to an increment in the activity too, since comparing the performance of both catalyst under the same conditions, the one made using PEG displayed an increase in the conversion of about 40% when compared with the catalyst prepare without PEG addition, despite having less amount of ruthenium.

3.5 Modeling

In order to calculate the kinetics of the system, a series of reactions at different hydrogen pressures, temperatures and initial D-Xylose concentrations were carried out in an isothermal semi-batch reactor, which worked with a fixed mass of catalyst. In this setup, the hydrogen was continuously added, thereby it can be supposed that the concentration throughout the reaction is constant, and so the pressure. All this triggers that the energy balance is omitted.

Furthermore, owing to the high stirring speed used, mass transfer limitation can be despised, which makes the reaction take place under kinetic regime. In addition, despite the sampling, the reaction volume can be also considered constant, since the change in liquid volume due to reaction is quite minor.

With regard to the kinetic mechanism, sugar hydrogenation is widely known as an irreversible reaction [78, 80, 81, 103, 120, 121]. Moreover, two byproducts could be also observed, D-Arabitol and Erythritol. Despite their concentrations were ranging the detection limit of the HPLC, they both were taken into account and so modeled.

When it comes to proposing a reaction mechanism, various alternatives can be found in literature. They both state the presence of D-Xylulose as a reaction intermediate when forming D-Arabitol. Since for this work D-Xylulose was not detected whatsoever, it has not been taken

into account when modeling, working instead with a direct isomerization from D-Xylitol. Moreover, regarding the erythritol reaction, it has been supposed to come directly from D-Xylose [119], and the other byproducts also presented in the reaction have also been ruled out since they were not detected when analyzing.

In order to simplificate the reaction rates, the adsorption affinity of the produced sugar alcohols has been neglected since it was shown to be significantly lower than the main sugars they come from [78]. Moreover, as a first approach, the catalyst surface was taken as ideal, so the Langmuir model could easily be applied.

3.5.1 Proposed Reaction Pathway

Therefore, the proposed reaction mechanism is the one shown in Figure 3.30.

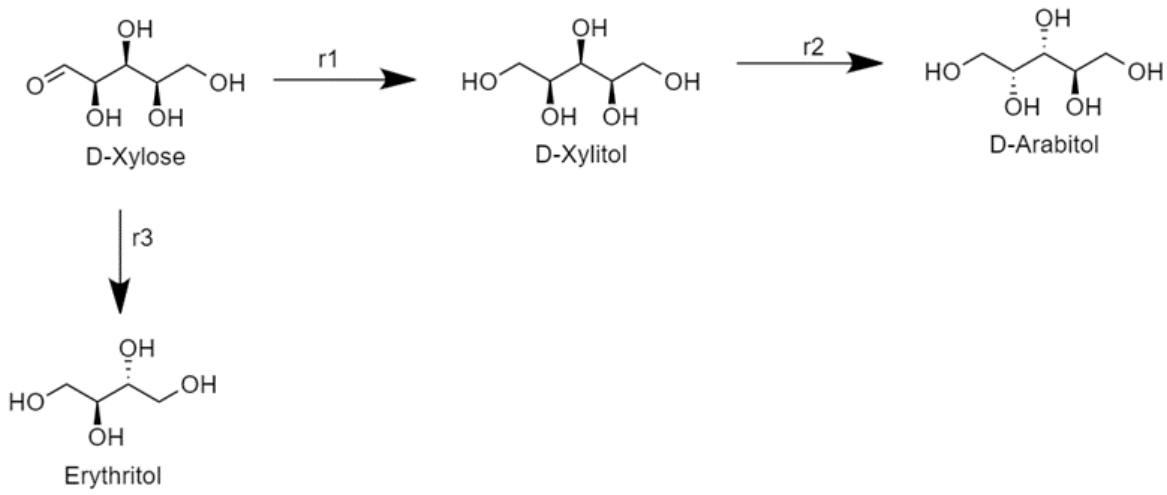

Figure 3.30: *Proposed reaction pathway for the hydrogenation of D-Xylose.*

Where, according to what was stated previously, the mole balance for a chemical species (i) involved in the reaction turned out to be as follows, since both volume and catalyst mass were supposed to be constant along the reaction.

$$\frac{dC_i}{dt} = r_i \cdot \frac{m_{cat}}{V_L} \tag{3.1}$$

Thus, the mole balance system for all the main components to be modeled is:

$$\frac{dS}{dt} = (-r_1 - r_3) \cdot \rho_B \tag{3.2}$$

$$\frac{dS_{OH}}{dt} = (r_1 - r_2) \cdot \rho_B \tag{3.3}$$

$$\frac{dAra}{dt} = r_2 \cdot \rho_B \tag{3.4}$$

$$\frac{dEry}{dt} = r_3 \cdot \rho_B \tag{3.5}$$

$$\rho_B = \frac{m_{cat}}{v_L} \tag{3.6}$$

3.5.2 Derivation of the Rate Expressions for the Kinetic Model

Assuming the reaction pathway stated above, the reactions that are set to take place are shown below. θ denotes a catalyst free site.

$$S + \theta \overset{\text{Ks}}{\leftrightarrow} \theta S \tag{3.7}$$

$$H_2 + \theta \overset{KH_2}{\leftrightarrow} \theta H_2 \tag{3.8}$$

$$\theta H_2 + \theta S \overset{K1}{\rightarrow} \theta S_{\text{OH}} + \theta \tag{3.9}$$

$$\theta S_{\text{OH}} \overset{KS_{\text{OH}}}{\leftrightarrow} S_{\text{OH}} + \theta \tag{3.10}$$

$$\theta S_{\text{OH}} \overset{K2}{\rightarrow} \theta Ara \tag{3.11}$$

$$\theta Ara \overset{\text{Kara}}{\rightarrow} \theta + Ara \tag{3.12}$$

$$\theta S \overset{K3}{\rightarrow} \theta Ery \tag{3.13}$$

$$\theta Ery \overset{\text{Kery}}{\rightarrow} \theta + Ery \tag{3.14}$$

A competitive kinetic mechanism based on molecular adsorption was selected, according to Sifontes Herrera et al. [78], where the hydrogen is supposed to "compete" against the D-Xylose for the active site. In reality, this is more complex, and it turns out to be a sort of semi-competitive system [16] but, in order to make the model simpler, a competitive mechanism was selected. From this one, the adsorption-desorption quasi-equilibria for the involved molecules is expressed by:

$$Ks = \frac{S\theta}{S \cdot \theta} \tag{3.15}$$

$$KH_2 = \frac{\theta H_2}{H_2 \cdot \theta} \tag{3.16}$$

$$KS_{OH} = \frac{\theta S_{OH}}{S_{OH} \cdot \theta} \tag{3.17}$$

$$KAra = \frac{\theta Ara}{Ara \cdot \theta} \tag{3.18}$$

$$KEry = \frac{\theta Ery}{Ery \cdot \theta} \tag{3.19}$$

Moreover, the balance of the catalyst sites necessary to relate all the species adsorbed on the surface results [78]:

$$\theta + \theta\ S + \theta\ H_2 + \theta\ S_{OH} + \theta\ Ara + \theta\ Ery = 1 \tag{3.20}$$

Considering now that the surface reaction between the adsorbed sugar molecules and the hydrogen is the rate-determining step, the rate equations can be written as it follows:

$$r_1 = K_1 \cdot \theta\ S \cdot \theta\ H_2 \tag{3.21}$$

$$r_2 = K_2 \cdot \theta\ S_{OH} \tag{3.22}$$

$$r_3 = K_3 \cdot \theta\ S \tag{3.23}$$

Where, mixing now equations and , the rates transform to:

$$r_1 = K_1 \cdot Ks \cdot S \cdot H_2 \cdot K_{H_2} \cdot \theta^2 \tag{3.24}$$

$$r_2 = K_2 \cdot Ks_{OH} \cdot S_{OH} \cdot \theta \tag{3.25}$$

$$r_3 = K_3 \cdot Ks \cdot S \cdot \theta \tag{3.26}$$

And adding now the balance of the catalyst sites:

$$r_1 = \frac{K_1 \cdot K\ s \cdot S \cdot H_2 \cdot K_{H_2}}{(1 + Ks \cdot S + K_{H_2} \cdot H_2 + Ks_{OH} \cdot S_{OH} + KAra \cdot A\ r\ a + KEry \cdot E\ r\ y\ )^2} \tag{3.27}$$

$$r_2 = \frac{K_2 \cdot K\ s_{OH} \cdot S_{OH}}{1 + Ks \cdot S + K_{H_2} \cdot H_2 + Ks_{OH} \cdot S_{OH} + \ KAra\ \cdot A\ r\ a\ +\ KEry\ \cdot E\ r\ y} \tag{3.28}$$

$$r_3 = \frac{K_3 \cdot K\ s \cdot S}{1 + Ks \cdot S + K_{H_2} \cdot H_2 + Ks_{OH} \cdot S_{OH} + \ KAra\ \cdot A\ r\ a\ +\ KEry\ \cdot E\ r\ y} \tag{3.29}$$

As mentioned before, the adsorption affinity of the produced sugar alcohols can be neglected since it was shown to be significantly lower than the main sugars they come from [78]. Thus, the reaction rates get simplified to:

$$r_1 = \frac{K_1 \cdot K\ s \cdot S \cdot H_2 \cdot K_{H_2}}{(1 + Ks \cdot S + K_{H_2} \cdot H_2\ )^2} \tag{3.30}$$

$$r_2 = \frac{K_2 \cdot K\ s_{OH} \cdot S_{OH}}{1 + Ks \cdot S + K_{H_2} \cdot H_2} \tag{3.31}$$

$$r_3 = \frac{K_2 \cdot K\ s \cdot S}{1 + Ks \cdot S + K_{H_2} \cdot H_2} \tag{3.32}$$

If the reactions are presumed to follow the Arrhenius law, the temperature dependence of the merged parameter can be expressed as:

$$K'_i = \ A_i \cdot \ e^{\left(\frac{-Ea_i}{R \cdot T}\right)} \tag{3.33}$$

Finally, mixing eqs and, the final expresions off the reaction can be written as:

$$r_1 = \frac{A_1 \cdot \ e^{\left(\frac{-Ea_1}{R \cdot T}\right)} \cdot S \cdot H_2}{(1 + Ks \cdot S + K_{H_2} \cdot H_2\ )^2} \tag{3.34}$$

$$r_2 = \frac{A_2 \cdot \ e^{\left(\frac{-Ea_2}{R \cdot T}\right)} \cdot S_{OH}}{1 + Ks \cdot S + K_{H_2} \cdot H_2} \tag{3.35}$$

$$r_3 = \frac{A_3 \cdot \ e^{\left(\frac{-Ea_3}{R \cdot T}\right)} \cdot S}{1 + Ks \cdot S + K_{H_2} \cdot H_2} \tag{3.36}$$

3.5.3 Parameter Estimation

The kinetic parameters were estimated by minimizing the sum of residual squares of the following objective function, by using the Nelder-Mead optimization method. In addition, the ordinary differential equation system (ODE) was solved with the programming language Python through the LSODA solver.

$$OF = \sum_{i=1}^{n} \left(C_{Exp_i} - C_{Calc_i}\right)^2 \tag{3.37}$$

As first approach, the equations 3.56, 3.57, 3.58 were firstly solved for one individual temperature, obtaining the merged kinetic parameter for each one and then computing the Arrhenius-Van't Hoff equation parameters. The experimental series at 40 bar was selected for this purpose (90, 100, 120°C). . The linearized Arrhenius plots for r1, r2 and r3 are shown in Figure 3.31:

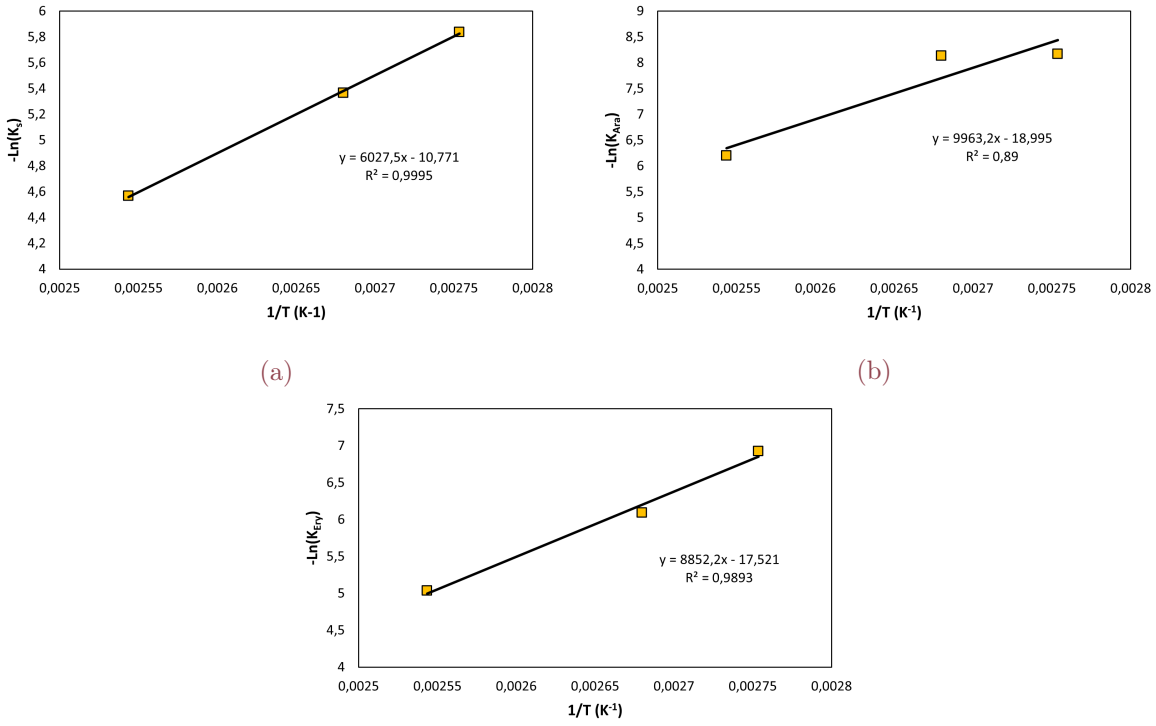

Figure 3.31: *Arrhenius plots for the estimated k'_s parameters: a) D-Xylitol, b) D-Arabitol and c) Erythritol.*

Where a high correlation coefficient was achieved for reaction 1, the one corresponding to D-xylose hydrogenation to xylitol. For the other two, r2 and r3, a smaller coefficient was accomplished. This can be ascribed to the small concentration the involved products are ranging, since as mentioned above, their concentrations are close to the detection limit the equipment was working with. Despite that, a good first parameter estimation could be conducted, dropping the next results:

With these parameters, a more than acceptable good point was achieved to start the opti-

Table 3.4: *Arrhenius parameters determined by linear regression.*

K	As' ($L \cdot gRu^{-1} \cdot min^{-1} \cdot mol^{-1} \cdot bar^{-1}$)	Ea' (KJ·mol-1)
1	47637	-50.113
2	177513601	-82.834
3	40670454	-73.596

mization process from. The coefficient of correlation for the model was computed from equation , varying from 0-100%, considering that a good degree of explanation is achieved for values of R2 in the range of 95-99% for the sugar hydrogenation step.

$$R^2 = \left(1 - \frac{\sum_{i=1}^{n} (C_{Exp,i} - C_{Calc.i})^2}{\sum_{i=1}^{n} (C_{Exp,i} - C_{mean})^2}\right) \cdot \tag{3.38}$$

The model-fitting results achieved are shown as follows, illustrating how the proposed model accurately characterized the experimental concentration profiles at various temperatures.

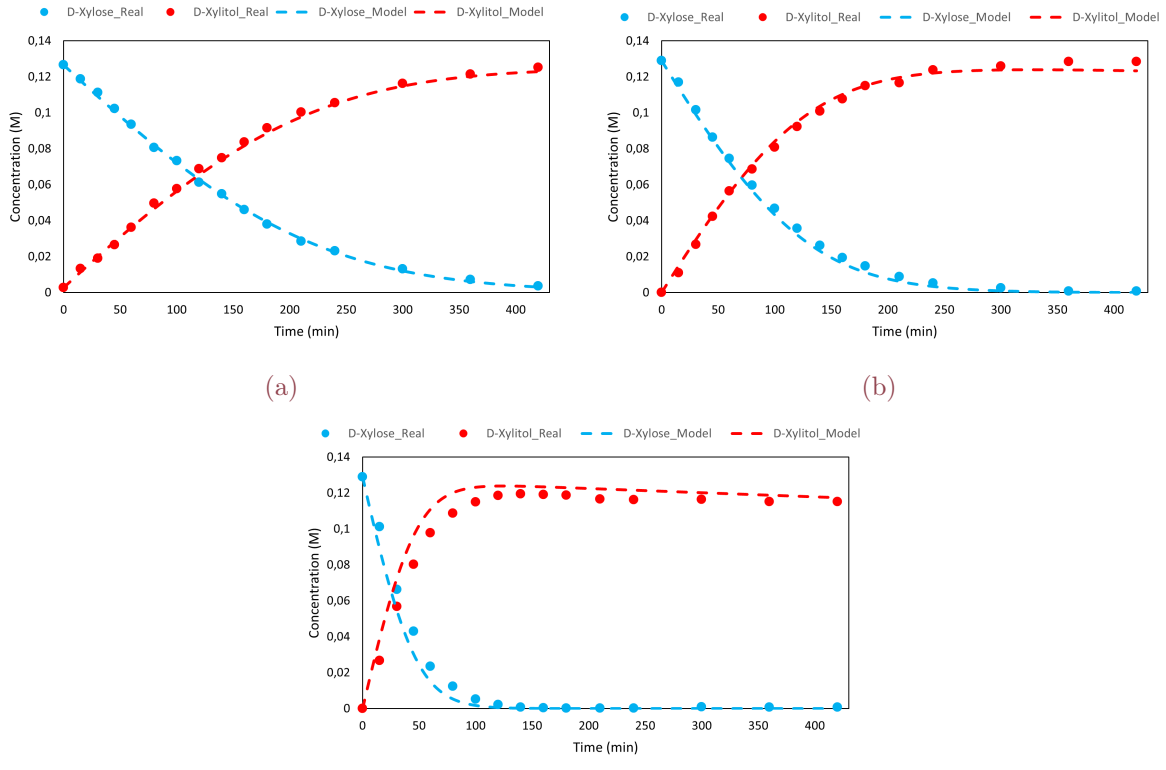

Figure 3.32: *Modelling results for D-xylose and D-xylitol at 40 bar: a) 90°C, b) 100°C and c) 120°C (Competitive model).*

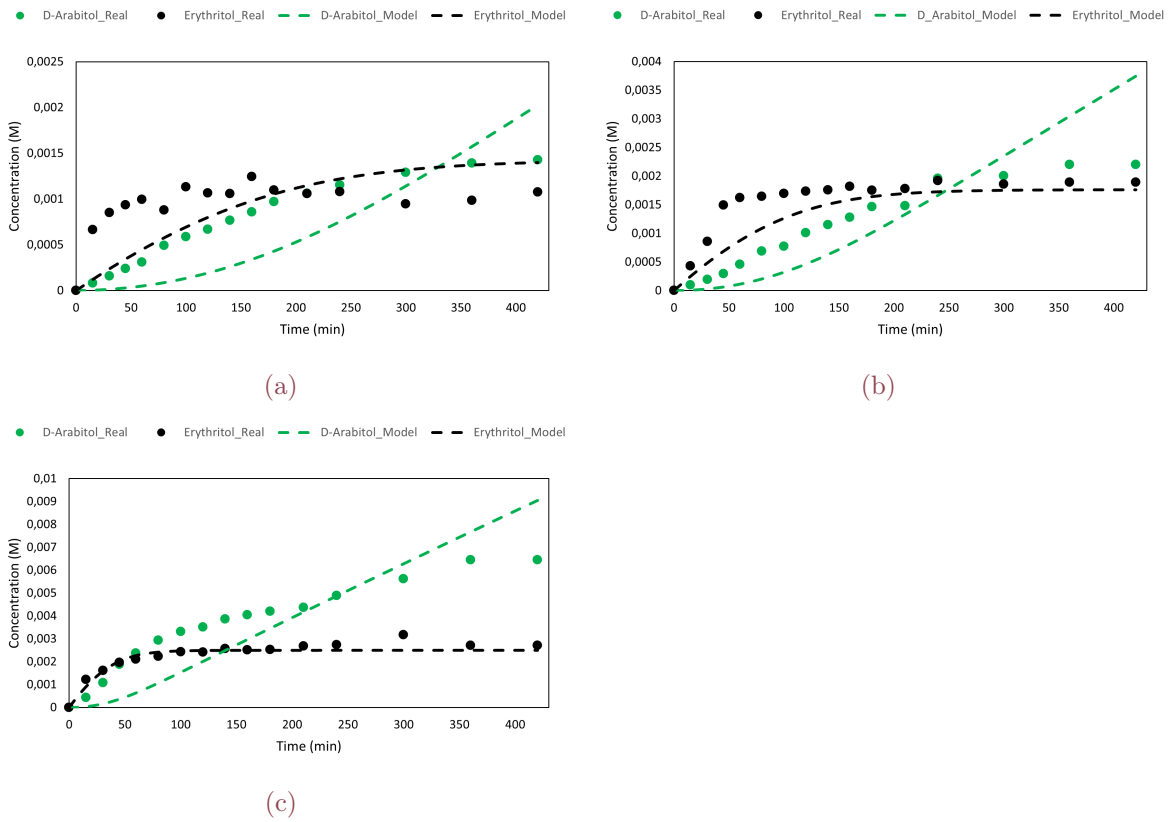

Figure 3.33: *Modelling results for the byproducts at 40 bar: a) 90°C, b) 100°C and c) 120°C (Competitive model).*

The optimum fitted parameters obtained by regression are presented in Table 3.34:

Figure 3.34: *Estimated kinetic parameters (Competitive model).*

K	As' ($L \cdot gRu^{-1} \cdot min^{-1} \cdot mol^{-1} \cdot bar^{-1}$)	Ea' (KJ·mol-1)
1	1756180	-61.088
2	1310	-44.131
3	744549528	-82.618

Where **Ks** found an optimum at **5.014** $L \cdot mol^{-1}$ and **KH2** at **0.000681** bar^{-1}. With regard to the SRS (Sum of the residual squares), the optimum was achieved around 0.000441 $mol^2 \cdot L^{-2}$ and the correlation coefficient turned out to be 0.9837 for the sugar and sugar alcohol system, whereas it was 0.3173 for the byproducts one.

A more than acceptable SRS value along with high correlation ones shown a good performance of the proposed model when it comes to representing the real results. The byproducts correlation factor was not as good as the sugar system since the concentrations were very small, which makes the experimental/analytical errors be more notorious.

Despite that, the activation energy value along with the preexponential one seemed to match outstandingly with the literature [81]. The adsorption parameter was also higher for D-Xylose

than for Hydrogen, which made sense and was expected owing to the huge molecule-size difference between them.

3.5.4 Sensitivity Analysis

In order to assure that the parameters obtained were the optimum ones a sensitivity analysis was also carried out, thus plotting the parameter values against the associated objective function while remaining the other ones constant and equal to the best-fitting from the model. The appearance of sharp valleys denotes that the parameters were well-defined, and they all contribute significantly to the overall model. The sensitivity analysis results are shown as follows:

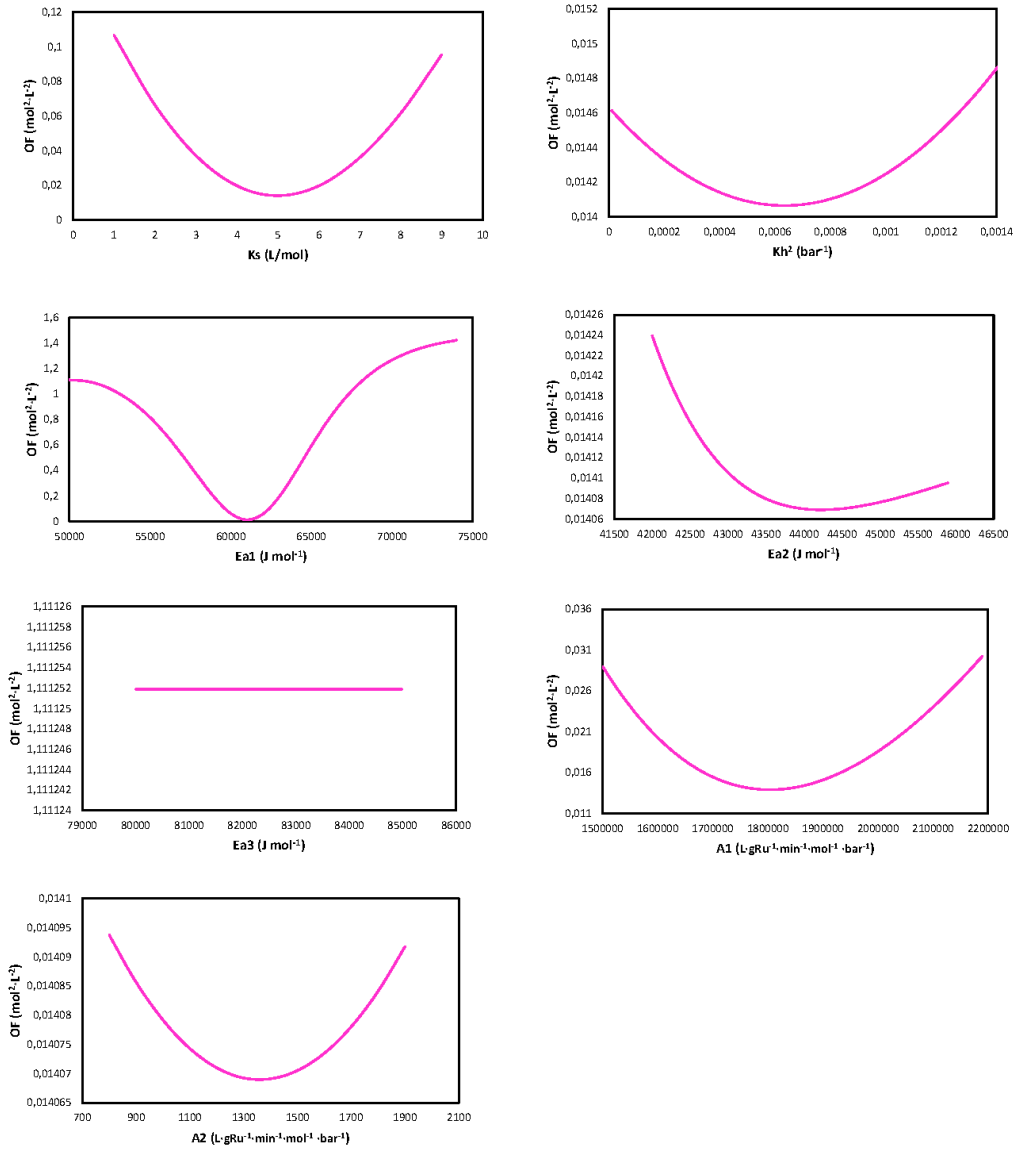

Figure 3.35: *Sensitivity analysis of fitted parameters.*

3.5.5 Model performance under different conditions

In order to check how reliable the proposed model is when performing out of the conditions it was optimized for ,(40 bar and temperatures from 90 to 120°C) , same temperatures were attempted but changing the pressure to 30 and 20 bars, since the model allows to play with the pressure. Thus, the results between reality and model are shown as follows.

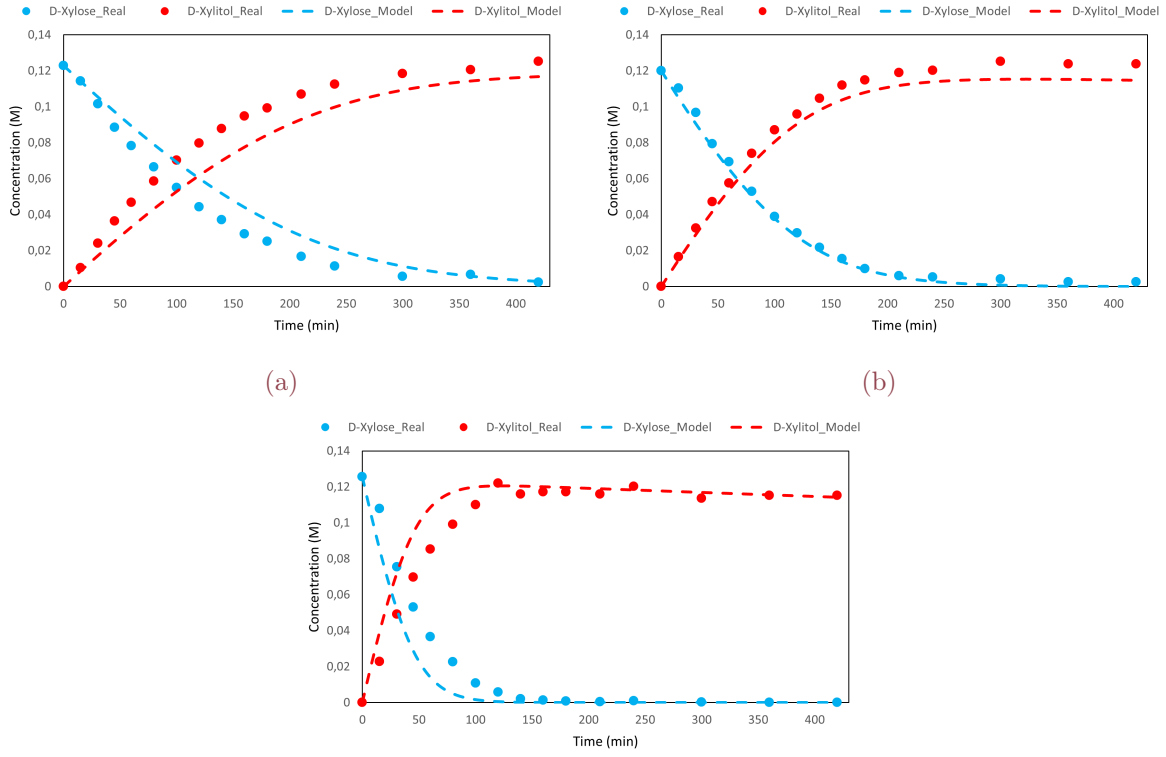

Figure 3.36: *Modelling results for D-xylose and D-xylitol at 30 bar: a) 90°C, b) 100°C and c) 120°C (Competitive model).*

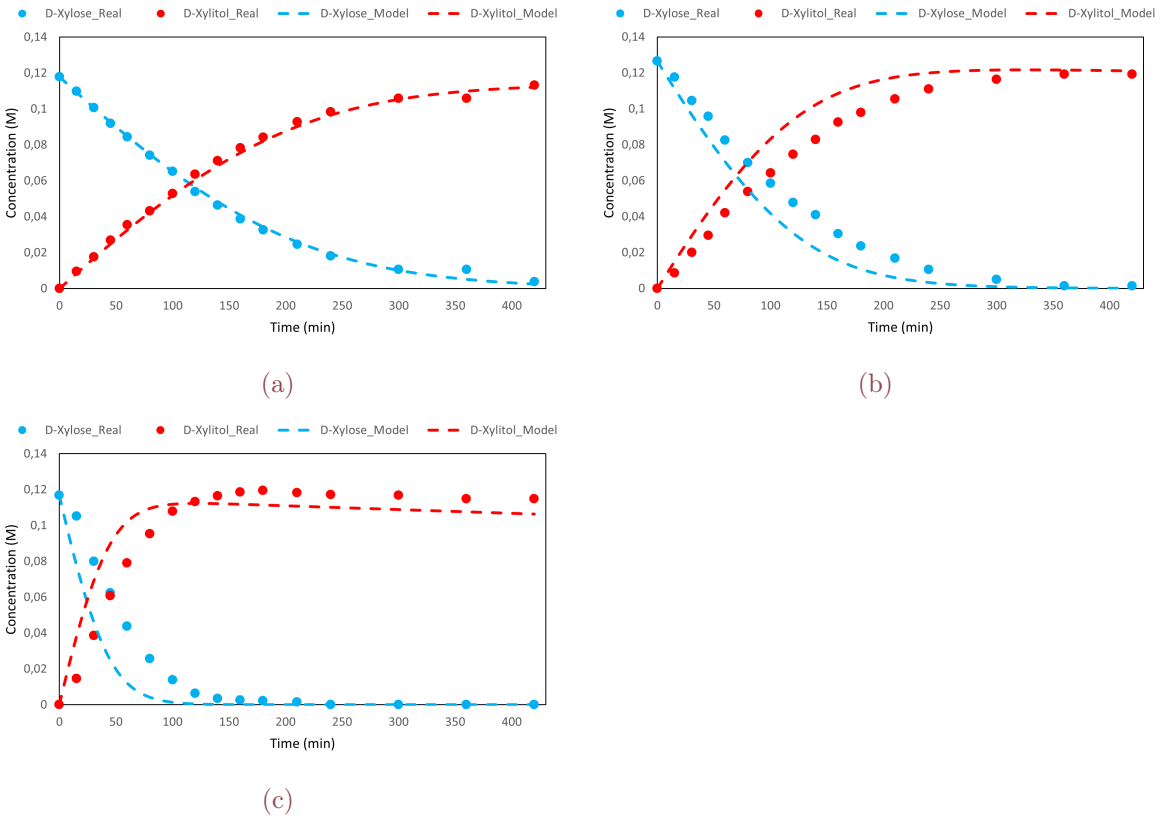

Figure 3.37: *Modelling results for the byproducts at 20 bar: a) 90°C, b) 100°C and c) 120°C (Competitive model).*

The proposed model managed to work also under different pressures it was not fitted for, thereby ending up reasonably close to the real data points. Hence, the model developed and fitted in this thesis was able to work in the range of 90-120^{o}C for different pressures in a very precise way, as the error between real and fitted data is small enough.

3.6 Non-competitive adsorption reaction pathway

In order to investigate what model fits the best with the real data, a non competitive adsoprtion reaction pathway model has been attempted. Being θ an active site for sugar adsorption and θ' site for hydrogen adsorption. Hence, the new kinetic equations are:

$$S + \ \theta \ \overset{\text{Ks}}{\leftrightarrow} \theta S \tag{3.39}$$

$$H_2 + \ \theta' \ \overset{K_{H_2}}{\leftrightarrow} H_2\theta' \tag{3.40}$$

$$H_2\theta' + \theta S \ \overset{K1}{\rightarrow} \ \theta S_{\text{OH}} + \ \theta' \tag{3.41}$$

$$\theta S_{\text{OH}} \ \overset{K_{S_{\text{OH}}}}{\leftrightarrow} \ S_{\text{OH}} + \ \theta \tag{3.42}$$

$$\theta S_{\text{OH}} \ \overset{K2}{\rightarrow} \theta Ara \tag{3.43}$$

$$\theta Ara \overset{\text{Kara}}{\rightarrow} \theta + \ Ara \tag{3.44}$$

$$\theta S \overset{K3}{\rightarrow} \theta Ery \tag{3.45}$$

$$\theta Ery \overset{\text{Kery}}{\rightarrow} \ \theta + \ Ery \tag{3.46}$$

Which, at the end, results in the following equations:

$$r_1 = \frac{K_1 \cdot K\ s \cdot S \cdot H_2 \cdot K_{H_2}}{(1 + Ks \cdot S + Ks_{OH} \cdot S_{OH} + \ KAra\ \cdot A\ r\ a\ +\ KEry\ \cdot E\ r\ y\ ) \cdot (1 + K_{H_2} \cdot H_2)} \tag{3.47}$$

$$r_2 = \frac{K_2 \cdot K\ s_{OH} \cdot S_{OH}}{(1 + Ks \cdot S + Ks_{OH} \cdot S_{OH} + \ KAra\ \cdot A\ r\ a\ +\ KEry\ \cdot E\ r\ y\ ) \cdot (1 + K_{H_2} \cdot H_2)} \tag{3.48}$$

$$r_3 = \frac{K_2 \cdot K\ s \cdot S}{(1 + Ks \cdot S + Ks_{OH} \cdot S_{OH} + \ KAra\ \cdot A\ r\ a\ +\ KEry\ \cdot E\ r\ y\ ) \cdot (1 + K_{H_2} \cdot H_2)} \tag{3.49}$$

Resulting in a simplified model such as:

$$r_1 = \frac{A_1 \cdot \ e^{\left(\frac{-Ea_1}{R \cdot T}\right)} \cdot S \cdot H_2}{(1 + Ks \cdot S) \cdot (1 + K_{H_2} \cdot H_2\ )} \tag{3.50}$$

$$r_2 = \frac{A_2 \cdot \ e^{\left(\frac{-Ea_2}{R \cdot T}\right)} \cdot S_{OH}}{(1 + Ks \cdot S) \cdot (1 + K_{H_2} \cdot H_2\ )} \tag{3.51}$$

$$r_3 = \frac{A_3 \cdot \ e^{\left(\frac{-Ea_3}{R \cdot T}\right)} \cdot S}{(1 + Ks \cdot S) \cdot (1 + K_{H_2} \cdot H_2\ )} \tag{3.52}$$

Thus, the fitting and the kinetic parameters obtained from the optimization are:

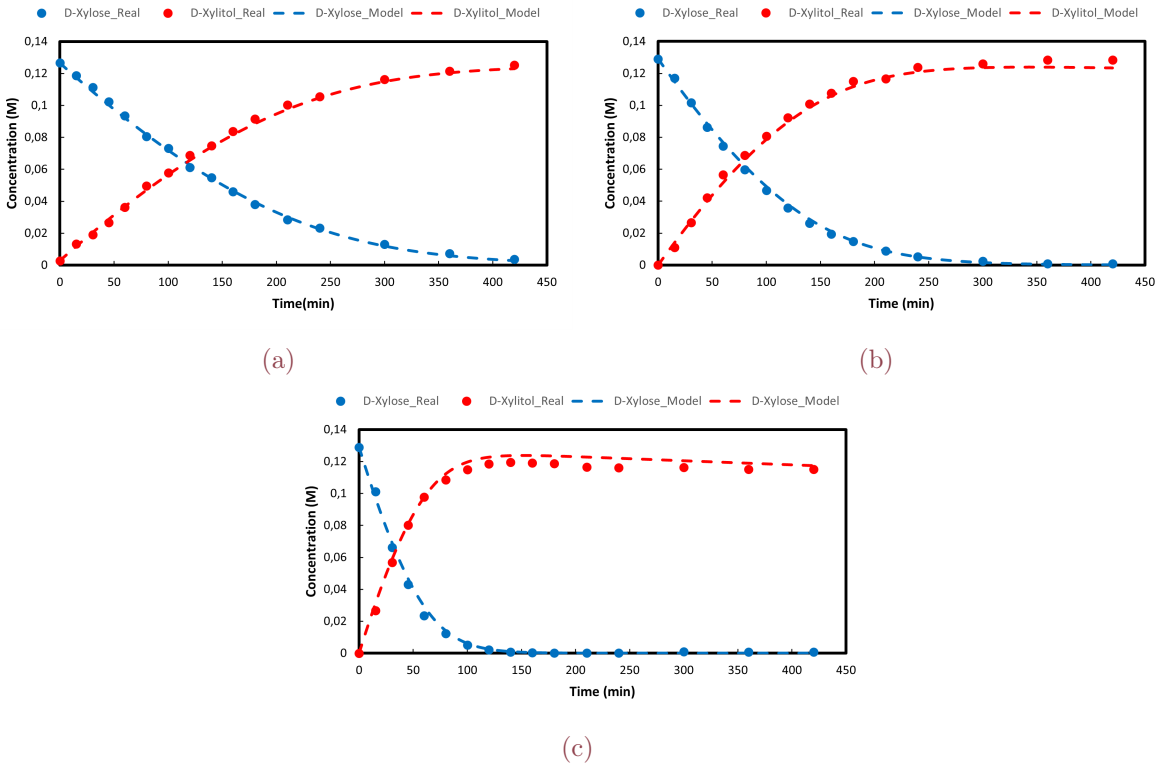

Figure 3.38: *Modelling results for D-xylose and D-xylitol at 40 bar: a) 90°C, b) 100°C and c) 120°C (Non-competitive model).*

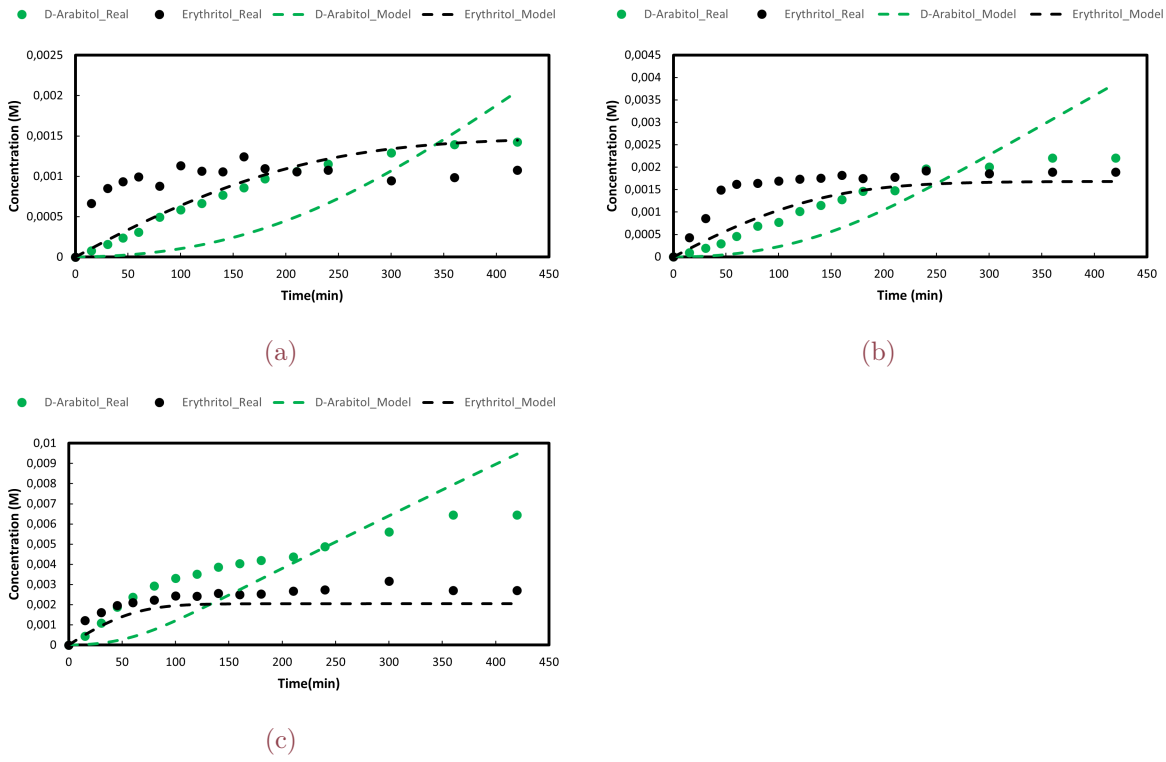

Figure 3.39: *Modelling results for the byproducts at 40 bar: a) 90°C, b) 100°C and c) 120°C. (Non-competitive model).*

Table 3.5: *Estimated kinetic parameters (Non-Competitive model).*

K	As' ($L \cdot gRu^{-1} \cdot min^{-1} \cdot mol^{-1} \cdot bar^{-1}$)	Ea' (KJ·mol-1)
1	58680	-50.685
2	728	-41.851
3	1656105	-63.028

Where **Ks** found an optimum at **13.54** $L \cdot mol^{-1}$ and **KH2** at **0.0009** bar^{-1}. With regard to the SRS (Sum of the residual squares), the optimum was achieved around 0.00055 $mol^2 \cdot L^{-2}$ and the correlation coefficient turned out to be 0.9957 for the sugar and sugar alcohol system, whereas it was 0.451 for the byproducts one.

In order to check how reliable the proposed model is when performing out of the conditions it was optimized for ,(40 bar and temperatures from 90 to 120°C) , same temperatures were attempted but changing the pressure to 30 and 20 bars. Thus, the results between reality and model are shown as follows:

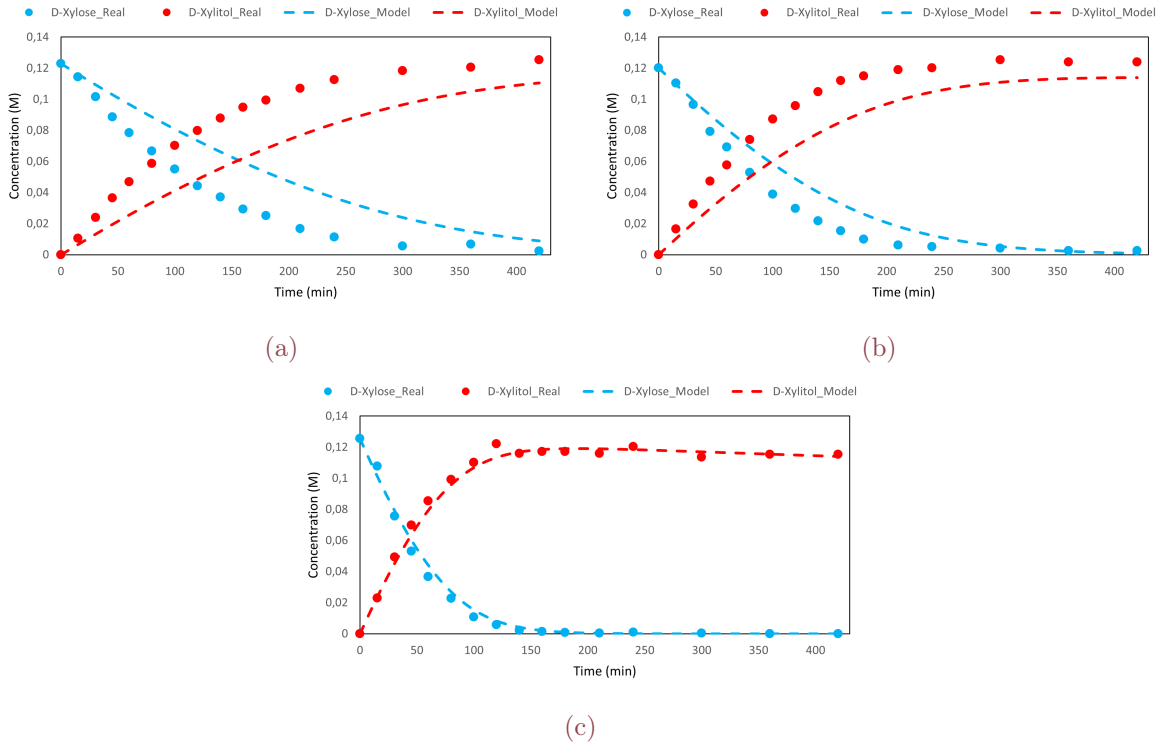

Figure 3.40: *Modelling results for D-xylose and D-xylitol at 30 bar: a) 90°C, b) 100°C and c) 120°C (Non-Competitive model).*

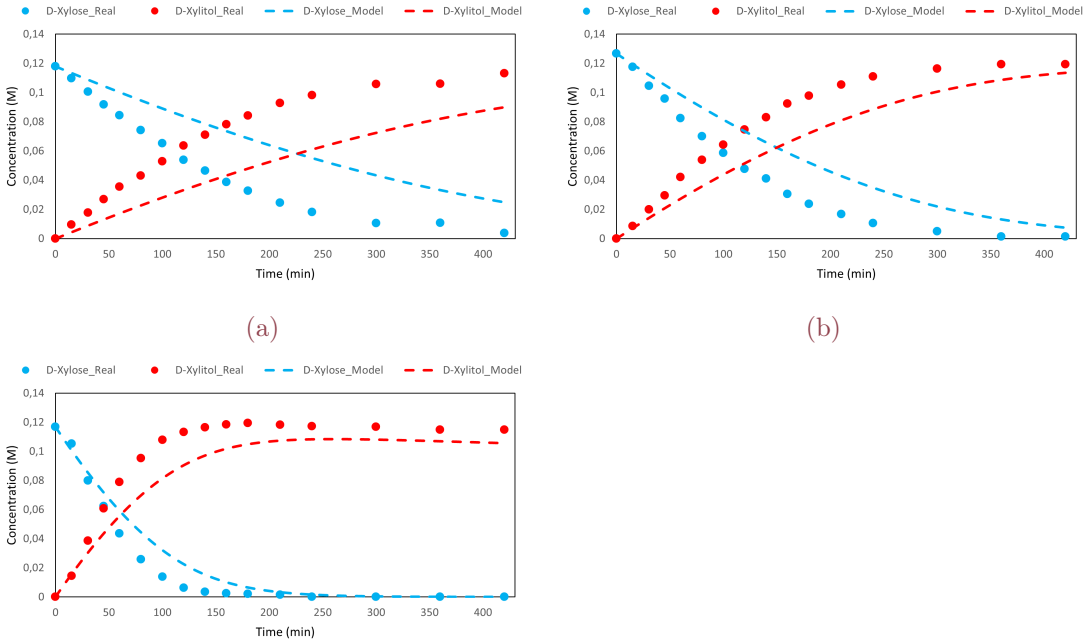

Figure 3.41: *Modelling results for D-xylose and D-xylitol at 20 bar: a) 90°C, b) 100°C and c) 120°C (Non-Competitive model).*

3.7 Semi-empirical adsorption reaction pathway.

A semi-empirical adsorption model was also attempted, thus obtaining the following equations:

$$r_1 = \frac{K_1 \cdot K\ s \cdot S \cdot H_2 \cdot K_{H_2}}{(1 + Ks \cdot S + K_{H_2} \cdot H_2 + Ks_{OH} \cdot S_{OH} + \ KAra\ \cdot A\ r\ a\ +\ KEry\ \cdot E\ r\ y\ \ )} \tag{3.53}$$

$$r_2 = \frac{K_2 \cdot K\ s_{OH} \cdot S_{OH}}{1 + Ks \cdot S + K_{H_2} \cdot H_2 + Ks_{OH} \cdot S_{OH} + \ KAra\ \cdot A\ r\ a\ +\ KEry\ \cdot E\ r\ y} \tag{3.54}$$

$$r_3 = \frac{K_3 \cdot K\ s \cdot S}{1 + Ks \cdot S + K_{H_2} \cdot H_2 + Ks_{OH} \cdot S_{OH} + \ KAra\ \cdot A\ r\ a\ +\ KEry\ \cdot E\ r\ y} \tag{3.55}$$

Which can be simplified to:

$$r_1 = \frac{K_1 \cdot K\ s \cdot S \cdot H_2 \cdot K_{H_2}}{(1 + Ks \cdot S + K_{H_2} \cdot H_2\ )} \tag{3.56}$$

$$r_2 = \frac{K_2 \cdot K\ s_{OH} \cdot S_{OH}}{1 + Ks \cdot S + K_{H_2} \cdot H_2} \tag{3.57}$$

$$r_3 = \frac{K_2 \cdot K\ s \cdot S}{1 + Ks \cdot S + K_{H_2} \cdot H_2} \tag{3.58}$$

Thus, the fitting and the kinetic parameters obtained from the optimization are:

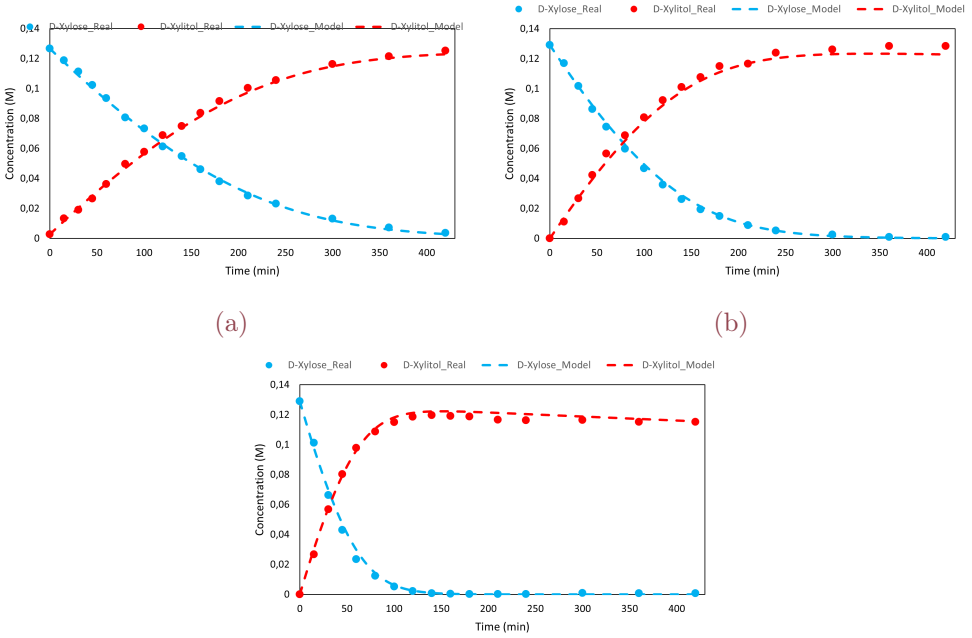

Figure 3.42: *Modelling results for D-xylose and D-xylitol at 40 bar: a) 90°C, b) 100°C and c) 120°C (Semi-empirical model).*

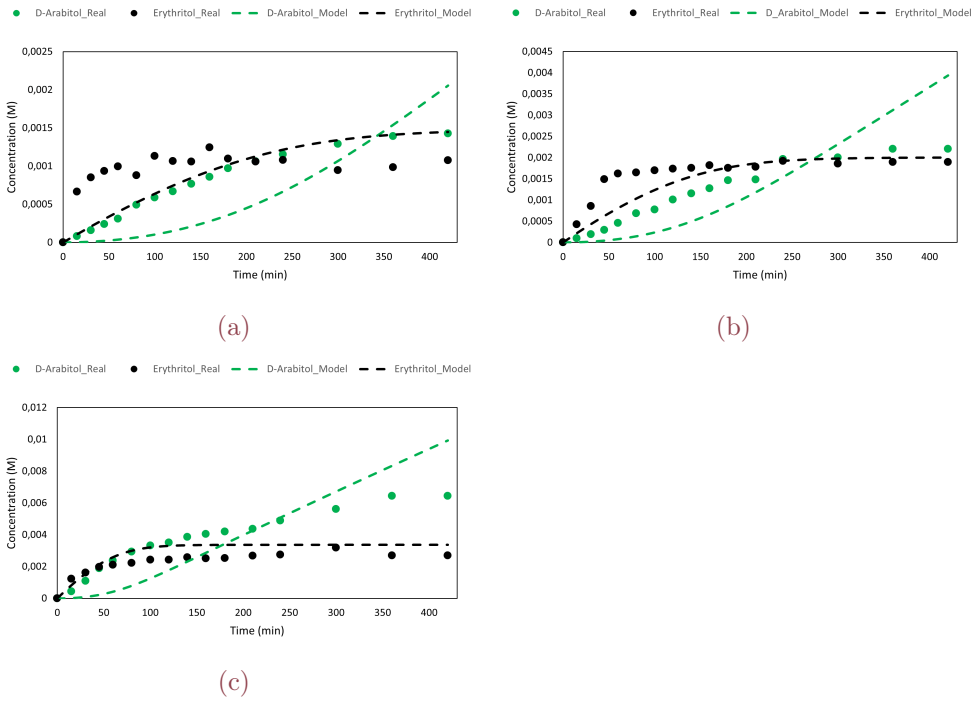

Figure 3.43: *Modelling results for the byproducts at 40 bar: a) 90°C, b) 100°C and c) 120°C. (Semi-empirical model).*

Table 3.6: *Estimated kinetic parameters (Non-Competitive model).*

K	As' ($L \cdot gRu^{-1} \cdot min^{-1} \cdot mol^{-1} \cdot bar^{-1}$)	Ea' (KJ·mol-1)
1	47739	-50.085
2	1598	-44.250
3	1002756296	-82.392

Where **Ks** found an optimum at **13.93** $L \cdot mol^{-1}$ and **KH2** at **0.000696** bar^{-1}. With regard to the SRS (Sum of the residual squares), the optimum was achieved around 0.00055 $mol^2 \cdot L^{-2}$ and the correlation coefficient turned out to be 0.9965 for the sugar and sugar alcohol system, whereas it was 0.3863 for the byproducts one.

Testing it now for conditions it was not optimized for:

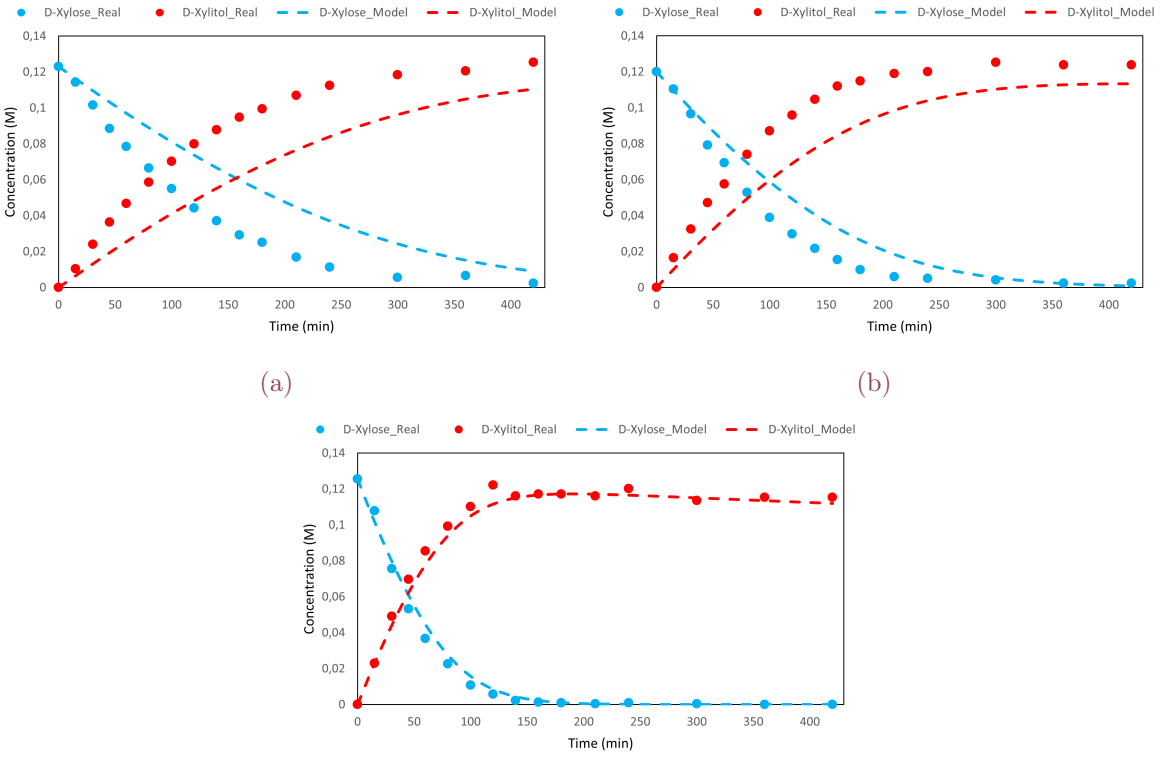

Figure 3.44: *Modelling results for D-xylose and D-xylitol at 30 bar: a) 90°C, b) 100°C and c) 120°C (Semi-empirical model).*

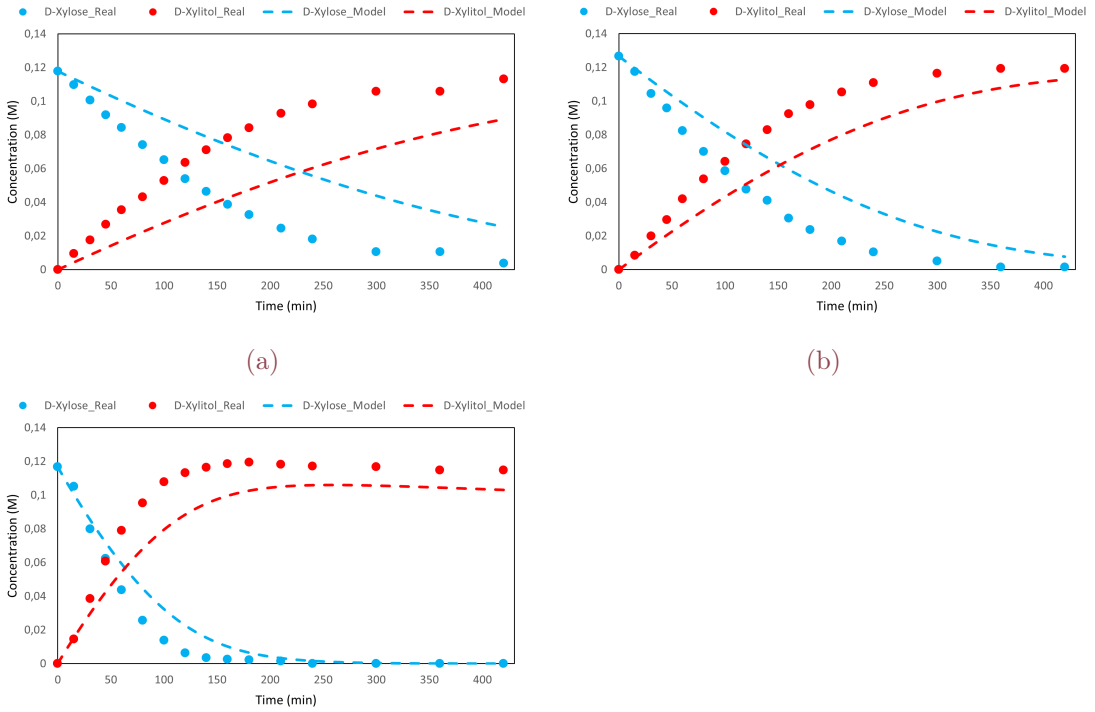

Figure 3.45: *Modelling results for D-xylose and D-xylitol at 20 bar: a) 90°C, b) 100°C and c) 120°C (Semi-empirical model).*

3.8 D-Arabitol coming directly from D-Xylose

For this supposition, the new reaction pathway would result in:

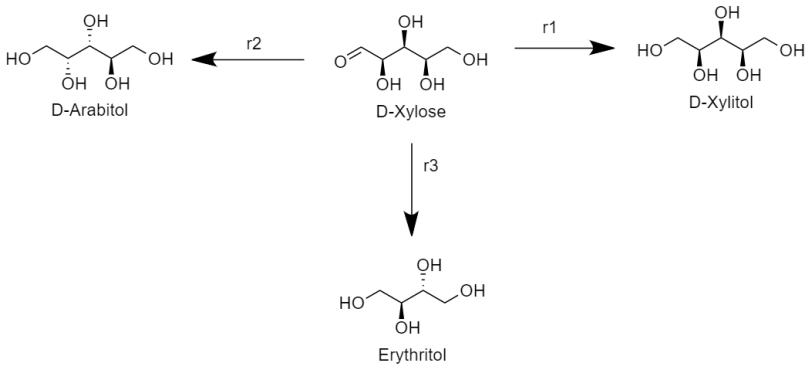

Figure 3.46: *Proposed reaction pathway 2.*

Hence, supposing a competitive model the kinetic equations would change to:

$$\frac{dS}{dt} = (-r_1 - r_2 - r_3) \cdot \rho_B \tag{3.59}$$

$$\frac{dS_{OH}}{dt} = r_1) \cdot \rho_B \tag{3.60}$$

$$\frac{dAra}{dt} = r_2 \cdot \rho_B \tag{3.61}$$

$$\frac{dEry}{dt} = r_3 \cdot \rho_B \tag{3.62}$$

$$\rho_B = \frac{m_{cat}}{v_L} \tag{3.63}$$

And adding now the balance of the catalyst sites:

$$r_1 = \frac{K_1 \cdot K\ s \cdot S \cdot H_2 \cdot K_{H_2}}{(1 + Ks \cdot S + K_{H_2} \cdot H_2 + Ks_{OH} \cdot S_{OH} + \ KAra\ \cdot A\ r\ a\ +\ KEry\ \cdot E\ r\ y\ )^2} \tag{3.64}$$

$$r_2 = \frac{K_2 \cdot K\ s \cdot S}{1 + Ks \cdot S + K_{H_2} \cdot H_2 + Ks_{OH} \cdot S_{OH} + \ KAra\ \cdot A\ r\ a\ +\ KEry\ \cdot E\ r\ y} \tag{3.65}$$

$$r_3 = \frac{K_3 \cdot K\ s \cdot S}{1 + Ks \cdot S + K_{H_2} \cdot H_2 + Ks_{OH} \cdot S_{OH} + \ KAra\ \cdot A\ r\ a\ +\ KEry\ \cdot E\ r\ y} \tag{3.66}$$

That finally result in:

$$r_1 = \frac{A_1 \cdot \ e^{\left(\frac{-Ea_1}{R \cdot T}\right)} \cdot S \cdot H_2}{(1 + Ks \cdot S + K_{H_2} \cdot H_2\ )^2} \tag{3.67}$$

$$r_2 = \frac{A_2 \cdot \ e^{\left(\frac{-Ea_2}{R \cdot T}\right)} \cdot S}{1 + Ks \cdot S + K_{H_2} \cdot H_2} \tag{3.68}$$

$$r_3 = \frac{A_3 \cdot \ e^{\left(\frac{-Ea_3}{R \cdot T}\right)} \cdot S}{1 + Ks \cdot S + K_{H_2} \cdot H_2} \tag{3.69}$$

Thus, the fitting and the kinetic parameters obtained from the optimization are:

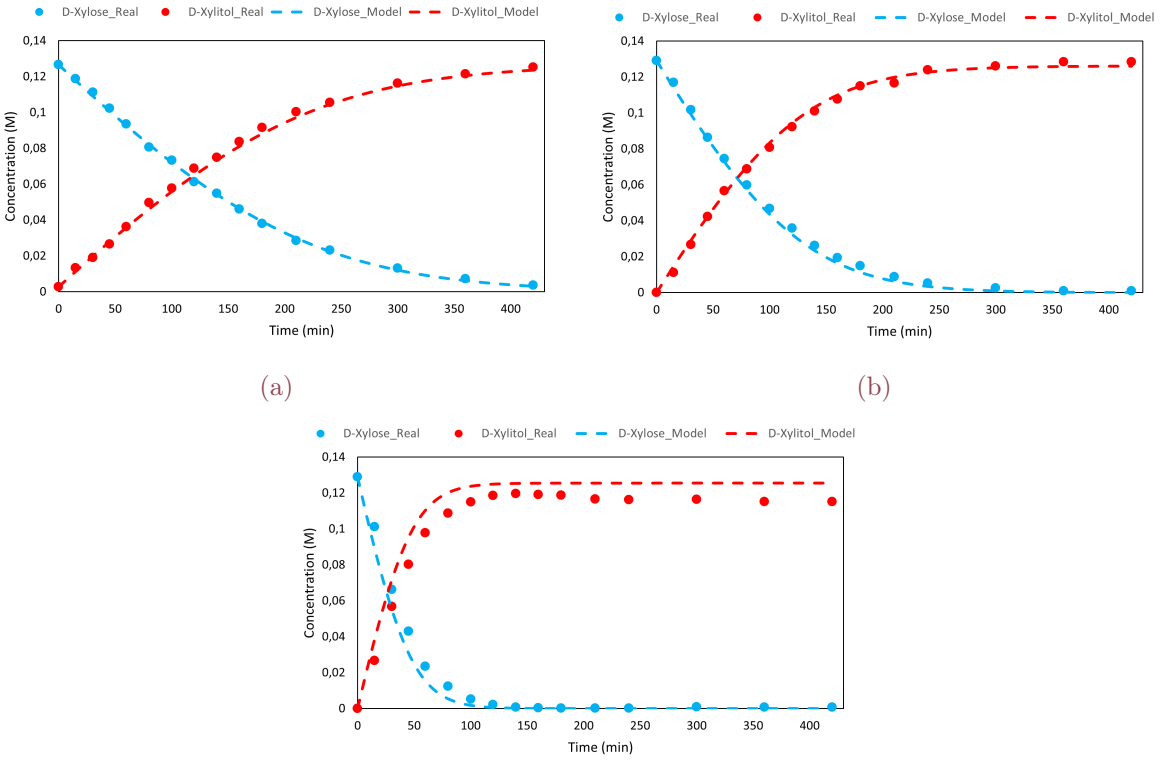

Figure 3.47: *Modelling results for D-xylose and D-xylitol at 40 bar: a) 90°C, b) 100°C and c) 120°C (Prposed reaction pathway 2 and Competitive model).*

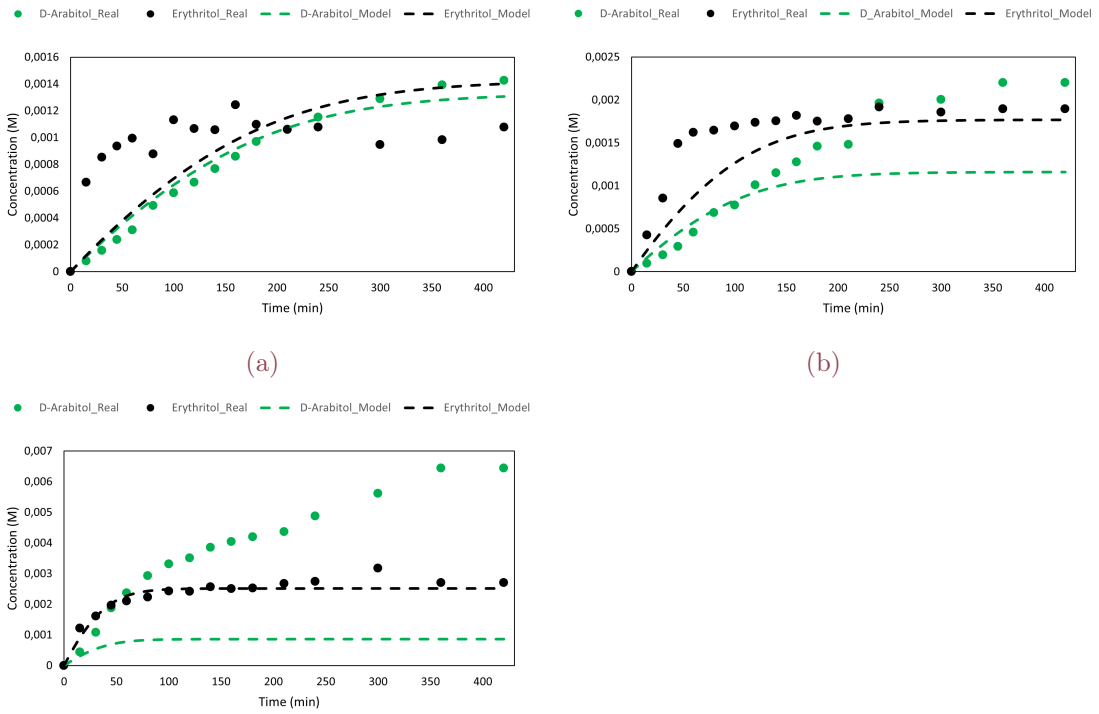

Figure 3.48: *Modelling results for the byproducts at 40 bar: a) 90°C, b) 100°C and c) 120°C (Proposed reaction pathway 2 and Competitive model).*

Table 3.7: *Estimated kinetic parameters for proposed reaction pathway 2 (Competitive model).*

K	As' ($L \cdot gRu^{-1} \cdot min^{-1} \cdot mol^{-1} \cdot bar^{-1}$)	Ea' (KJ·mol-1)
1	1643912	-60.881
2	1347	-42.877
3	757803548	-82.642

Where **Ks** found an optimum at **5.068** $L \cdot mol^{-1}$ and **KH2** at **0.00074** bar^{-1}. With regard to the SRS (Sum of the residual squares), the optimum was achieved around 0.00040 $mol^2 \cdot L^{-2}$ and the correlation coefficient turned out to be 0.9812 for the sugar and sugar alcohol system, whereas it was 0.0467 for the byproducts one.

With this proposed pathway, the main sugars D-xylose and D-xylitol are represented in an accurate way, but the byproducts are not. Since D-arabitol, the one that has been supposed to come directly from the main sugar D-xylose, it's the worst one, since the model is not capable of predicting its behaviour.

It could be concluded then that D-arabitol, for this case, does not come from D-xylose but from D-xylitol, as it was modeled in Section 3.5.

3.9 Model comparison.

The coefficients of determination for the models tested are presented in Table 3.8 :

Table 3.8: *Coefficients of determination for the models studied.*

	Pathway a)		Pathway b)	
	Sugar Hydrog.	*By Products*	*Sugar Hydrog.*	*By Products*
Competitive	0.9837	0.3173	0.9812	0.0467
Non Competitive	0.9957	0.451	-	-
Semi-empirical	0.9965	0.3863	-	-

Although the pathway b) option is able to represent the sugar hydrogenation system accurately, 98% of determination, it is, on the other hand, not capable of doing the same with the byproducts, thus being the pathway a) the best option, since higher coefficients are achieved for both systems.

For this proposition, the non competitive model turned out to be the most promising one when describing the process, since the highest fitting coefficients are achieved, 99 and 45%.

Chapter 4

Conclusions

The aim of this work was to improve the catalyst developed by German [16], whilst studying the reaction kinetics of the selective hydrogenation of D-Xylose into D-Xylitol and its respective byproducts.

The thesis is divided into 3 parts. The first one has to do with the catalyst preparation, covering the necessary steps carried out as well as the results of each. The second one was dedicated to study the kinetic data, carrying out experiments under typical hydrogen conditions, with temperatures ranging from 60 to 120°C, pressures between 20 and 60 bar and initial D-Xylose concentrations of 0.065, 0.13 and 0.26M. The third part focused on the modelling, obtaining kinetic parameters to be able to model all the identified byproducts as well as the pressure term.

Starting from the open-cell catalyst foam developed by German, the addition of PEG, when coating the foam, exhibited an increase in the average pore width from around 1 until even 40 nm, thereby increasing 40% the conversion. The limit amount of PEG to work with resulted in 20% wt, since no carbon remained on the foam after pyrolysis.

A water-washing step was also added to the recipe, in order to assure no polymer remained on the catalyst surface. Finally, through incipient wetness impregnation, the average Ru nanoparticle turned out to be around 4 nm.

With regard to the kinetics, conversions in the range of 60-100% were accomplished, depending on the working conditions. Moreover, D-Xylitol yields around 58-99% were achieved. When it comes to D-Xylitol selectivity, the developed open-cell was very selective, as purities in the range of 95-98.7% were achieved. In addition, a selectivity barrier was found around 98.5-7%, and it could not be overcome by changing neither the temperature nor the pressure. Despite that, temperature and pressure seemed to have an important influence on this parameter, since the highest purities were found at low temperatures and high pressures. The optimum conditions, taking into account selectivity and velocity, was found to be around 90ºC and pressures around 40 bar or even higher. 60°C temperatures were not recommended due to the slow kinetics it performs with.

A kinetic model based on a competitive and non-competitive adsorption behaviour between the sugar molecules and hydrogen was fitted to experimental data, adding also the pressure term.

A very successful match between real and simulated concentration profiles were achieved for the pair D-Xylose and D-Xylitol, being able to simulate the sugars under different pressures. Regarding the byproducts, they were also fitted but with more difficulties, since its concentration profiles were a bit noisy, owing to the fact that its concentrations were on the detection limit of the HPLC.

It was also attempted a reaction pathway in which the D-Arabitol comes directly from D-xylose, but the results were not that accurate, which means that this compound is produced directly from D-xylitol, the main supposition, and not from D-xylose.

After 180h of use, some catalyst deactivation was observed, since the conversion decreased around 13% after 100 minutes of reaction. The agglomeration of the Ru nanoparticles was found to be the main deactivation reason through TEM micrographs. The particles grew from around 4 nm to 8 nm. Despite that, the catalyst exhibited good selectivity, activity and stability.

No Ru leaching, under the experimental conditions, was neither detected (detection limit:$<$0.03 mg/L).

Many research opportunities can be derived from the results of this study, such as the scaling up of the carbon coating and anodic oxidation methods, reducing the number of impregnation stages for the ruthenium inclusion technique, discus if the catalyst cleaning step is necessary...

In terms of industrial scaling up, the next step may be to employ the created foam catalyst in a continuous mode in a reactor structure that takes advantage of the high mass and heat transfer rates, as well as the low resistance to diffusion, associated with this type of catalyst. Furthermore, higher pressures and longer reaction times might as well be attempted, in order to give the final "push" to the selectivity.

Bibliography

[1] G. Bhutada. Visualizing the history of energy transitions. [Online]. Available: https://www.visualcapitalist.com/visualizing-the-history-of-energy-transitions/

[2] B. p.l.c. Statistical review of world energy | energy economics | home. [Online]. Available: https://www.bp.com/en/global/corporate/energy-economics/statistical-review-of-world-energy.html

[3] N. US Department of Commerce. Global monitoring laboratory - carbon cycle greenhouse gases. [Online]. Available: https://gml.noaa.gov/ccgg/trends/global.html

[4] C. P. Morice, J. J. Kennedy, N. A. Rayner, and P. D. Jones, "Quantifying uncertainties in global and regional temperature change using an ensemble of observational estimates: The HadCRUT4 data set: THE HADCRUT4 DATASET," vol. 117, pp. n/a–n/a. [Online]. Available: http://doi.wiley.com/10.1029/2011JD017187

[5] "Biorefineries: Targeting energy, high value products and waste valorisation," ser. Lecture Notes in Energy, M. Rabaçal, A. F. Ferreira, C. A. M. Silva, and M. Costa, Eds. Springer International Publishing, vol. 57. [Online]. Available: http://link.springer.com/10.1007/978-3-319-48288-0

[6] I. Ghosh. All the biomass of earth, in one graphic. [Online]. Available: https://www.visualcapitalist.com/all-the-biomass-of-earth-in-one-graphic/

[7] Y. M. Bar-On, R. Phillips, and R. Milo, "The biomass distribution on earth," vol. 115, no. 25, pp. 6506–6511. [Online]. Available: https://pnas.org/doi/full/10.1073/pnas.1711842115

[8] A. Horvat, "A study of the uncertainty associated with tar measurement and an investigation of tar evolution and composition during the air-blown fluidised bed gasification of torrefied and non-torrefied grassy biomass," accepted: 2017-03-03T15:25:55Z Publisher: University of Limerick. [Online]. Available: https://ulir.ul.ie/handle/10344/5583

[9] Sugar alcohol market size & share | industry analysis 2020-2027. [Online]. Available: https://www.alliedmarketresearch.com/sugar-alcohol-market-A09022

[10] R. a. M. ltd. Global xylitol market by form (powder and liquid), by application (chewing gum, confectionery, bakery & other foods, oral care, and others), by regional outlook, industry analysis report and forecast, 2021 - 2027. [Online]. Available: https://www.researchandmarkets.com/reports/5514636/global-xylitol-market-by-form-powder-and

[11] Xylitol market size, report | 2022 - 27 | forecast, trends. [Online]. Available: https://www.mordorintelligence.com/industry-reports/xylitol-market

[12] Google trends. [Online]. Available: https://trends.google.com/trends/explore?date=all&q=xylitol,arabitol,galactitol,sorbitol,mannitol

[13] Stock comparison. [Online]. Available: https://portfolioslab.com/tools/stock-comparison

[14] TIKR: Institutional-grade investing for individuals. [Online]. Available: https://app.tikr.com

[15] P. H. Ho, M. Ambrosetti, G. Groppi, E. Tronconi, R. Palkovits, G. Fornasari, A. Vaccari, and P. Benito, "Structured catalysts-based on open-cell metallic foams for energy and environmental applications," in *Studies in Surface Science and Catalysis*. Elsevier, vol. 178, pp. 303–327. [Online]. Available: https://linkinghub.elsevier.com/retrieve/pii/B978044464127400015X

[16] G. Araujo-Barahona, K. Eränen, J. P. Oña, D. Murzin, J. García-Serna, and T. Salmi, "Solid foam ru/c catalysts for sugar hydrogenation to sugar alcoholspreparation, characterization, activity, and selectivity," vol. 61, no. 7, pp. 2734–2747. [Online]. Available: https://pubs.acs.org/doi/10.1021/acs.iecr.1c04501

[17] S. I. Mussatto, "Application of xylitol in food formulations and benefits for health," in *D-Xylitol*, S. S. da Silva and A. K. Chandel, Eds. Springer Berlin Heidelberg, pp. 309–323. [Online]. Available: http://link.springer.com/10.1007/978-3-642-31887-0_14

[18] World population clock: 7.95 billion people (2022) - worldometer. [Online]. Available: https://www.worldometers.info/world-population/

[19] D. Hoornweg, P. Bhada-Tata, and C. Kennedy, "Environment: Waste production must peak this century," vol. 502, no. 7473, pp. 615–617, number: 7473 Publisher: Nature Publishing Group. [Online]. Available: https://www.nature.com/articles/502615a

[20] H. Ritchie, M. Roser, and P. Rosado, "CO and greenhouse gas emissions." [Online]. Available: https://ourworldindata.org/co2-and-other-greenhouse-gas-emissions

[21] D. J. Wuebbles, D. W. Fahey, and K. A. Hibbard, "Climate science special report: fourth national climate assessment, volume i," 2017.

[22] K. S. Deffeyes, *Hubbert's Peak: The Impending World Oil Shortage - New Edition*. Princeton University Press, publication Title: Hubbert's Peak. [Online]. Available: https://www.degruyter.com/document/doi/10.1515/9781400829071/html

[23] 5 global issues to watch in 2020. [Online]. Available: https://unfoundation.org/blog/post/5-global-issues-to-watch-in-2020/

[24] Renewable carbon publications. [Online]. Available: https://renewable-carbon.eu/publications/

[25] "Climate change 2021: The physical science basis. contribution of working group i to the sixth assessment report of the intergovernmental panel on climate change."

[26] W. E. Mabee, D. J. Gregg, and J. N. Saddler, "Assessing the emerging biorefinery sector in canada," vol. 123, no. 1, pp. 0765–0778. [Online]. Available: http://link.springer.com/10.1385/ABAB:123:1-3:0765

[27] C. D. Pinales-Márquez, R. M. Rodríguez-Jasso, R. G. Araújo, A. Loredo-Treviño, D. Nabarlatz, B. Gullón, and H. A. Ruiz, "Circular bioeconomy and integrated biorefinery in the production of xylooligosaccharides from lignocellulosic biomass: A review," vol. 162, p. 113274. [Online]. Available: https://linkinghub.elsevier.com/retrieve/pii/S0926669021000388

[28] T. Arai, P. Biely, I. Uhliariková, N. Sato, S. Makishima, M. Mizuno, K. Nozaki, S. Kaneko, and Y. Amano, "Structural characterization of hemicellulose released from corn cob in continuous flow type hydrothermal reactor," vol. 127, no. 2, pp. 222–230. [Online]. Available: https://linkinghub.elsevier.com/retrieve/pii/S1389172318302640

[29] J. Xu, B. Liu, L. Wu, J. Hu, H. Hou, and J. Yang, "A waste-minimized biorefinery scenario for the hierarchical conversion of agricultural straw into prebiotic xylooligosaccharides, fermentable sugars and lithium-sulfur batteries," vol. 129, pp. 269–280. [Online]. Available: https://linkinghub.elsevier.com/retrieve/pii/S0926669018310549

[30] O. Ajao, M. Marinova, O. Savadogo, and J. Paris, "Hemicellulose based integrated forest biorefineries: Implementation strategies," vol. 126, pp. 250–260. [Online]. Available: https://linkinghub.elsevier.com/retrieve/pii/S0926669018308872

[31] D. L. Aguilar, R. M. Rodríguez-Jasso, E. Zanuso, D. J. de Rodríguez, L. Amaya-Delgado, A. Sanchez, and H. A. Ruiz, "Scale-up and evaluation of hydrothermal pretreatment in isothermal and non-isothermal regimen for bioethanol production using agave bagasse," vol. 263, pp. 112–119. [Online]. Available: https://linkinghub.elsevier.com/retrieve/pii/S0960852418306230

[32] S. L. Baptista, L. C. Carvalho, A. Romaní, and L. Domingues, "Development of a sustainable bioprocess based on green technologies for xylitol production from corn cob," vol. 156, p. 112867. [Online]. Available: https://linkinghub.elsevier.com/retrieve/pii/S0926669020307846

[33] S. González-García, P. C. Morales, and B. Gullón, "Estimating the environmental impacts of a brewery waste–based biorefinery: Bio-ethanol and xylooligosaccharides joint production case study," vol. 123, pp. 331–340. [Online]. Available: https://linkinghub.elsevier.com/retrieve/pii/S0926669018306034

[34] M. S. Pino, R. M. Rodríguez-Jasso, M. Michelin, A. C. Flores-Gallegos, R. Morales-Rodriguez, J. A. Teixeira, and H. A. Ruiz, "Bioreactor design for enzymatic hydrolysis of biomass under the biorefinery concept," vol. 347, pp. 119–136. [Online]. Available: https://linkinghub.elsevier.com/retrieve/pii/S1385894718306235

[35] J. Esteban, P. Yustos, and M. Ladero, "Catalytic processes from biomass-derived hexoses and pentoses: A recent literature overview," vol. 8, no. 12, p. 637. [Online]. Available: http://www.mdpi.com/2073-4344/8/12/637

[36] T. A. Werpy, J. E. Holladay, and J. F. White, "Top value added chemicals from biomass: I. results of screening for potential candidates from sugars and synthesis gas," pp. PNNL–14 808, 926 125. [Online]. Available: http://www.osti.gov/servlets/purl/926125-eeUkhS/

[37] M. K. Islam, H. Wang, S. Rehman, C. Dong, H.-Y. Hsu, C. S. K. Lin, and S.-Y. Leu, "Sustainability metrics of pretreatment processes in a waste derived lignocellulosic biomass biorefinery," vol. 298, p. 122558. [Online]. Available: https://linkinghub.elsevier.com/retrieve/pii/S0960852419317882

[38] N. Bhagavan, "Simple carbohydrates," in *Medical Biochemistry*. Elsevier, pp. 133–151. [Online]. Available: https://linkinghub.elsevier.com/retrieve/pii/B9780120954407500111

[39] C. van Loveren, "Sugar alcohols: What is the evidence for caries-preventive and caries-therapeutic effects?" vol. 38, no. 3, pp. 286–293. [Online]. Available: https://www.karger.com/Article/FullText/77768

[40] Global sugar alcohol market report and forecast 2022-2027. [Online]. Available: https://www.expertmarketresearch.com/reports/sugar-alcohol-market

[41] International journal of advance research in engineering technology and sciences. [Online]. Available: http://www.ijarets.org/current-issue-part.php?journalId=85

[42] O. N. L. \. O. N. L. Bakal, A., *Alternative sweeteners*.

[43] M. Gliemmo, A. Calviño, O. Tamasi, L. Gerschenson, and C. Campos, "Interactions between aspartame, glucose and xylitol in aqueous systems containing potassium sorbate," vol. 41, no. 4, pp. 611–619. [Online]. Available: https://linkinghub.elsevier.com/retrieve/pii/S0023643807001843

[44] M. C. A. Maia, A. P. G. L. K. Galvão, R. C. D. Modesta, and N. Pereira Júnior, "Avaliação do consumidor sobre sorvetes com xilitol," vol. 28, no. 2, pp. 341–347. [Online]. Available: http://www.scielo.br/scielo.php?script=sci_arttext&pid=S0101-20612008000200011&lng=pt&nrm=iso&tlng=pt

[45] F. Ronda, "Effects of polyols and nondigestible oligosaccharides on the quality of sugar-free sponge cakes," vol. 90, no. 4, pp. 549–555. [Online]. Available: https://linkinghub.elsevier.com/retrieve/pii/S0308814604003607

[46] U. Manz, E. Vanninen, and F. Voirol, "Xylitol: its properties and use as a sugar substitute in foods."

[47] T. Pepper and P. Olinger, "Xylitol in sugar-free confections," vol. 42, no. 10, pp. 98–106.

[48] A. Bakal, L. O'Brien Nabors, and L. O'Brien Nabors, "Alternative sweeteners," publisher: Dekker: New York.

[49] R. Ylikahri, "Metabolic and nutritional aspects of xylitol," in *Advances in Food Research*. Elsevier, vol. 25, pp. 159–180. [Online]. Available: https://linkinghub.elsevier.com/retrieve/pii/S0065262808602372

[50] E. Vieira-Neto, C. Pereira, and A. Fonseca, "Avaliação do desempenho de rastreamento neonatal de deficiência de glicose-6-fosfato desidrogenase em amostras de sangue em papel filtro," no. 119, pp. 98–104.

[51] L. Luzzatto, C. Nannelli, and R. Notaro, "Glucose-6-phosphate dehydrogenase deficiency," vol. 30, no. 2, pp. 373–393. [Online]. Available: https://linkinghub.elsevier.com/retrieve/pii/S0889858815001938

[52] J. Van Eys, "Xylitol as a therapeutic agent in glucose-6-phosphate dehydrogenase deficiency." pp. 613–631, publisher: Academic Press.

[53] K. K. Mäkinen, J. Olak, S. Russak, M. Saag, T. Seedre, R. Vasar, T. Vihalemm, M. Mikelsaar, and P.-L. Mäkinen, "Polyol-combinant saliva stimulants: a 4-month pilot study in young adults," vol. 56, no. 2, pp. 90–94. [Online]. Available: http://www.tandfonline.com/doi/full/10.1080/00016359850136049

[54] J. T. Autio, "Effect of xylitol chewing gum on salivary streptococcus mutans in preschool children," vol. 69, no. 1, pp. 81–86.

[55] D. Kandelman, "Sugar, alternative sweeteners and meal frequency in relation to caries prevention: new perspectives," vol. 77, pp. S121–S128. [Online]. Available: https://www.cambridge.org/core/product/identifier/S0007114597000147/type/journal_article

[56] J. Erramouspe and C. A. Heyneman, "Treatment and prevention of otitis media," vol. 34, no. 12, pp. 1452–1468. [Online]. Available: http://journals.sagepub.com/doi/10.1345/aph.19391

[57] T. Kontiokari, M. Uhari, and M. Koskela, "Effect of xylitol on growth of nasopharyngeal bacteria in vitro," vol. 39, no. 8, pp. 1820–1823. [Online]. Available: https://journals.asm.org/doi/10.1128/AAC.39.8.1820

[58] M. Uhari, T. Kontiokari, and M. Niemelä, "A novel use of xylitol sugar in preventing acute otitis media," vol. 102, no. 4, pp. 879–884. [Online]. Available: https://publications.aap.org/pediatrics/article/102/4/879/65538/A-Novel-Use-of-Xylitol-Sugar-in-Preventing-Acute

[59] P. T. Mattila, M. J. Svanberg, K. K. Mäkinen, and M. L. Knuuttila, "Dietary xylitol, sorbitol and d-mannitol but not erythritol retard bone resorption in rats," vol. 126, no. 7, pp. 1865–1870. [Online]. Available: https://doi.org/10.1093/jn/126.7.1865

[60] J. Zabner, M. P. Seiler, J. L. Launspach, P. H. Karp, W. R. Kearney, D. C. Look, J. J. Smith, and M. J. Welsh, "The osmolyte xylitol reduces the salt concentration of airway surface liquid and may enhance bacterial killing," vol. 97, no. 21, pp. 11 614–11 619. [Online]. Available: https://pnas.org/doi/full/10.1073/pnas.97.21.11614

[61] T. Tapiainen, T. Kontiokari, L. Sammalkivi, I. Ikäheimo, M. Koskela, and M. Uhari, "Effect of xylitol on growth of *Streptococcus pneumoniae* in the presence of fructose and sorbitol," vol. 45, no. 1, pp. 166–169. [Online]. Available: https://journals.asm.org/doi/10.1128/AAC.45.1.166-169.2001

[62] H. Mitchell, *Sweeteners and sugar alternatives in food technology*. John Wiley & Sons.

[63] Xylitol market size & share | industry report, 2020-2028. [Online]. Available: https://www.grandviewresearch.com/industry-analysis/xylitol-market

[64] M. Guisnet, J. Barbier, J. Barrault, D. Duprez, C. Montassier, and G. Perot, *Heterogeneous catalysis and fine chemicals III: proceedings of the 3rd international symposium, Poitiers, April 5-8, 1993*. Elsevier, open Library ID: OL1417159M.

[65] B. J. Arena, "Deactivation of ruthenium catalysts in continuous glucose hydrogenation," vol. 87, no. 2, pp. 219–229. [Online]. Available: https://linkinghub.elsevier.com/retrieve/pii/0926860X9280057J

[66] K. van Gorp, "Catalytic hydrogenation of fine chemicals: sorbitol production," vol. 52, no. 2, pp. 349–361. [Online]. Available: https://linkinghub.elsevier.com/retrieve/pii/S0920586199000875

[67] J. Wisnlak and R. Simon, "Hydrogenation of glucose, fructose, and their mixtures," vol. 18, no. 1, pp. 50–57. [Online]. Available: https://pubs.acs.org/doi/abs/10.1021/i360069a011

[68] J. Wisniak, M. Hershkowitz, and S. Stein, "Hydrogenation of xylose over platinum group catalysts," vol. 13, no. 4, pp. 232–236. [Online]. Available: https://pubs.acs.org/doi/abs/10.1021/i360052a004

[69] E. Redina, O. Tkachenko, and T. Salmi, "Recent advances in c5 and c6 sugar alcohol synthesis by hydrogenation of monosaccharides and cellulose hydrolytic hydrogenation over non-noble metal catalysts," vol. 27, no. 4, p. 1353. [Online]. Available: https://www.mdpi.com/1420-3049/27/4/1353

[70] P. Gallezot, P. Cerino, B. Blanc, G. Fleche, and P. Fuertes, "Glucose hydrogenation on promoted raney-nickel catalysts," vol. 146, no. 1, pp. 93–102. [Online]. Available: https://linkinghub.elsevier.com/retrieve/pii/0021951794900124

[71] Q. Y. Chen, J. Brocato, F. Laulicht, and M. Costa, "Mechanisms of nickel carcinogenesis," in *Essential and Non-essential Metals*, A. Mudipalli and J. T. Zelikoff, Eds. Springer International Publishing, pp. 181–197, series Title: Molecular and Integrative Toxicology. [Online]. Available: http://link.springer.com/10.1007/978-3-319-55448-8_8

[72] S. G. Akpe, S. H. Choi, and H. C. Ham, "Conversion of cyclic xylose into xylitol on ru, pt, pd, ni, and rh catalysts: a density functional theory study," vol. 23, no. 46, pp. 26 195–26 208. [Online]. Available: http://xlink.rsc.org/?DOI=D1CP04660H

[73] H. Kruszyna, R. Kruszyna, J. Hurst, and R. P. Smith, "Toxicology and pharmacology of some ruthenium compounds: Vascular smooth muscle relaxation by nitrosyl derivatives of ruthenium and iridium," vol. 6, no. 4, pp. 757–773. [Online]. Available: http://www.tandfonline.com/doi/abs/10.1080/15287398009529895

[74] C. O. Malécot, V. Bito, and J. A. Argibay, "Ruthenium red as an effective blocker of calcium and sodium currents in guinea-pig isolated ventricular heart cells: Ruthenium red block of heart ca and na channels," vol. 124, no. 3, pp. 465–472. [Online]. Available: http://doi.wiley.com/10.1038/sj.bjp.0701854

[75] I. Kostova, "Ruthenium complexes as anticancer agents," vol. 13, no. 9, pp. 1085–1107. [Online]. Available: http://www.eurekaselect.com/openurl/content.php?genre=article&issn=0929-8673&volume=13&issue=9&spage=1085

[76] V. Brabec and O. Novakova, "DNA binding mode of ruthenium complexes and relationship to tumor cell toxicity," vol. 9, no. 3, pp. 111–122. [Online]. Available: https://linkinghub.elsevier.com/retrieve/pii/S1368764606000252

[77] T. N. Pham, A. Samikannu, A.-R. Rautio, K. L. Juhasz, Z. Konya, J. Wärnå, K. Kordas, and J.-P. Mikkola, "Catalytic hydrogenation of d-xylose over ru decorated carbon foam catalyst in a SpinChem® rotating bed reactor," vol. 59, no. 13, pp. 1165–1177. [Online]. Available: http://link.springer.com/10.1007/s11244-016-0637-4

[78] V. A. Sifontes Herrera, O. Oladele, K. Kordás, K. Eränen, J.-P. Mikkola, D. Y. Murzin, and T. Salmi, "Sugar hydrogenation over a ru/c catalyst," vol. 86, no. 5, pp. 658–668. [Online]. Available: https://onlinelibrary.wiley.com/doi/10.1002/jctb.2565

[79] V. A. Sifontes, D. Rivero, J. P. Wärnå, J.-P. Mikkola, and T. O. Salmi, "Sugar hydrogenation over supported ru/c—kinetics and physical properties," vol. 53, no. 15, pp. 1278–1281. [Online]. Available: http://link.springer.com/10.1007/s11244-010-9582-9

[80] T. Salmi, D. Y. Murzin, J.-P. Mikkola, J. Wärnå, P. Mäki-Arvela, E. Toukoniitty, and S. Toppinen, "Advanced kinetic concepts and experimental methods for catalytic three-phase processes," vol. 43, no. 16, pp. 4540–4550. [Online]. Available: https://pubs.acs.org/doi/10.1021/ie0307481

[81] J. Kuusisto, J. Mikkola, M. Sparv, J. Warna, H. Karhu, and T. Salmi, "Kinetics of the catalytic hydrogenation of d-lactose on a carbon supported ruthenium catalyst," vol. 139, no. 1, pp. 69–77. [Online]. Available: https://linkinghub.elsevier.com/retrieve/pii/S1385894707005244

[82] G. Araujo Barahona, K. Eränen, D. Murzin, J. García Serna, and T. Salmi, "Reaction mechanism and intrinsic kinetics of sugar hydrogenation to sugar alcohols on solid foam ru/c catalysts – from arabinose and galactose to arabitol and galactitol," vol. 254, p. 117627. [Online]. Available: https://linkinghub.elsevier.com/retrieve/pii/S0009250922002111

[83] A. Najarnezhadmashhadi, J. Wärnå, K. Eränen, H. L. Trajano, D. Murzin, and T. Salmi, "Modelling of kinetics, mass transfer and flow pattern on open foam structures in

tubular reactors: Hydrogenation of arabinose and galactose on ruthenium catalyst," vol. 233, p. 116385. [Online]. Available: https://linkinghub.elsevier.com/retrieve/pii/S0009250920309179

[84] J.-P. Mikkola, T. Salmi, and R. Sjöholm, "Modelling of kinetics and mass transfer in the hydrogenation of xylose over raney nickel catalyst," vol. 74, no. 7, pp. 655–662. [Online]. Available: https://onlinelibrary.wiley.com/doi/10.1002/(SICI)1097-4660(199907)74:7<655::AID-JCTB96>3.0.CO;2-G

[85] P. Avila, M. Montes, and E. E. Miró, "Monolithic reactors for environmental applications," vol. 109, no. 1, pp. 11–36. [Online]. Available: https://linkinghub.elsevier.com/retrieve/pii/S1385894705000793

[86] F. García-Moreno, "Commercial applications of metal foams: Their properties and production," vol. 9, no. 2, p. 85. [Online]. Available: http://www.mdpi.com/1996-1944/9/2/85

[87] L.-P. Lefebvre, J. Banhart, and D. Dunand, "Porous metals and metallic foams: Current status and recent developments," vol. 10, no. 9, pp. 775–787. [Online]. Available: https://onlinelibrary.wiley.com/doi/10.1002/adem.200800241

[88] J. Qi, Y. Sun, Z. Xie, M. Collins, H. Du, and T. Xiong, "Development of cu foam-based ni catalyst for solar thermal reforming of methane with carbon dioxide," vol. 24, no. 6, pp. 786–793. [Online]. Available: https://linkinghub.elsevier.com/retrieve/pii/S2095495615000704

[89] A. Montebelli, C. G. Visconti, G. Groppi, E. Tronconi, S. Kohler, H. J. Venvik, and R. Myrstad, "Washcoating and chemical testing of a commercial cu/ZnO/al2o3 catalyst for the methanol synthesis over copper open-cell foams," vol. 481, pp. 96–103. [Online]. Available: https://linkinghub.elsevier.com/retrieve/pii/S0926860X14003196

[90] P. W. A. M. Wenmakers, J. van der Schaaf, B. F. M. Kuster, and J. C. Schouten, ""hairy foam": carbon nanofibers grown on solid carbon foam. a fully accessible, high surface area, graphitic catalyst support," vol. 18, no. 21, p. 2426. [Online]. Available: http://xlink.rsc.org/?DOI=b718673h

[91] ——, "Comparative modeling study on the performance of solid foam as a structured catalyst support in multiphase reactors," vol. 49, no. 11, pp. 5353–5366. [Online]. Available: https://pubs.acs.org/doi/10.1021/ie900644e

[92] F. Rodríguez-reinoso, "The role of carbon materials in heterogeneous catalysis," vol. 36, no. 3, pp. 159–175. [Online]. Available: https://linkinghub.elsevier.com/retrieve/pii/S0008622397001735

[93] F.-C. Buciuman and B. Kraushaar-Czarnetzki, "Preparation and characterization of ceramic foam supported nanocrystalline zeolite catalysts," vol. 69, no. 1, pp. 337–342. [Online]. Available: https://linkinghub.elsevier.com/retrieve/pii/S092058610100387X

[94] L. Giani, C. Cristiani, G. Groppi, and E. Tronconi, "Washcoating method for pd/-al2o3 deposition on metallic foams," vol. 62, no. 1, pp. 121–131. [Online]. Available: https://linkinghub.elsevier.com/retrieve/pii/S0926337305002833

[95] F. Lali, G. Böttcher, P.-M. Schöneich, S. Haase, S. Hempel, and R. Lange, "Preparation and characterization of pd/al2o3 catalysts on aluminum foam supports for multiphase hydrogenation reactions in rotating foam reactors," vol. 94, pp. 365–374. [Online]. Available: https://linkinghub.elsevier.com/retrieve/pii/S026387621400389X

[96] P. Wenmakers, J. van der Schaaf, B. Kuster, and J. Schouten, "Enhanced liquid–solid mass transfer by carbon nanofibers on solid foam as catalyst support," vol. 65, no. 1, pp. 247–254. [Online]. Available: https://linkinghub.elsevier.com/retrieve/pii/S0009250909003856

[97] F. Glenk, T. Knorr, M. Schirmer, S. Gütlein, and B. J. M. Etzold, "Synthesis of microporous carbon foams as catalyst supports," pp. NA–NA. [Online]. Available: https://onlinelibrary.wiley.com/doi/10.1002/ceat.201000005

[98] T. Knorr, A. Schwarz, and B. J. M. Etzold, "Comparing different synthesis procedures for carbide-derived carbon-based structured catalyst supports," vol. 37, no. 3, pp. 453–461. [Online]. Available: https://onlinelibrary.wiley.com/doi/10.1002/ceat.201300582

[99] F. Lali, S. Gärtner, S. Haase, and R. Lange, "Preparation method for ruthenium catalysts supported by carbon-coated aluminum foams," vol. 38, no. 8, pp. 1353–1361. [Online]. Available: https://onlinelibrary.wiley.com/doi/10.1002/ceat.201400676

[100] T. Vergunst, F. Kapteijn, and J. Moulijn, "Preparation of carbon-coated monolithic supports," vol. 40, no. 11, pp. 1891–1902. [Online]. Available: https://linkinghub.elsevier.com/retrieve/pii/S0008622302000349

[101] C. Moreno-Castilla, O. Mahajan, P. Walker, H.-J. Jung, and M. Vannice, "Carbon as a support for catalysts—III glassy carbon as a support for iron," vol. 18, no. 4, pp. 271–276. [Online]. Available: https://linkinghub.elsevier.com/retrieve/pii/0008622380900500

[102] M. Choura, N. M. Belgacem, and A. Gandini, "Acid-catalyzed polycondensation of furfuryl alcohol: Mechanisms of chromophore formation and cross-linking," vol. 29, no. 11, pp. 3839–3850. [Online]. Available: https://pubs.acs.org/doi/10.1021/ma951522f

[103] A. Najarnezhadmashhadi, K. Eränen, S. Engblom, A. Aho, D. Murzin, and T. Salmi, "Continuous hydrogenation of monomeric sugars and binary sugar mixtures on a ruthenium catalyst supported by carbon-coated open-cell aluminum foam," vol. 59, no. 30, pp. 13 450–13 459. [Online]. Available: https://pubs.acs.org/doi/10.1021/acs.iecr.0c01565

[104] P. Munnik, P. E. de Jongh, and K. P. de Jong, "Recent developments in the synthesis of supported catalysts," vol. 115, no. 14, pp. 6687–6718. [Online]. Available: https://pubs.acs.org/doi/10.1021/cr500486u

[105] R. B. Mason, "Effect of aluminum sulfate in the sulfuric acid electrolyte on anodic polarization," vol. 103, no. 8, p. 425. [Online]. Available: https://iopscience.iop.org/article/10.1149/1.2430373

[106] M. S. Strano, H. Agarwal, J. Pedrick, D. Redman, and H. C. Foley, "Templated pyrolytic carbon: the effect of poly (ethylene glycol) molecular weight on the pore size distribution of poly (furfuryl alcohol)-derived carbon," *Carbon*, vol. 41, no. 13, pp. 2501–2508, 2003.

[107] I. L. Simakova, Y. S. Demidova, J. Gläsel, E. V. Murzina, T. Schubert, I. P. Prosvirin, B. J. M. Etzold, and D. Y. Murzin, "Controlled synthesis of PVP-based carbon-supported ru nanoparticles: synthesis approaches, characterization, capping agent removal and catalytic behavior," vol. 6, no. 24, pp. 8490–8504. [Online]. Available: http://xlink.rsc.org/?DOI=C6CY02086K

[108] O. Sanz, L. C. Almeida, J. M. Zamaro, M. A. Ulla, E. E. Miró, and M. Montes, "Washcoating of pt-ZSM5 onto aluminium foams," vol. 78, no. 1, pp. 166–175. [Online]. Available: https://linkinghub.elsevier.com/retrieve/pii/S0926337307002937

[109] N. Burgos, M. Paulis, and M. Montes, "Preparation of al2o3/al monoliths by anodisation of aluminium as structured catalytic supports," vol. 13, no. 6, p. 1458. [Online]. Available: http://xlink.rsc.org/?DOI=b212242a

[110] C. C. Chen, J. H. Chen, and C. G. Chao, "Post-treatment method of producing ordered array of anodic aluminum oxide using general purity commercial (99.7%) aluminum," vol. 44, no. 3, pp. 1529–1533. [Online]. Available: https://iopscience.iop.org/article/10.1143/JJAP.44.1529

[111] A. Kozhukhova, S. du Preez, and D. Bessarabov, "The effects of pore widening and calcination on anodized aluminum oxide prepared from al6082," vol. 383, p. 125234. [Online]. Available: https://linkinghub.elsevier.com/retrieve/pii/S0257897219312241

[112] P. McKendry, "Energy production from biomass (part 1): overview of biomass," vol. 83, no. 1, pp. 37–46. [Online]. Available: https://linkinghub.elsevier.com/retrieve/pii/S0960852401001183

[113] A. M. Ruppert, K. Weinberg, and R. Palkovits, "Hydrogenolysis goes bio: From carbohydrates and sugar alcohols to platform chemicals," vol. 51, no. 11, pp. 2564–2601. [Online]. Available: https://onlinelibrary.wiley.com/doi/10.1002/anie.201105125

[114] Sugar alcohol market size, share | global forecast [2020-2027]. [Online]. Available: https://www.fortunebusinessinsights.com/sugar-alcohol-market-102956

[115] E. M. Cepollaro, D. Caputo, S. Cimino, N. Gargiulo, and L. Lisi, "Synthesis and characterization of activated carbon foam from polymerization of furfuryl alcohol activated by zinc and copper chlorides," vol. 6, no. 3, p. 45. [Online]. Available: https://www.mdpi.com/2311-5629/6/3/45

[116] P. Koopman, "Characterization of ruthenium catalysts as studied by temperature programmed reduction," vol. 69, no. 1, pp. 172–179. [Online]. Available: https://linkinghub.elsevier.com/retrieve/pii/0021951781901391

[117] S. Rio, G. Peru, B. Léger, F. Kerdi, M. Besson, C. Pinel, E. Monflier, and A. Ponchel, "Supported ruthenium nanoparticles on ordered mesoporous carbons using

a cyclodextrin-assisted hard-template approach and their applications as hydrogenation catalysts," vol. 383, pp. 343–356. [Online]. Available: https://linkinghub.elsevier.com/retrieve/pii/S0021951719305238

[118] I. L. Simakova, Y. S. Demidova, E. V. Murzina, A. Aho, and D. Y. Murzin, "Structure sensitivity in catalytic hydrogenation of galactose and arabinose over ru/c catalysts," *Catalysis Letters*, vol. 146, no. 7, pp. 1291–1299, 2016.

[119] F. van der Klis, L. Gootjes, J. van Haveren, D. S. van Es, and J. H. Bitter, "Selective terminal c–c scission of c5-carbohydrates," vol. 17, no. 7, pp. 3900–3909. [Online]. Available: http://xlink.rsc.org/?DOI=C5GC01012H

[120] V. A. Sifontes Herrera, F. Saleem, B. Kusema, K. Eränen, and T. Salmi, "Hydrogenation of l-arabinose and d-galactose mixtures over a heterogeneous ru/c catalyst," vol. 55, no. 7, pp. 550–555. [Online]. Available: http://link.springer.com/10.1007/s11244-012-9833-z

[121] E. Crezee, "Three-phase hydrogenation of ?-glucose over a carbon supported ruthenium catalyst—mass transfer and kinetics," vol. 251, no. 1, pp. 1–17. [Online]. Available: https://linkinghub.elsevier.com/retrieve/pii/S0926860X03005878

Appendices

Appendix A

HPLC Calibration

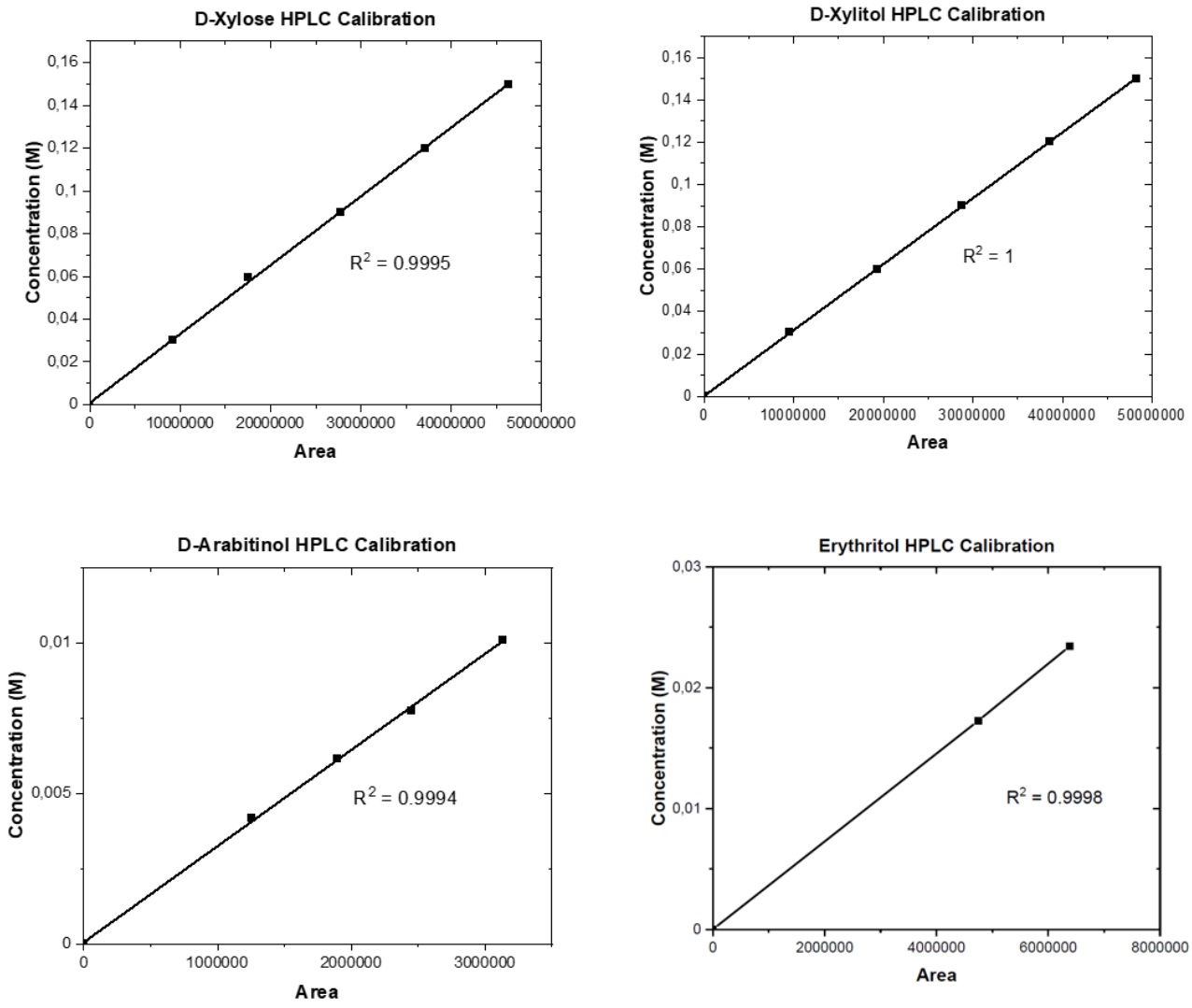

Figure A.1: *HPLC calibration curves.*

Appendix B

HPLC Chromatograph

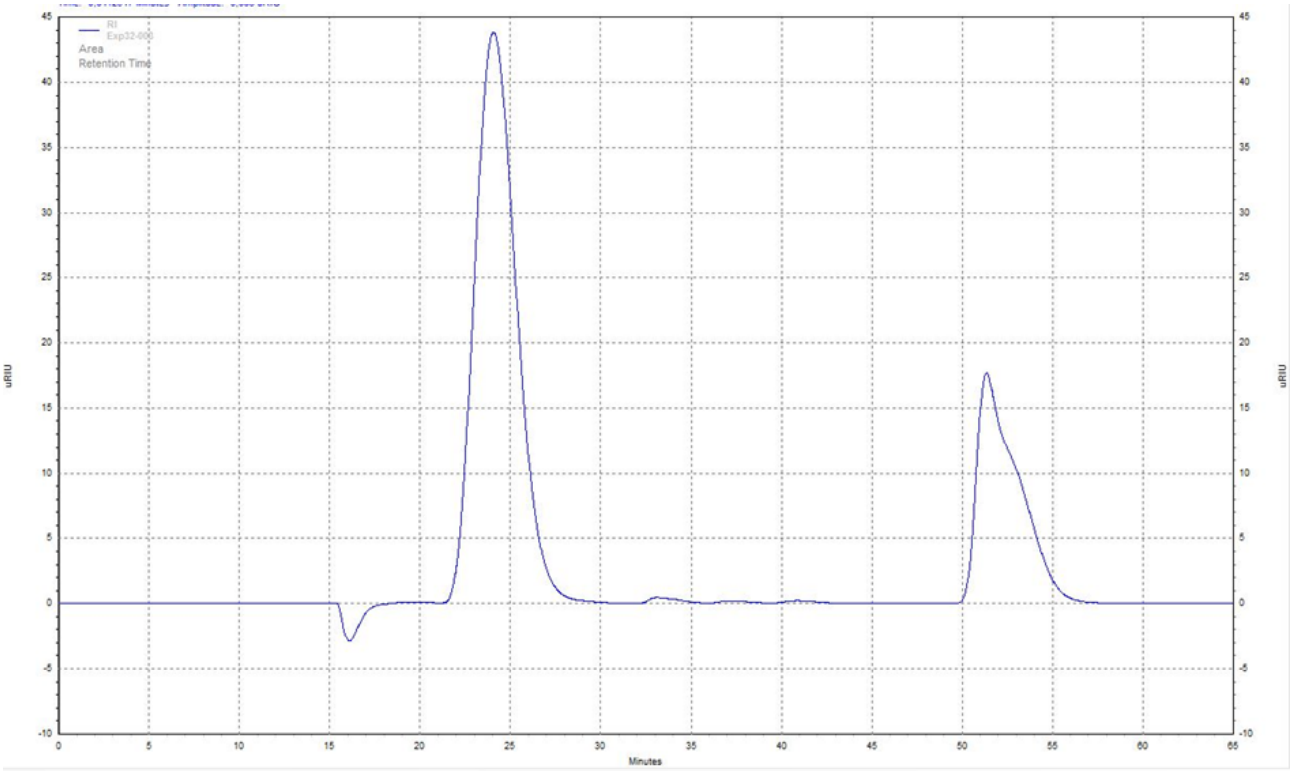

Figure B.1: *HPLC chromatograph.*

Appendix C

Kinetic 3D Charts

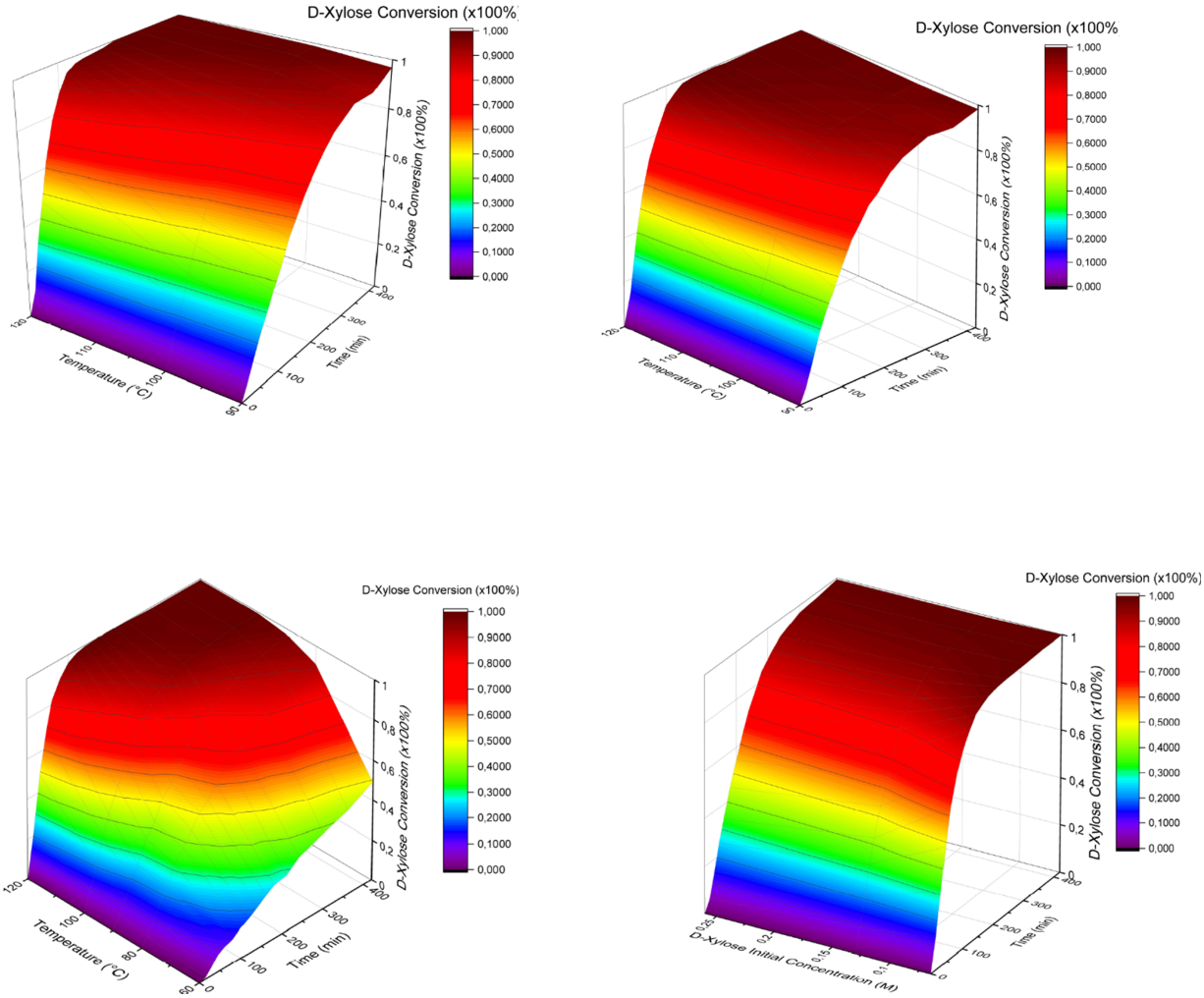

Figure C.1: *3D temperature influence charts under 40 bar, 30 bar, 20 bar, and concentration influence under 40 bar and 100°C.*

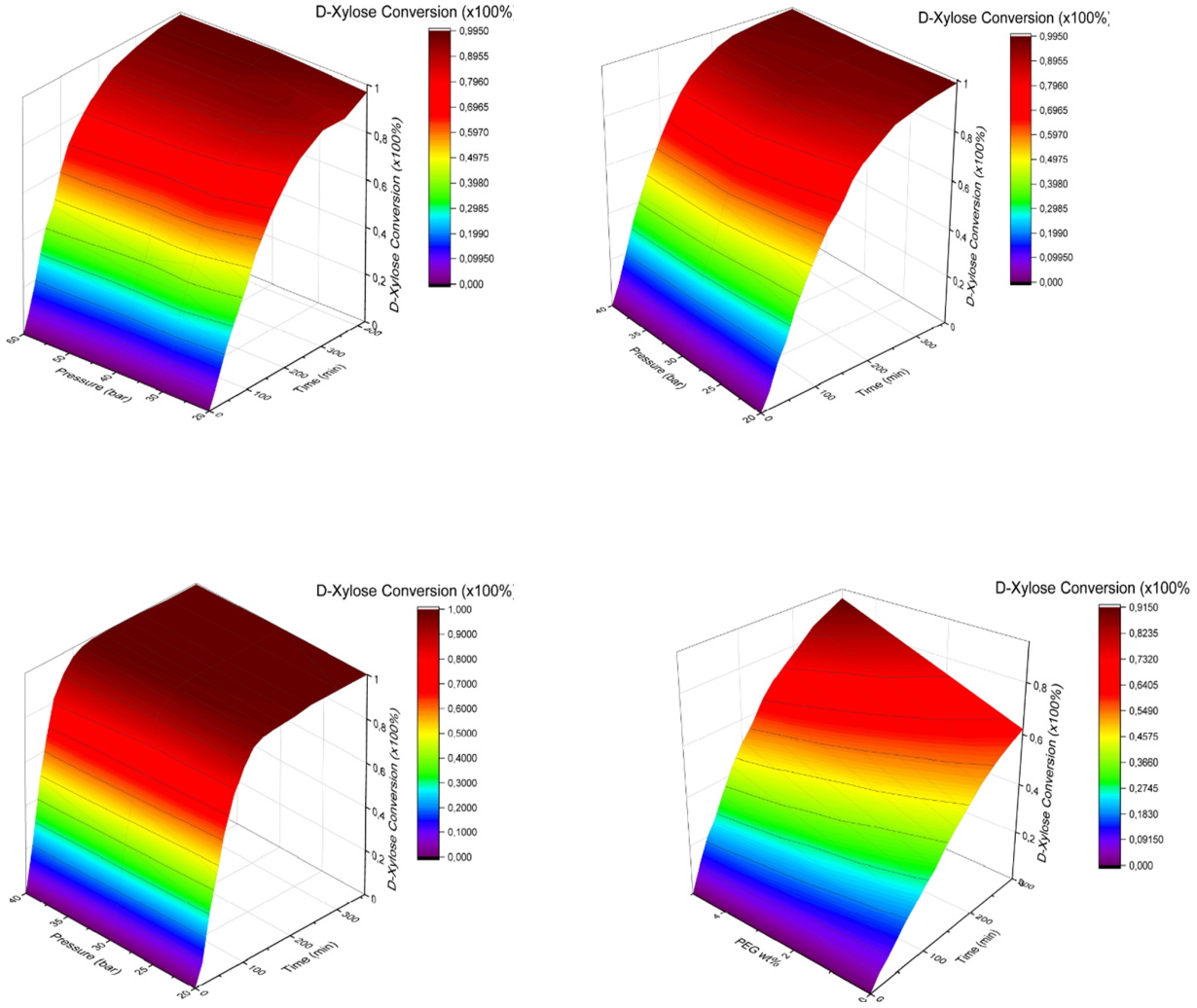

Figure C.2: *Pressure influence under 90°C, 100°C and 120°C, and PEG influence under 90°C and 30 bar.*

Appendix D

D-Xylitol Selectivity against Erythritol's

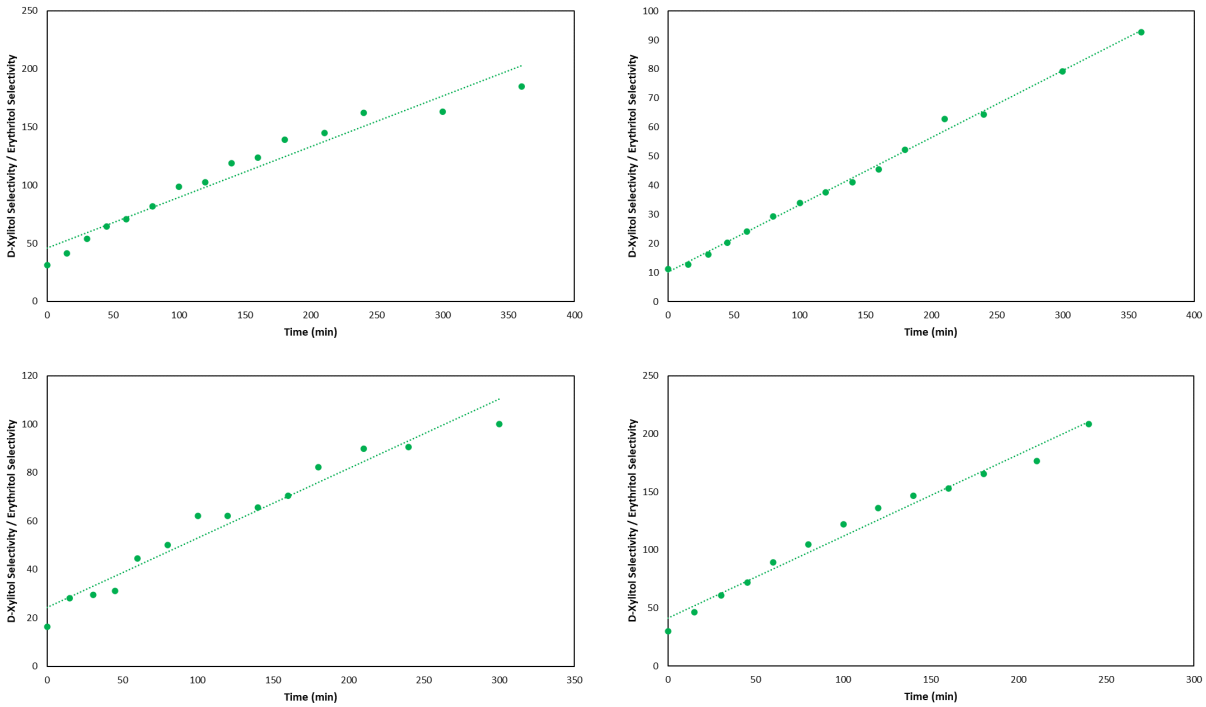

Figure D.1: *D-Xylitol selectivity against erythritol's chart.*

The concentratrion of D-xylitol vs the concentrion of erythritol results in a straight line, which suggests that both reactions occur paralally, since:

$$r_1 = \frac{K_1 \cdot S}{Denominator} \tag{D.1}$$

$$r_3 = \frac{K_3 \cdot S}{Denominator} \tag{D.2}$$

$$\frac{dCS_{OH}}{dt} = r_1 \cdot \rho_B \tag{D.3}$$

$$\frac{dCEry}{dt} = r_3 \cdot \rho_B \tag{D.4}$$

So:

$$\frac{dCS_{OH}}{dCEry} = \frac{r_1}{r_3} = cte \tag{D.5}$$